Elucidating mechanisms of unreduced gamete formation in *Arabidopsis thaliana*

Dissertation
zur Erlangung des
Doktorgrades der Naturwissenschaften (Dr. rer. nat.)

der

Naturwissenschaftlichen Fakultät III
Agrar- und Ernährungswissenschaften,
Geowissenschaften und Informatik

der Martin-Luther-Universität Halle-Wittenberg

vorgelegt von

Frau Ewa Weronika Piskorz
Geb. am 21.07.1993 in Wrocław, Poland

Datum der Verteidigung: 16.05.2022

Gutachter:

Jun.-Prof. Hua Jiang – Martin-Luther-Universität Halle-Wittenberg

Assoc. Prof. Aleš Pečinka – Institute of Experimental Botany of the Czech Academy of Sciences

Table of Contents

1. Introduction

1.1 Polyploidy in plants

Polyploidy is a widespread phenomenon among eukaryotes, considered as a major speciation and adaptation mechanism. Numerous studies reported on the existence of polyploid species within fungi and animal kingdoms (Albertin & Marullo, 2012; Dowling & Secor, 1997; Kellis et al., 2004; McLysaght et al., 2002); however, it is the plant kingdom that is particularly enriched in polyploids, as up to 70% of angiosperms are estimated to be polyploid (Bretagnolle & Thompson, 1995). The term "polyploid" refers to a cell or an organism with more than two complete copies of the genome. Depending on the origin of the genomes, polyploids are classified as autopolyploids and allopolyploids. Autopolyploidy results from the genome doubling within or between populations of a single species (intraspecific), whereas allopolyploidy derives from the hybridization between different species (interspecific), followed by no reduction of the chromosome content or fusion of unreduced gametes (Comai, 2005; De Storme & Geelen, 2013).

Plants are strongly benefited from polyploidization in their ancestral lineages. First of all, polyploids display heterosis that is defined as “the increase in performance displayed by hybrids compared to their inbred parents” (Comai, 2005). The improvement of vigor is observed not only in allopolyploids but also in autopolyploids. However, it is worth noting that some autopolyploid inbreds often show stronger inbreeding depression than the corresponding diploid inbreds, possibly due to the allelic dosage effect (Birchler et al., 2003, Kidwell et al., 1994). Heterozygosity is another important feature of polyploids, which enables the progenies to be more genetically diverse. In allopolyploids, heterozygosity reaches high levels due to the combination of two different genomes. The genetic inheritance of homologous chromosomes coming from the same diploid ancestor fixes heterozygous traits of the progenies (Sattler et al., 2016). Increased heterozygosity is also expected to occur in autopolyploids due to polysomic inheritance (Moody et al., 1993). Moreover, heterozygosity positively affects vigor in multiple autotetraploid hybrid plant species (Katepa-Mupondwa et al., 2002; Mendoza & Haynes, 1974).

Another advantage is that due to gene redundancy, recessive alleles are masked more often by the dominant wild-type alleles. While a heterozygous diploid organism produces 1/4 of recessive homozygous progenies, heterozygous allotetraploid produces only 1/16 of such progenies, and heterozygous autotetraploid – between 1/36 and 1/22 (Comai, 2005). It is especially important in isolated and bottlenecked populations, which are forced to save continuity of their lineage by inbreeding, or in the case of deleterious

recessive mutations spread in a population. Moreover, some redundant genes might diversify to acquire novel functions since polyploids have multiple genome copies (Adams & Wendel, 2005).

Polyploids can also utilize asexual reproduction through apomixis, producing embryos only from maternal tissues without the sexual mate (Bicknell & Koltunow, 2004). By selecting the asexual means of reproduction, polyploids can bypass the so-called 'triploid block' – the malfunction of the endosperm, observed when a polyploid progeny is backcrossed to a diploid parent or as a result of meiotic restitution in triploids (Köhler et al., 2010). Taken together, the advantages granted by polyploidy resulted in the increased genomic variation and subsequent chances of more efficient adaptation to new environments than their diploid ancestors.

The benefits of polyploidy have been utilized in cultivation of many important crops and ornamental plants. The most well-known allopolyploid crop displaying heterosis is hexaploid bread wheat (*Triticum aestivum*), which arose naturally through multiple hybridizations (Haider, 2013). Moreover, two types of tetraploid cotton, *Gossypium hirsutum* and *G. barbadense*, present fiber quality superior to their diploid parents (Renny-Byfield & Wendel, 2014). Darwin hybrid tulips, including diploid, triploid, and tetraploid cultivars, display increased flower size and overall plant vigor (Marasek-Ciolakowska et al., 2012). Autotetraploid rye (*Secale cereal*e) displays stiff straw and improved quality for baking by induced polyploidization (Schlegel, 2006). The resistance to root-knot nematodes could be transferred from *Nicotiana repanda* to *Nicotiana tabacum* only through *Nicotiana sylvestris*, which was capable of hybridizing with both species and therefore served as a "bridge" (Burk, 1967). A sterile intergeneric hybrid, *Chitalpa taskentensis,* gained fertility upon autopolyploidization through oryzalin treatment (Olsen et al., 2006). More examples are listed in the comprehensive review by Sattler, Carvalho, and Clarindo (Sattler et al., 2016).

Polypoid generation can be divided into two main categories: natural and artificial. Artificial methods utilize chemicals such as colchicine, oryzalin, or nitrous oxide to induce chromosome doubling in somatic tissues. They act by binding to tubulin, the main component of mitotic and meiotic spindles, thus inhibiting its polymerization and arresting the dividing cell in metaphase until chromosomes return to their interphase structure (Ascough et al., 2008; Kitamura et al., 2009; Nebei, 1937). However, this approach is time-consuming, laborious, and inefficient (Sato et al., 2005). Moreover, the obtained polyploid plants are often less fit and more variable than naturally generated polyploids, as shown by McCoy and Rowe in their study on alfalfa (McCoy & Rowe, 1986).

Another disadvantage of artificially induced polyploidy is that treatment with chemicals can be detrimental to plantlet's vigor, while yielding higher ploidy levels than anticipated. It is thus not surprising, that much effort is put into understanding mechanisms of natural polyploidization, which can be utilized in breeding without issues linked to usage of chemicals. Since from the perspective of both evolution and breeding, polyploids capable of reproduction are of utmost importance, this thesis focuses on the natural mechanisms which lead to their production.

1.1.1 Natural polyploidization

Whole-genome duplication (WGD) – a transient multiplication of an organism's entire genome – is thought to be the basis of the angiosperm species diversification and a driving force for their evolutionary success. It is believed that all extant angiosperms share two whole-genome duplications in their lineages – one in the common ancestor of the seed plants, and one in the common ancestor of the angiosperms themselves (Jiao et al., 2011). On top of that, many plant species underwent more than two WGD events, i.e. at least three in maize, soybean, and *Arabidopsis thaliana* (Blanc et al., 2000, 2003), and most eudicots are reported to originate from a common hexaploid progenitor (Jaillon et al., 2007; Jiao et al., 2011). A change in ploidy usually causes genome instability, such as substantial gene loss and genomic rearrangement, leaving many genes as a single-copy locus. On the other hand, if both copies survive, one of them might diverge to adopt a different function (reviewed in Sémon & Wolfe, 2007).

Polyploids are believed to be continuously generated in nature through the most common natural route: the defects in meiosis progression (Brownfield & Köhler, 2011). Meiosis is a specific type of cell division, that aims to produce gametes. In this process, a single round of DNA replication is followed by two consecutive rounds of nuclear division, resulting in the generation of four daughter cells and the reduction of parental DNA content by half. Meiotic divisions are referred to as reductional (also: first or meiosis I) and equational (also: second or meiosis II). During reductional nuclear division, homologous chromosomes synapse, exchange genetic material, and segregate, whereas sister chromatids separate during the equational division, which strongly resembles mitosis. In flowering plants, the products of meiosis are four haploid cells, that undergo subsequent mitotic divisions to develop into mature gametophytes. Any deviation from the standard course of meiosis results in the formation of abnormal meiotic products, among which are unreduced gametes. Unreduced gametes contain the somatic chromosome number and mature into the unreduced, albeit viable spores capable of reproduction. An example would be a diploid plant producing diploid pollen instead of the expected, haploid ones.

As a side note, it is worth noting that depending on the plant species, diploid sperm nuclei can be disadvantaged in the race with the haploid ones to fertilize the ovule. In most angiosperms, diploid pollen germinates slower than the haploid one (Kang & Zhu, 1997), or at the same pace but later, as in *Citrus grandis* (Tuyet et al., 2011). On the other hand, in *Solanum phureja,* 2n pollen was proved to be more viable than 1n pollen (Simon & Peloquin, 1976), while in its relative, *Solanum tuberculosum*, pollen tubes grew faster on the stigmata (Van Breukelen, 1982). Therefore, the capability of forming a certain number of unreduced gametes may not mean producing the equal amount of polyploid offspring.

In order to propagate smoothly, most polyploids need to have an even number of chromosome sets. The best example is a tetraploid plant, which can be generated through three routes: by self- or cross-fertilization of unreduced gametes, or through an unstable triploid intermediate, which circumvents the so-called 'triploid block'. The failure of endosperm, which causes triploid seed abortion, is the result of excess of either maternal or paternal genomes, deviating from the '2 maternal and 1 paternal genome' composition required for correct endosperm development. Under normal conditions, the homodiploid central cell is fertilized by one of the two haploid sperm nuclei before developing into the endosperm. The endosperm thus becomes triploid and is capable of providing nutrients for the developing embryo (Lopes & Larkins, 1993). When reduced and unreduced gametes are involved in the fertilization process, either during a cross between a diploid and a tetraploid plant, or during triploid's self-propagation, the balance of maternal and paternal genome contribution is disturbed. If the female gametophyte is unreduced, the proliferation of the endosperm is inhibited. Unreduced male gametophytes yield an endosperm excess (Haig & Westoby 1991; Scott et al., 1998). Both usually lead to endosperm failure and subsequently increased seed abortion. The viable offspring is a triploid plant. Triploids are morphologically normal, and their biomass as well as organ size is usually greater than those of their diploid and tetraploid relatives (Morgan et al., 2004; Riddle et al., 2006; Liqin et al., 2019). They are, however, mostly infertile. Their almost complete sterility upon self-fertilization arises from the random pairing and imbalanced chromosome segregation of mono-, di and trivalents caused by the presence of odd-numbered chromosome sets. However, triploids can produce a subset of seeds, which are capable of germinating. Most of the progenies are aneuploid, i.e., contain more or less individual chromosomes or large chromosomal segments than the wild type. Aneuploids usually show severe phenotypic defects, such as disturbed development, partial sterility and morphological abnormalities (Birchler & Veitia, 2007; Makarevitch et al., 2008). But more importantly, some of the viable seeds which overcame the 'triploid block' are tetraploid and can successfully self-propagate.

1.1.2 Polyploidization through unreduced gametes as an evolutionary mechanism

The interest in polyploidy eventually led to the question if it is just a meiotic mishap, or whether it should be considered an important evolutionary mechanism. Mason and Pires in their review discussed this issue and put forward arguments, that support the latter belief. According to their observations, a wide range of mechanisms that cause unreduced gamete formation are present in a variety of species from most eukaryotic kingdoms (Dowling & Secor, 1997; Wyatt et al., 1988; Wood et al., 2009; Albertin & Marullo, 2012). These mechanisms are also involved in viable interspecies crosses, as well as crosses between ploidy levels, which further outline the great role of unreduced gametes in facilitating polyploidy (reviewed in Köhler et al., 2010). Moreover, unreduced gametes are regularly produced by many interspecific hybrids, such as the spruce bark beetle (Führer, 2004), intergeneric hybrids of the frog genus Xenopus (Bogart, 1980) or hybrid angiosperm species (Ramsey & Schemske, 1998). Last but not least, many reports show that unreduced gametes are produced upon environmental stresses. This is especially well documented in studies on flowering plants subjected to, among others, cold stress, heat stress, osmotic stress, or nutrient deficiency (Grant, 1953; De Storme & Geelen, 2014). Nevertheless, it is still unknown whether the initial unreduced gamete formation incident was an exception that became a heritable, advantageous feature, or an event that facilitated the course of evolutionary adaptation (Gould & Vrba, 1982). Regardless of the answer, unreduced gametes production remains to be the most important mechanism of polyploid formation in plants, which provides a lot of profits for breeding. The ability of plants to produce unreduced gametes can facilitate crosses between plants with varying ploidy levels – a process advantageous for transferring beneficial genes between species or masking the ones with a negative effect on breeding (Ogburia et al., 2002; Carputo et al., 2000; Ortiz et al., 1997). Unreduced gametes are also utilized to generate new auto- and allopolyploids of formerly diploid species in order to increase genetic diversity and make use of heterosis for the enhanced biomass and overall performance (Ogburia et al., 2002; Consiglio et al., 2004). The prevalence and importance of polyploids, as well as the important role of the unreduced gamete formation in the facilitation of polyploidy, are the reasons why the origin of unreduced gametes is the main focus of this study.

1.2 Meiosis in plants

Meiosis is a conserved process among eukaryotes (Dawe, 1998). Upon leaving the premeiotic S-phase, when the genome content is doubled due to the generation of sister chromatids in each chromosome, the cell enters prophase I - the first and also the longest stage of meiosis, which consists of five phases. Leptotene, the first phase of prophase I,

begins with chromosome condensation and the onset of homologous chromosomes pairing. Each chromosome finds its homolog by zygotene, during which the synaptonemal complex (SC) polymerizes in order to guide synapsis – the close alignment of maternal and paternal chromosome axes. Once it is fully reached at pachytene, double-strand breaks occur, enabling cross-over between non-sister chromatids represented by chiasmata – tight physical connections between bivalents (homologous chromosomes in each pair). Crossovers warrant not only genetic diversity in the offspring, but also guarantee – after equatorial alignment of the bivalents during metaphase I – correct segregation of homologous chromosomes during anaphase I, resulting in reduced chromosome numbers in the daughter cells. At diplotene, the SC disassembles and chromosomes further condense. During diakinesis, chromosomes reach maximal condensation while still being connected within each pair by chiasmata. At this stage, the nuclear envelope finally breaks and prophase I is completed. During metaphase I, highly condensed chromosomes move to the cell equator and align, while spindle microtubules attach to the kinetochores at the centromeres of both homologs of each bivalent. Anaphase I starts when homologous chromosomes separate from each other and move along the spindles to opposite poles. In telophase I, chromosomes reach the poles and briefly decondense, while the nuclear envelope temporarily re-emerges. The second meiotic division begins with prophase II, in which the separated homologous chromosomes condense again as univalent, move towards the cell equator during prometaphase II and reach perfect alignment in metaphase II, when the meiotic spindles once attach to the sister centromeres.

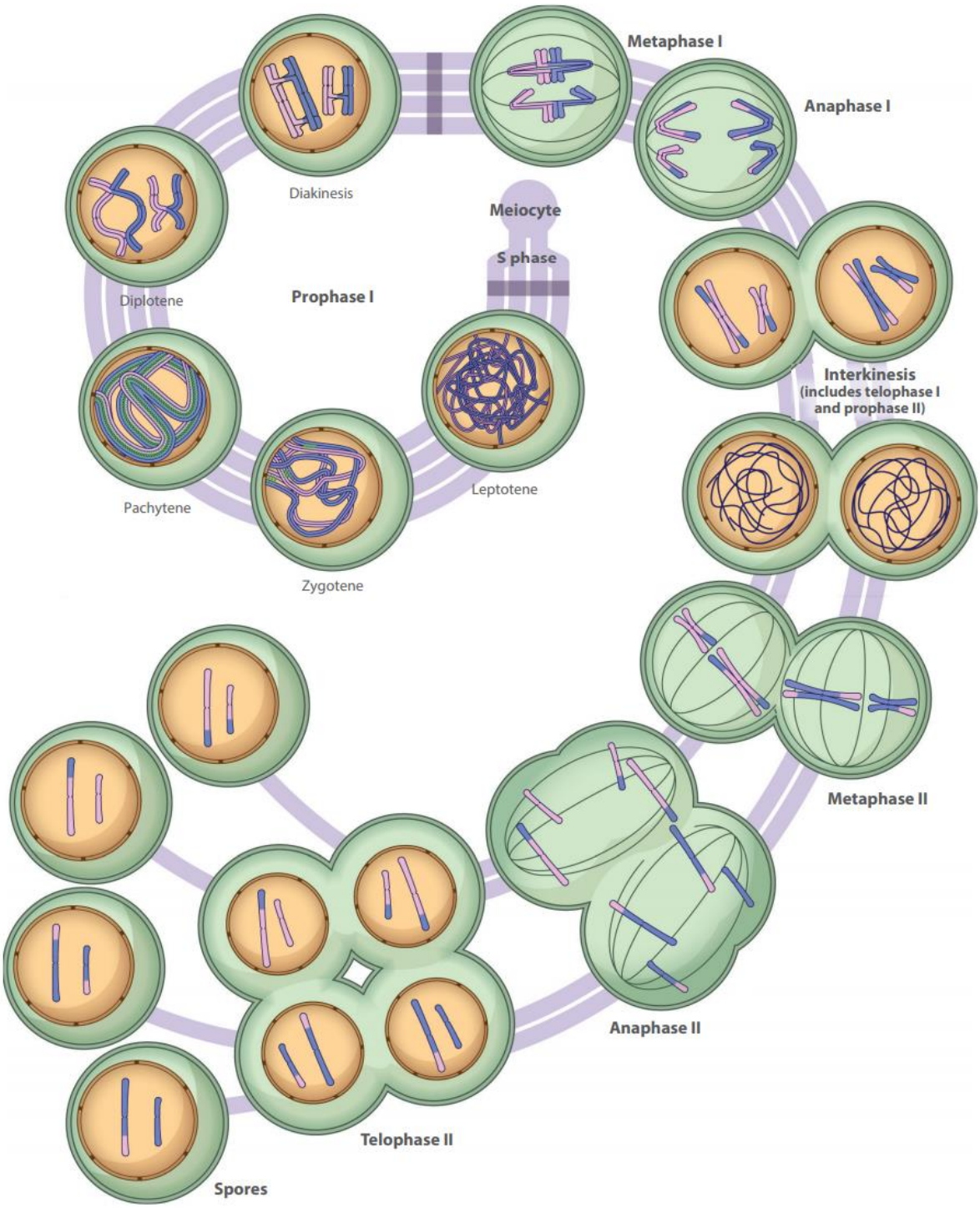

Figure 1 Overview of meiosis [modified from Mercier et al., 2015].

During anaphase II, sister chromatids segregate to opposite cell poles, and finally decondense during telophase II, creating four haploid nuclei (Fig. 1). In Arabidopsis male meiosis, their spatial organization is tetrahedral, although linear, T-shaped, tetragonal and rhomboidal configurations can be observed in other plant species (reviewed in De Storme & Geelen, 2013). This diversity is caused first and foremost by the type of cytokinesis that occurs in the meiotic cell, which can be either successive or simultaneous. Successive

cytokinesis can be observed usually in monocotyledonous plants and is characterized by two rounds of cytokinesis. The first leads to the formation of a cell wall after telophase I, yielding a "transitory" dyad, which physically separates two groups of chromosomes. Their sister chromatids segregate during meiosis II, which ends with the second cytokinesis. On the other hand, simultaneous cytokinesis is more common in dicotyledonous plants, such as Arabidopsis. In such plants, cytokinesis occurs only after telophase II, dividing the mother cell into four daughter cells at once (Fig. 2).

1.2.1 Roles of the cytoskeleton in meiosis

To produce four reduced gametes from a spore mother cell during meiosis, all cellular components need to cooperate in an organized manner. One of such components is the cytoskeleton, which is found in the cytoplasm of every eukaryotic cell and consists mostly of microtubules and microfilaments. The main roles of the cytoskeleton are maintaining the shape of the cell and anchoring some organelles in place, while providing movement for other organelles as well as for the cell itself.

Microtubules are built from α- and β-tubulin heterodimers and have polarized ends – stable minus ends are at the origin site, while plus ends radiate outwards and elongate. In animals and algae, the structure at the minus end of microtubules, which is responsible for their nucleation, is called Microtubule Organizing Centre (MTOC, also known as centrosome). Its main compound is a pair of centrioles. Interestingly, most higher plants' cells lack such kind of MTOCs (Ovechkina & Oakley, 2001). Various microscopic analyses show a more disorganized distribution of nucleation sites, as they appear both in the cytoplasm and/or the endomembrane system. Shaw et al. showed the dispersed and migratory plant MTOCs on the example of cortical microtubules (Shaw et al., 2003). The same findings were presented in spindles (Shimamura et al., 2004). Nonetheless, various studies on eukaryotic cells show that the common component of eukaryotic microtubule nucleation centers is y-tubulin in a complex with several proteins at the minus end (reviewed by Oakley, 2000). y-tubulin does not form heterodimers and, in contrast to α- and β-tubulin, it is not the main component of microtubular arrays. In plants, it creates a Tubulin Ring Complex (TuRC) with GCP2 to GCP6 proteins, which acts as a nucleation center at the spindle poles and alongside the phragmoplast (Miao et al., 2019).

Plants' microtubules are capable of initiating a wide range of arrays, including radial arrays, cortical arrays, preprophase band, spindles and phragmoplast (Falconer et al., 1988). The chromosome segregation is guided by the spindles, which form during metaphase. Their minus ends are bound to a diffused plant MTOC, while plus ends

elongate towards chromosomes and attach to the centromeres to initiate the segregation of homologous chromosomes in meiosis I and of sister chromatids in meiosis II. Another well-known microtubular array is the phragmoplast – a structure made of two sets of multiple short, parallel microtubules, whose plus ends overlap at the cell equator. It forms at the division plane and serves as a track for the transport of Golgi-derived vesicles carrying membrane components for the growing cell plate (reviewed by Hamada, 2014). In plants, whose PMCs undergo successive cytokinesis, it appears in late telophase I, but in contrast to mitotic cytokinesis, the division plane is not established by the cortical microtubule array arranged into the preprophase band (PPB), but rather by the central spindle fibers in meiosis I. They remain in the cell midzone after anaphase I and form a phragmoplast-like structure that expands centrifugally and increases in number of more and more curved fibers (Shamina et al., 2007). On the other hand, in meiocytes with simultaneous cytokinesis, no PPB nor phragmoplast is formed. Instead, microtubules emanating from the nuclear membrane of telophase II nuclei, together with actin filaments, form radial microtubule arrays (RMAs), which are responsible for marking the position of the future cell wall by creating furrows of the callose wall of PMCs. Those furrows then grow centripetally, not restricted by the pre-determined PPB, but rather by the spatial organization of the nuclei present in the cell (Brown & Lemmon, 1989, 1992, 2001; Traas et al., 1989) (Fig. 2).

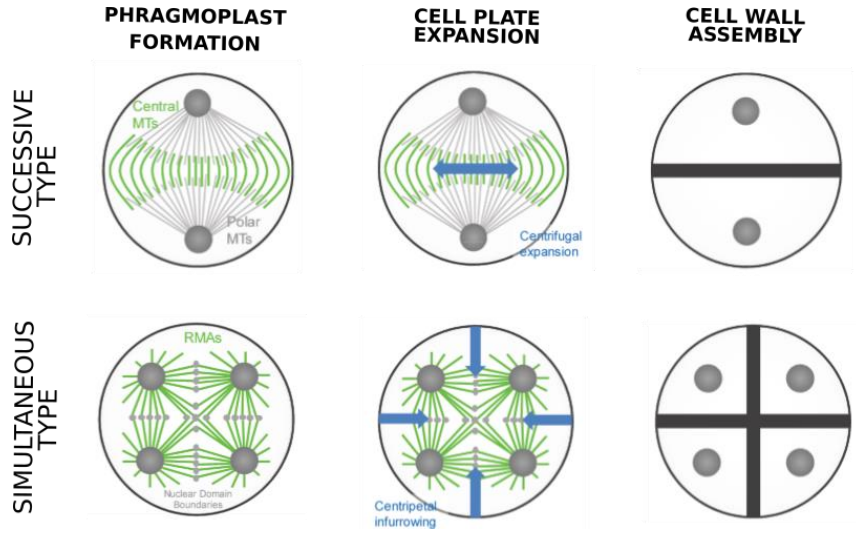

Figure 2 Microtubule array formation in male meiotic cytokinesis. Upper panel represents the first cell division and a "transitory dyad" in plants with successive cytokinesis, whereas the lower panel shows the singular cytokinesis event in plants with simultaneous cytokinesis. Green represents phragmoplast and RMA microtubules. Blue represents the newly formed cell plate and associated deposition of callose. Gray represents polar MT bundles [modified from De Storme & Geelen, 2013].

Less is known about the role of actin during meiotic division. The functional form of actin is filamentous actin (F-actin), which assembles from globular actin (G-actin) monomers into a helical structure (Li et al., 2015). Generally, F-actin is present in the cytoplasm of plant cells throughout their lives, including karyo- and cytokinesis. Moreover, various studies show a special enrichment of microfilaments in the spindles and/or phragmoplast of plant cells (Sheldon & Hawes, 1988; Dinis & Mesquita, 1993; Staiger & Cande, 1991; Van Lammeren et al., 1989). Dinis and Mesquita, upon analysis of F-actin distribution in microspores of *Magnolia soulangeana*, described its four main configurations: peripheral filaments (cortical network), filaments dispersed in the cytoplasm (central cytoplasmic network), filaments associated with the meiotic spindles and filaments associated with the phragmoplast. They claim, however, that despite co-distribution of F-actin with microtubules necessary for correct meiotic progression, actin's role might be limited to cytoplasmic cleavage during cytokinesis. A study on the effect of cytochalasin-B, the inhibitor of F-actin polymerization, which also damages the preexisting filaments (Brown & Spudich, 1979; Hartwig & Stossel, 1979), on microsporangia of *Psilotum nudum* seems to corroborate this notion. Upon treatment with cytochalasin-B, meiosis was disturbed as no typical actin structures were present, organelles did not form the organelle band, and normally separated nuclei were chaotically dispersed in the cytoplasm, often coming close together (Dorota Tchórzewska & Bednara, 2011). Another work, which studied the effect of cold stress on actin distribution in wheat male meiosis, also showed disorganized phragmoplast and insufficient deposition of callose on the cell plate, pointing towards the relationship between actin cytoskeleton and the formation of the cell plate (Xu et al., 2013).

More about cytoskeleton’s role in meiotic progression can be learned through studying motor proteins. These proteins utilize energy from the hydrolysis of ATP to actively move along the cytoskeleton filaments and carry out regulatory, reorganizing and transporting tasks. Although three types of motor proteins can be found in mammals and fungi, plants possess only two of them: kinesins, which travel on microtubules, and myosins, which traverse microfilaments.

Kinesins and myosins share structural similarities. All kinesins are made of two (or more) heavy chains and several light chains which stabilize and regulate them. Heavy chains consist of four domains: 1) the motor (head) domain, which hydrolyzes ATP to generate energy for the movement; 2) a neck domain, which is a flexible linker with the stalk; 3) the stalk – a coiled-coil domain, which can dimerize in order to couple two or more kinesins to act as a single unit; and 4) a tail domain, responsible for binding cargo. Different functions of kinesins result from the fourth domain, the variable, non-motor tail,

depending on what cargo it binds. Similar to kinesins, myosins contain motor domains on the N-terminus and a cargo-binding domain on their C-terminus. Myosin necks are, however, longer than those of kinesins, which allow them to take longer "steps" and thus generate cytoplasmic streaming – the motion of the cytoplasm, caused by myosins transporting their cargo along microfilaments.

The role of kinesins during both mitosis and meiosis is indispensable, although up to date the exact function of many kinesin families' members remains elusive. Kinesins participate in microtubular spindle assembly, nuclear envelope breakdown, attachment of microtubules to sister chromatids, parallel positioning of the chromosomes during metaphase, movement of chromosomes along the spindles and spindle elongation (reviewed in Lee & Liu, 2007). KCH, a minus-end-directed kinesin, was found to balance the plus-end-directed motor protein ARK during nuclear positioning (Augustine, 2018), whereas another minus-end-directed kinesin, KINDR in maize, is responsible for the motility of heterochromatic knobs during anaphase in meiosis, thus participating in the chromosome segregation (Dawe et al., 2018). In rice, chromosome dynamics in male meiosis was discovered to be controlled by *PSS1* – a kinesin-1-like protein (Zhou et al., 2011).

Among kinesin families, two are involved in the regulation of microtubular spindle: kinesin-14 and kinesin-5 families. In Arabidopsis, the first family has two members localized to the mitotic and male meiotic spindle poles: ATK1 and ATK5. Both of them are minus-end-directed, and as such they generate the inward forces that shorten the spindle. The *atk1-1* mutant is characterized by loss of spindle bipolarity, abnormal chromosome segregation and eventual reduction in male fertility (Chen et al., 2002). On the other hand, *atk5* mutant displays broader and longer mitotic spindles than those of wild-type (Ambrose & Cyr, 2007; Ambrose et al., 2005; Marcus et al., 2003; Marcus et al., 2002). The *atk1;atk5* double mutant was found to be unrecoverable, which points towards the necessity of minus-end-directed kinesins' function in spindle assembly (Bannigan et al., 2008). Two other kinesin-14 family members in maize, DV1 (*Divergent spindle-1*) and ZmKin11, control the spindle shape by possibly crosslinking microtubules from two different spindle poles, leading to broader and longer spindles, chromosome lagging in anaphase and eventually lower pollen viability (Higgins et al., 2016). Kinesin-14's inward force is balanced by plus-end-directed kinesin-5's outward force, which separates the spindle halves in anaphase. Kinesin-5 proteins function also at the mitotic spindle midzone, where they stabilize it by crosslinking antiparallel microtubules. In the *radially swollen 7* mutant, with a point mutation in the kinesin-5 gene AtKRP125c, spindles were

found to be highly deformed as the spindle poles collapsed towards each other, most likely due to imbalance in the inward/outward forces (Wiedemeier et al., 2002).

Up to date the best described kinesins' cargo are Golgi-derived vesicles, which are being delivered by the members of kinesin-10 and kinesin-12 families to the phragmoplast for the formation of a new cell wall. *Arabidopsis* PAKRP2, a kinesin-10 family member, was found to be localized to the phragmoplast midzone most likely upon being activated by the association with its cargo, the Golgi vesicles (Lee et al., 2001). Although the evidence was indirect, gathered from i.e. brefeldin A treatment, studies on AtPAKRP2 homologs in rice and moss corroborated its function in the regulation of phragmoplast organization (Hiwatashi et al., 2014; Fang et al., 2018).

Myosins are also involved in the phragmoplast formation. In moss and tobacco, myosin VIII was found to guide phragmoplast expansion possibly by linking its microtubules ends to the cortical division site with the use of actin filaments (Wu & Bezanilla, 2014). Moreover, myosin is believed to affect the dynamics and organization of actin through their movement along the microfilaments. In the triple and quadruple *Arabidopsis* mutants of myosin XI isoforms, thick and parallel bundles of actin in the leaf epidermis cells were exchanged for the thinner and disorganized ones, possibly by a lack of regular myosin movement, which in wild-type brings filaments together (Peremyslov et al., 2010; Ueda et al., 2010).

Myosins transport multiple different cargos within the cell, the main ones being organelles such as ER, Golgi, mitochondria or peroxisomes. Interestingly, various studies showed a low specificity of myosin isoforms towards their cargo, as loss of function of selected isoforms often resulted in decreased movement of more than one type of organelle (Peremyslov et al., 2008; Ueda et al., 2010).

Growing evidence suggests the existence of a cross-talk between kinesins and actin filaments, and myosins and microtubules. One example is a bi-functional kinesin KCH of various plant species, which contains actin- and microtubule-binding domains and most likely transports microfilaments along microtubules (Xu et al., 2007). Another example is myosin XI, which accumulates in the apical dome of growing protonemata, presumably co-existing with polymerizing plus-ends of microtubules before the accumulation of actin filaments in the same area (Furt et al., 2013; Nebenführ & Dixit, 2018). These examples emphasize the importance of motor proteins for the regulation of cytoskeleton dynamics, both as positive and negative effectors.

1.2.2 Organelles' function during meiosis

Another important aspect regarding meiotic division is the position of organelles during its course. In 1899, Fullmer observed that karyo- and cytokinesis are accompanied by a spatial rearrangement of cellular organelles (chondrion), such as mitochondria and plastids (Fullmer, 1899). Later studies showed that this rearrangement was not random but highly organized, potentially required for the equal inheritance of organelles by the dividing cells (Marquette, 1907, 1908; Michaelis, 1955). This mode of organelle segregation into daughter cells during cell division was termed "chondriokinesis". However, chondriokinesis is not only important for proper distribution of organelles, but it also prevents fusion of karyokinetic spindles, which is especially crucial in meiosis with simultaneous cytokinesis. Positioning organelles in the equatorial plane of the dividing cell provides a physical barrier and splits the cell into two compartments, with two separate chromosome sets on each side of the plate (Fig. 3). This particular localization of organelles and a proper arrangement of the microtubular cytoskeleton are believed to hinder the spindles from coming into contact and ensure a proper cell division (Brownfield et al., 2015; Tchórzewska, 2017; Marciniec et al., 2019).

The first classification of chondriokinesis was based on the organelles' arrangement during telophase I and metaphase I (Bakowski, 1938). Four main categories (and their combinations) were proposed: equatorial, neutral, capsular, and polar. Equatorial chondriokinesis is characterized by organelles forming aggregates on both sides of the metaphase I chromosome plate, which gradually disperse to create a band between nuclei in telophase I. Neutral type is observed when organelles are evenly dispersed in the cytoplasm and do not form any identifiable clusters. Capsular chondriokinesis occurs when organelles surround both nucleus and meiotic spindles from late prophase I to the end of cytokinesis. In polar type, organelles in metaphase I group on the opposite cell poles and remain there until the first cell division, upon which they redistribute in the cytoplasm (Tchórzewska, 2017).

In Arabidopsis, chondriokinesis is neutral and equatorial during meiotic telophase, which is characteristic for plants with simultaneous cytokinesis (Fig. 3). In this case, organelles are evenly distributed in the cytoplasm until anaphase I, during which they start moving to the equatorial plane to form a "plate" at telophase I. This organization persists throughout prophase II and metaphase II, and is referred to as the "organelle band" in various other publications. The organelle band changes into a cross-like structure during anaphase II, to separate the four nuclei in telophase II and to determine division plane for subsequent cytokinesis.

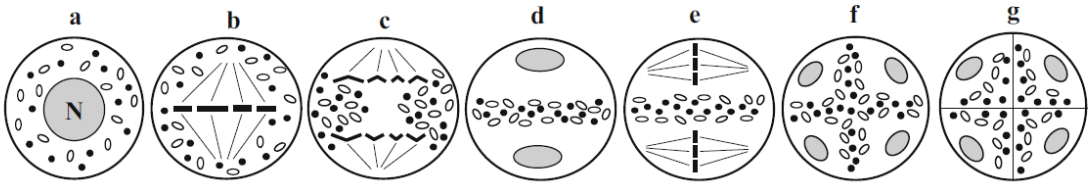

Figure 3 Neutral chondriokinesis equatorial during telophase in cells with simultaneous cytokinesis, such as *Arabidopsis*. *a* – prophase I, *b* – metaphase I, *c* – anaphase I, *d* – telophase I, *e* – anaphase II, *f* – early telophase II, *g* – late telophase II [modified from Tchórzewska, 2017].

Since mitochondria and plastids contain their own DNA, their localization in the cell during meiosis can be visualized by DAPI (4',6-diamidino-2-phenylindole) staining, simultaneously with chromosomal DNA. However, these organelles are not the only ones present in the plant cell during the meiotic division. Golgi apparatus (GA), endoplasmic reticulum (ER), plasma membrane (PM), vacuoles, and various vesicles are components of the endomembrane system, participating in the synthesis and transport of proteins, lipids, and polysaccharides within the cell (Morita & Shimada, 2014). Compounds are transported inside vesicles through two main pathways. The first one is the secretory pathway, which starts at the ER, and leads through GA cisternae to the final destination at the vacuole or PM. The second one is endocytosis, during which vesicles are formed by the PM around the extracellular molecule, and carried into an early endosome for subsequent sorting (Fan et al., 2015). There are few studies on the localization and behavior of endomembrane system components during plant meiotic divisions. The studies on morphology and dynamics of the plant endomembrane system using the GFP and its spectral variants were reviewed by Kim and Brandizzi (Kim & Brandizzi, 2014). Marker lines for cellular components, in which cellular markers are fused with four different fluorescent proteins at their N- or C-termini, have been developed and have since become available for interested scientists (Geldner et al., 2009). Additionally, confocal microscopy can be used for optical sectioning and subsequent 3-D reconstruction of the imaged organelle (Kutsuna & Hasezawa, 2002). Furthermore, transmission electron microscopy (TEM) proved helpful in studying the endomembrane system and vesicle trafficking (reviewed by Liu et al., 2021).

So far, the best-documented cases of the relationship between the endomembrane system and plant cell division display the role of this systems' components in cell plate formation. KNOLLE, the syntaxin required for the membrane fusion, and *KEULE*, encoding its interactor, Sec1 homolog, are partially functionally redundant and necessary for the plant cytokinesis. Their mutants possess incomplete cell walls, formed by fusion of vesicles carrying material for cell wall construction, and a subset of unbound vesicles in the cytoplasm (Assaad et al., 2001; Waizenegger et al., 2000). Inhibition of the vesicle

trafficking through e.g., the repression of NACK1 and NACK2 (kinesis-like proteins) leads to defective cytokinesis (Nishihama et al., 2002). High-resolution electron tomography, performed on endosperm mitosis, showed the abundance of Golgi-derived vesicles in the close vicinity of the spindles and the phragmoplast, highlighting their role in cell wall component delivery (Otegui et al., 2001). The use of Brefeldin A, the inhibitor of the secretory pathway, hinders the formation of the cell plate (Yasuhara et al., 1995; Yasuhara & Shibaoka, 2000). The endocytic marker FM4-64 was shown to be delivered directly to the developing cell plate in at least three plant species, suggesting that endocytosis, as well as the secretory pathway, participate in cell plate formation during plant cytokinesis (Dhonukshe et al., 2006).

Three lines from the 'wave line collection' were used to study the male meiotic mutant *jason* (Brownfield et al., 2015; Geldner et al., 2009). These authors studied the localization of the JASON protein in roots and meiocytes and compared it with the localization of vacuole, GA, and PM markers. Both Golgi- and PM-derived vesicles were observed predominantly in the organelle band; the Golgi signal was registered at the cell periphery. Interestingly, no signal from the tonoplast (vacuole's membrane) was found in meiotic cells (Fig. 4) (Brownfield et al., 2015).

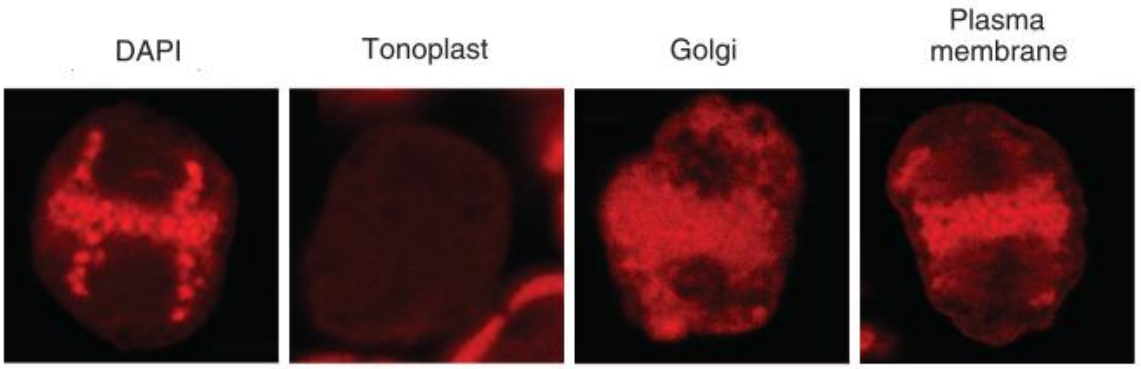

Figure 4 Localization of vacuole, Golgi, and plasma membrane proteins at metaphase II. DAPI staining shows the position of chromosomes and organelles forming the organelle band [modified from Brownfield et al., 2015].

1.2.3 Unreduced gamete formation

The normal product of male meiosis is a tetrad – four haploid cells enclosed within the callose wall that later undergo two rounds of mitotic divisions to generate fully developed haploid pollen grains. The term "unreduced gametes" in this context refers to a situation, in which meiotic defects lead to incorrect chromosome segregation and the formation of cells with a diploid (unreduced) chromosome set. If one mother cell gives rise to two haploid (reduced) daughter cells and one diploid (unreduced), such product is called a triad. If the only meiotic products are two diploid cells, such product is a dyad. Further

maturation of triads leads to the development of two haploid pollen grains and a diploid one, whereas dyads will develop into two diploid pollen grains. In addition to dyads and triads, other types of unreduced gametes, such as monads, pentads, hexads, or heptads, can be produced under certain conditions. A wide array of unreduced gametes was observed e.g., in *Brassica* interspecific hybrids exposed to cold temperatures (Mason et al., 2011). Yet another example is a polyad – a gamete with more than four nuclei – formed due to lagging chromosomes, such as the *spo-11-1-3* mutant (De Storme & Geelen, 2011).

In general, unreduced gametes result from meiotic nuclear restitution (also called: "meiotic nonreduction"). Failure at meiosis I is termed First Division Restitution (FDR). Homologous chromosome separation does not occur (or becomes reversed) after metaphase I, and the final meiotic products present an increased level of heterozygosity compared to the parental cell, due to recombination between non-sister chromatids during prophase I. The corresponding anomaly during meiosis II is named Second Division Restitution (SDR). Its meiotic products consist of sister chromatids with complete homozygosity. There is also an additional mechanism in *Lilium* interspecific hybrids called Indeterminate Meiotic Restitution (IMR), which leads to a mix of FDR and SDR gametes (Lim et al., 2001; Barba-Gonzalez et al., 2006).

The mutants of some genes that play a role in prophase I can produce a subset of viable unreduced gametes. One of them is the *SWITCH(SWI1)/DYAD* gene, which encodes a protein responsible for sister chromatid cohesion and recombination. The *swi1.2* mutant variant affects both male and female meiosis, although differently. In male meiosis, sister chromatid separation occurs already in meiosis I, hindering further meiotic progression, whereas female meiosis resembles a mitotic-like division, resulting in sterility. On the other hand, *swi1.1* allele, also known as the *dyad* mutant variant, affects only female gametophyte (Fig. 5) (Mercier et al., 2003; Mercier et al., 2001). Mutants produce only 1 to 10 seeds, and ca. 60% of them are triploid due to diploid ovules pollinated by haploid pollen (Ravi et al., 2008). Thus, *dyad* can be considered a mutant generating a low frequency of unreduced female gametes.

A larger proportion of unreduced gametes can be caused by cell cycle mutants. In Arabidopsis, the enzyme CDKA;1 (CYCLIN-DEPENDENT KINASE A1) and its activators, the cyclins of group A and B are responsible for cell cycle progression (Menges et al., 2005). Tight regulation of the cell cycle during meiosis is indispensable for the transition from meiosis I to meiosis II without passing an S-phase, as required for mitotic cycles. The levels of CDKA;1 need to be thoroughly controlled since a *cdka;1* knockout mutant is embryo lethal, while a hypomorphic mutant allele displays meiotic defects in female and male

meiosis, resulting in plant sterility (Dissmeyer et al., 2007). Mutations in genes encoding cyclins lead to the production of viable, unreduced gametes. One cyclin A gene is *CYCA1;2/TAM* (*TARDY ASYNCHRONOUS MEIOSIS*) (Magnard et al., 2001; Y. Wang et al., 2004). Homozygous null mutants produce mostly dyads during male meiosis and up to 30% of dyads during female meiosis, because most meiocytes cannot enter meiosis II and become arrested after the segregation of homologous chromosomes (Fig. 5). A point mutation of the same gene leads to hypomorphic activity of the cyclin, and to a delay of the cell cycle progression resulting in more haploid spores in addition to dyads. Another protein required for the transition into meiosis II is *OSD1* (*OMISSION OF SECOND DIVISION 1*), despite its yet unclear function. Meiocytes of the *osd1* mutant fail to enter the second meiotic division, giving rise to 100% of dyads as male and ~85% as female meiotic products (Fig. 5). These unreduced gametes are viable and produce polyploid offspring (D'Erfurth et al., 2009).

The documented cases on cytokinesis defects, which lead to the formation of unreduced gametes, involve the incorrect arrangement of RMAs. Such microtubular disorganization is found in the final stages of meiosis II in the *tetraspore (tes)/stud* mutant and prevents cytokinesis, yielding four nuclei in a common cytoplasm. The TES/STUD protein is predicted to be a kinesin based on homology to the tobacco NACK proteins, which are involved in the positive regulation of cell plate expansion through MAP (mitogen-activated protein) kinase cascade phosphorylation (Nishihama et al., 2002). The final meiotic product of the *tes/stud* mutant is a cell containing all four nuclei, some of which fuse with each other before the subsequent pollen mitotic division, and some complete their development into functional tetraploid pollen (Fig. 5). Interestingly, only RMAs seem to be defected and not spindles. Therefore, two rounds of mitotic divisions during pollen development occur seamlessly and may lead to the formation of functional sperm cells. Progenies of self-fertilized *tes/stud* mutants are thus a population of various ploidy levels, ranging from triploid to pentaploid (Spielman et al., 1997; Yang et al., 2003). A more severe phenotype can be observed in the mutant of the MAP kinase, MPK4. Since MAPK cascade is required for the control of plant cytokinesis, the homozygous *mpk4* mutant exhibits incomplete cell wall formation and enlarged, multinuclear cells, and on the organismic level: dwarfism, retarded root growth, meager flower development and very limited seed set (Kosetsu et al., 2010).

Defects in spindle organization may also lead to incorrect chromosome segregation and unreduced gamete formation. ATK1 is a putative kinesin, and its disruption results in a broad, multi-axial spindle during the first meiotic division, followed by abnormal

chromosome alignment in metaphase II and the occurrence of multiple spindles. *atk1-1* produces various microspores, which may contain any number of nuclei between three and ten. Thus, only few microspores matures into a viable pollen, rendering *atk1-1* plants largely infertile (Chen et al., 2002).

In Arabidopsis, cytokinesis happens simultaneously after the second division, so all four chromosome sets are within the cytoplasm of one cell. Therefore, a separate and perpendicular arrangement of both metaphase II spindles is necessary to ensure that segregation of chromosomes sets will not interfere with each other. The organelle band provides a physical barrier between the four chromosome sets. Two male meiotic mutants: *atps1* (*Arabidopsis parallel spindle 1*) and *jason* have similar phenotypes, manifested in the formation of tetrads, triads and dyads in different ratios, due to their metaphase II spindles displaying either parallel, fused, or tripolar orientation (Fig. 5). The arrangement of spindles is random, probably caused by loss of the organelle band in prometaphase II (*jason*) or metaphase II (*atps1*). However, they act on different genetic pathways, as *atps1;jason* double mutant shows an even stronger phenotype than the single mutants (Brownfield et al., 2015).

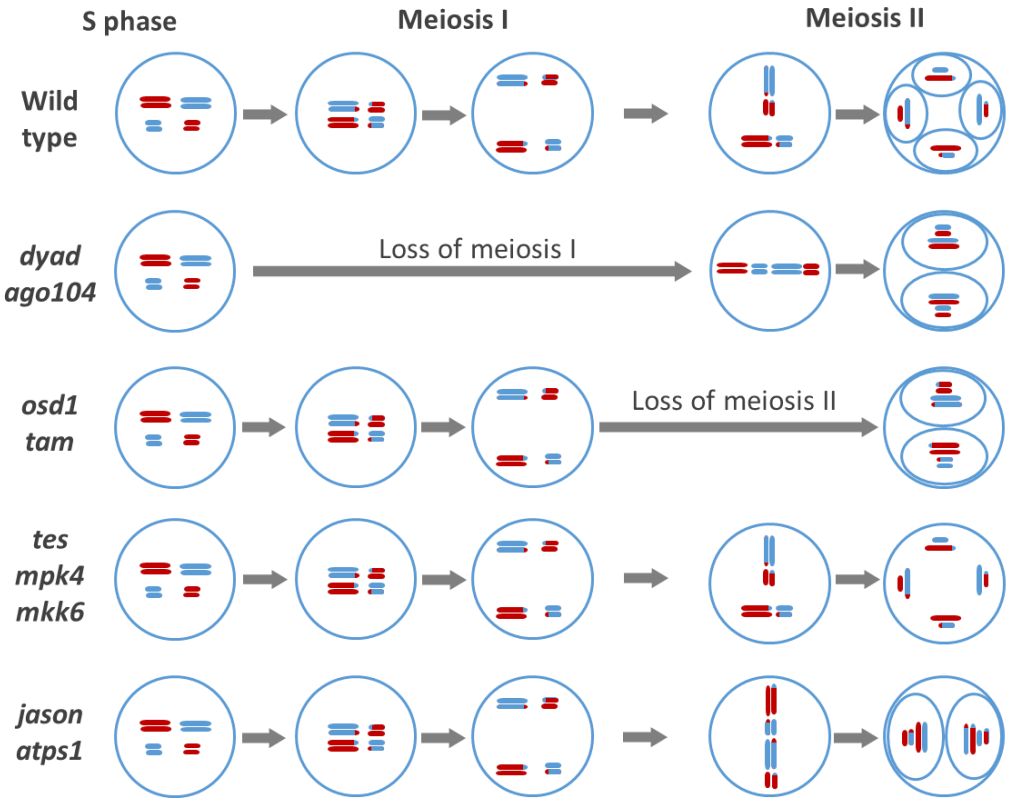

Figure 5 Examples of unreduced gamete formation [modified from Brownfield & Köhler, 2011].

Since this dissertation is focused predominantly on the *jason* mutant, JASON will be described in more detail in the next subchapter.

1.2.4 The meiotic mutant *jason*

JASON (At1g06660) was identified as a meiotic gene through ethyl methanesulfonate mutagenesis (EMS) on the Arabidopsis Landsberg *erecta (Ler)* ecotype (Erilova et al., 2009). EMS treatment generated a premature STOP codon in the fifth exon at position +1960 (C -> T), and this allele was numbered as *jas-1*. Three further alleles in the Columbia (Col) accession were found in T-DNA insertion libraries, among which *jas-3* (SAIL_813_H03) is the most commonly used one (Erilova et al., 2009).

The JASON protein has no domains of known functions, but its C-terminus domain is highly conserved in plants. The only related protein is the JAS-LIKE protein (At2g30820), which shows 64% similarity, but has a broader expression pattern. *JASON* is expressed mostly during reproductive development, consistent with its function during meiosis (Erilova et al., 2009). However, when fused with a green fluorescent protein (GFP) at the C-terminus, JASON was found in the roots of 4-6 days old seedlings, predominantly in the endomembrane system. Also, in meiocytes, JASON co-localizes with Golgi- and plasma membrane-derived vesicles in the organelle band (Brownfield et al., 2015).

An important characteristic of this gene is an alternative translation initiation site, from which a shorter form of JASON protein is produced. By mutating two ATGs at the N-terminus of the *JASON* gene sequence, the transcript was translated from ATG at the position +85, thus creating short*JASON* (Cabout et al., 2017), while a modification of ATG at the position +85 ensured that *JASON* is expressed only in the full, long-form (long*JASON*), enabling the comparison between the two forms. Both forms were fused with GFP and expressed under the native *JASON* promoter. Their subcellular localization in roots showed that the long*JAS* did not co-localize with the plasma membrane marker, whereas short*JAS* did not colocalize with the Golgi apparatus. Moreover, both forms were detected in meiocytes, but the shorter version was present predominantly in the organelle band, while the longer version appeared in other parts of the cell as well, suggesting that this form is more important for JASON function during meiosis (Cabout et al., 2017).

jason is a male meiotic mutant (Erilova et al., 2009). The *jason* phenotype, without organelle band in prometaphase II, enables the spindles to move freely in the cytoplasm with various abnormal orientations while keeping their structure unaffected. As a result, the distance between separating chromosome sets becomes shorter, sometimes leading

to intermingling, which disturbs correct segregation. Therefore, *jason* produces dyads and triads (Fig. 6), as well as normal tetrads (if parallel spindle orientation is followed by flawless cytokinesis). The proportion of the three types of gametes is roughly 33% each, and thus the ratio between haploid and diploid pollen should be about 2:1. Since the haploid ovule can be pollinated by either 1n or 2n pollen, *jason* produces both diploid and triploid seeds. The latter are lethal or give rise to triploid plants, depending on the ecotype of the *jason* mutant (Erilova et al., 2009; Brownfield et al., 2015).

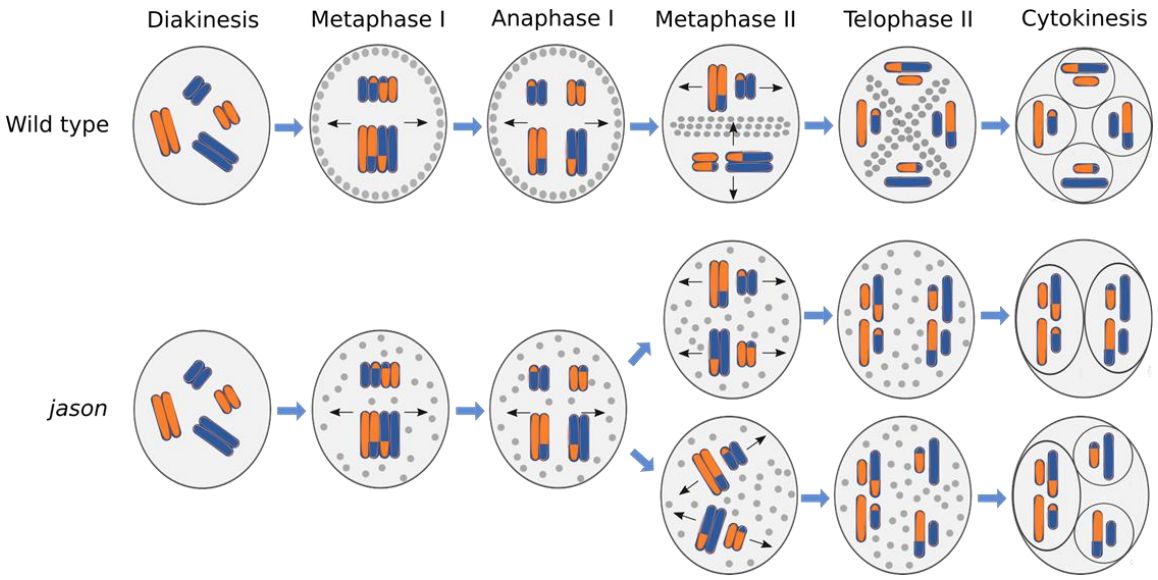

Figure 6 Simplified scheme depicting possibilities of unreduced gamete formation in the *jason* mutant. The meiotic products from top to bottom are tetrad, dyad, and triad. Grey dots represent organelles.

1.3 Aim of the thesis

From the evolutionary perspective, polyploidization is a major drive for plant diversity and speciation. It also confers various benefits, which, if utilized in breeding agriculturally-important plants, could improve desired crop features and eliminate (or prevent expression of) undesirable alleles by combining related species. The most common natural way of generating polyploids occurs through unreduced gametes, which carry the somatic DNA content. Unreduced gametes are generated after the meiotic chromosome segregation fails, e.g., by malfunctioning of cell cycle progression or cytokinesis defects. However, the genetic basis of most of these pathways is not fully understood.

One of the *Arabidopsis* male meiotic mutants, *jason*, produces a large subset of unreduced gametes through loss of the organelle band in metaphase II and consequently a random organization of meiotic spindles. JAS is co-localized with markers for the Golgi and the plasma membrane in the organelle band at metaphase II, indicating that a subset of the

Golgi apparatus and endomembrane vesicles are components of the organelle band. Maintaining the organelle band relies on the function of the JAS protein. To characterize the mechanism of the JAS function, a suppressor screen was performed to find mutants that form reduced gametes in the presence of the *jas* mutation. Further analysis of identified genes will elucidate novel genetic pathways that govern the formation of unreduced gametes and influence chromosome segregation during the second meiotic division. Understanding the intricacies of mechanisms leading to the formation of polyploids provides an immense agricultural potential, which is indispensable in times of a worldwide climate crisis.

2. Materials and methods

2.1 Plant material and propagation

Seeds of *Arabidopsis* T-DNA insertional mutants: *peleus* (SALK_209914C), *jas-3* (SAIL_813_H03), *atps1-1* (SALK_078818), *ubq-like1* (SALK_072154), *kiwi* (SAIL_693_F01), and *ap4b* (SAIL_796_A10) were obtained from the Nottingham Arabidopsis Stock Centre (NASC). The *jas-1* allele in the L*er* accession and the tubulin-GFP were kindly provided by Prof. Claudia Köhler. The seeds from the wave line collection are listed in the Supplemental table 1. The wild-type *Arabidopsis thaliana* ecotype used was Col-0, unless stated otherwise.

Seeds were stratified for 2 days at 4°C, in water and darkness, before being sowed on the soil. To sow them on MS plates (½MS, 1% sucrose, 0.8% plant agar), seeds were surface-sterilized with 70% (v/v) ethanol for 10 minutes and rinsed twice with 98% ethanol. Seeds were kept on plates for two weeks, before being replanted into soil.

Plants were propagated in a phytotron with 16 h light / 8 h dark photoperiod. Temperature in LD rooms was set to 22°C for day and 19°C for night, light intensity was 115 µmol·m-2·s-1 and humidity was at 70%.

2.2 Bacterial material and propagation

The *Escherichia coli* strains DH5α and TOP10, as well as *Agrobacterium tumefaciens* GV3101 were obtained from Prof. Andreas Houben Group (IPK Gatersleben).

E.coli and *Agrobacterium* upon transformation were plated on a Petri dish with solid LB medium (0.8% of micro-agar) containing adequate antibiotics. Liquid cultures were prepared by dipping a tip in the bacterial colony and transferring it to 5 ml of standard liquid LB medium with antibiotics. 500 µl of each liquid culture was mixed with 500 µl of 50% glycerol and stored in -80°C as a stock. For growth, *E.coli* strains were kept in an incubator (plates) or a shaking incubator (liquid cultures) at 37°C for 17 h. *Agrobacterium* was kept in respective incubators at 28°C for 24 h.

2.3 Plant material extraction

DNA for genotyping was extracted from fresh or frozen plant material using Edwards method (200 mM Tris-HCl pH 7.5, 250 mM NaCl, 25 mM EDTA, 0.5% SDS) (Edwards et al., 1991 with modification). Plant material was disrupted using polypropylene pestles or steel balls and Retsch Mill MM400. Upon dissolving in water, DNA pellets were stored at 4°C or -20°C, for short- or long-term storage respectively. High quality DNA was extracted from

plant material snap-frozen in liquid nitrogen using a DNeasy® Plant Mini Kit from Qiagen, according to the provided protocol. DNA was stored at -20°C.

2.4 Phenotyping techniques

2.4.1 Pollen size analysis

2-3 open flowers per plant were dipped in a drop of 1x PBS with 0.1% of Triton X-100. The pollen suspension was observed under 10x magnification using an optical microscope (SMZ1500 Nikon). Pollen size was measured using ImageJ, where the 'Area' category reflects the 2-D area of a pollen grain.

2.4.2 Seed set analysis

Nearly mature siliques of at least 6 weeks old plants were taped to a microscopic slide and gently opened with tweezers. Seeds were counted according to their size and color, with uniformly small, yellow, diploid Col-0 seeds as reference. Viable triploid seeds were bigger, often still green, aborted seeds were shrunk and black.

2.4.3 Root length measurement

Seeds were surface-sterilized and sowed on ½ MS plates supplemented with 1% sucrose and 1% plant agar. Petri dishes were placed at 4°C under cover for five days in order to ensure full stratification and synchronized germination. Following stratification, plates were transferred to an LD room and placed vertically. To check the germination efficiency, after 2 days of growth fully developed seedlings with roots and cotyledons were counted and compared with the total number of sowed seeds. After 6 days of growth, plates were photographed and each root was measured using ImageJ.

2.5 Cytological techniques

2.5.1 Tetrad analysis

Whole inflorescence from ca. 5 weeks old plants were fixed in Carnoy's fixative (ethanol:acetic acid, 3:1) for 4h at RT and stored at 4°C in fresh fixative until use. Fixed buds were washed twice with 1x PBS and viewed under a stereoscope. Flower buds were separated from the inflorescence, anthers were taken out from the buds and subsequently dissected. 0.1-0.2% toluidine blue solution was used to stain meiotic products, which were viewed at 10x magnification.

2.5.2 Chromosome spreading

Inflorescences were prepared as for tetrad formation analysis, but separated flower buds were digested in 10mM sodium citrate buffer, pH 4.5 in 0.3% cellulase and 0.3% pectinase for 20 min at 37°C. Buds were then washed three times in 1x PBS and viewed under stereoscope. Anthers were dissected from the buds, macerated into a homogeneous

suspension using sharp tweezers, and then shortly incubated in 60% acetic acid on a hot plate, before being washed with fresh Carnoy's fixative. Cells were air dried and covered with 2 µm/ml DAPI (Roth®) in antifade solution. Slides were viewed under 63x magnification using a Zeiss Axioplan 2 Imaging Fluorescent Microscope.

2.6 Microscopic imaging

2.6.1 Whole anther analysis

Inflorescences were prepared as for tetrad formation analysis. Flower buds were dissected to isolate intact anthers, which were incubated in DAPI buffer (0.4 µl of 2 µg/ml DAPI in 1x PBS + 0.15% Triton X-100) for 20 min and later covered with cover slip. Anthers were imaged using a confocal microscope (Zeiss LSM780) at 40x magnification. The excitation channel was chosen depending on the type of material – DAPI channel for organelle band imaging, EGFP for imaging of meiotic spindles, and mCherry for imaging of endomembrane system marker lines.

2.6.2 Visualizing cellular organelles

Inflorescences undergoing meiosis were fixed in methanol for 20 min at -20°C and washed thrice in 1x PBS. Anthers were subsequently removed from the buds and chopped using a fine needle on a slide and stained with Golgi/ER Staining Kit – Cytopainter (Abcam) according to the protocol for live, adherent cells. Organelles were imaged using a confocal microscope with DAPI channel for nuclei, FITC channel for Golgi Apparatus and Texas Red for Endoplasmic Reticulum.

2.6.3 Visualizing cytoskeleton components

In order to visualize tubulin in meiotic cells, seeds of a tubulin marker line were sowed on MS plates and 7 days old seedling roots were inspected using a confocal microscope to check the strength of the signal. Positive plants were transferred to soil and grown until flowering. Inflorescences undergoing meiosis were fixed in methanol for 20 min at -20°C and anthers were subsequently removed from flower buds. Intact anthers were treated with DAPI buffer for 20 min at RT and viewed under confocal microscope using the EGFP channel.

In order to visualize actin in meiotic cells, inflorescences undergoing meiosis were fixed in fresh 4% PFA for 20 min at RT and anthers were subsequently removed from the buds. Intact anthers were stained with an F-actin Staining Kit – Green Fluorescence – Cytopainter kit from Abcam for up to 1 h at RT and stained with DAPI. Actin was visualized under a confocal microscope in the FITC channel.

2.7 Genetic techniques

2.7.1 Molecular cloning

SnapeGene® Viewer was used to visualize gene and plasmid sequences, as well as to check for enzyme restriction sites. Restriction enzymes from Thermo Fisher Scientific and NEB were used to cut PCR products and plasmids. PCR for genotyping was done using 2x Taq Master Mix from Vazyme. PCR for cloning was done using Phusion™ High-Fidelity DNA Polymerase from Thermo Fisher Scientific or Phanta Max Super-Fidelity DNA Polymerase from Vazyme. Working concentration of primers was 10 µM. Reaction was performed in the Eppendorf Mastercycler, with temperatures of consecutive steps adjusted to polymerase manufacturer's guidelines. PCR products were purified from 1% agarose gel using scalpel and purified using FastPure Gel DNA Extraction Mini Kit from Vazyme. All steps were carried out according to provided protocol and DNA concentration was measured on NanoDrop™. Ligation was done using T4 ligase from Thermo Fisher Scientific. In-fusion cloning was carried out using ClonExpress Ultra One Step Cloning kit from Vazyme according to manufacturer's protocol. Plasmids were extracted from 5 ml of overnight culture using FastPure Plasmid Mini Kit from Vazyme. All steps were carried out according to provided protocol. Plasmid concentration and quality was measured using NanoDrop™ One from Thermo Fisher Scientific. Primers used in this study were synthesized by Eurofins Genomics Germany GmbH. The list of primers is provided in the Supplemental table 2.

2.7.2 DNA library construction

4 µg of high-quality DNA was sonicated using Bioruptor® from Diagenode into 200-300 bp fragments and the library was prepared according to the protocol of VAHTS Universal DNA Library Prep Kit for Illumina® from Vazyme. Quantity of the libraries was measured on Qubit Fluorometer from Thermo Fisher Scientific and quality was measured on the Agilent 2100 Bioanalyzer from Agilent Technologies. Libraries were sequenced at Novogene, UK and at least 15 million reads were produced for each sample. Reads were mapped to TAIR10 Col-0 genomes with HISAT2 (Kim et al., 2019).

2.7.3 GUS staining

Ca. 1.5 kb of promoter region of the gene of interest was cloned into destination vector carrying the GUS gene (pGWB533) and transformed into wild-type Col-0. Positive transformants were selected on ½ MS plates with hygromycin. Various organs were collected at different points of development, stained with GUS staining solution (50 mM phosphate buffer, 10 mM EDTA, 0.1% Triton X-100, 1 mM potassium ferricyanide III, 1 mM

potassium ferrocyanide II, 1 mg/ml X-Gluc), incubated over night at 37°C in the dark and washed with 70% ethanol until staining is resolved.

2.8 Microbiological techniques

2.8.1 Bacterial transformation

E. coli was transformed by incubating bacteria with plasmid for 30 min on ice, then transferring the tube to 42°C for 1.5 min and subsequently to ice for another 2 min. After adding LB buffer, *E.coli* was incubated for an hour in a shaker set at 37°C and 200 rpm. Regenerated bacteria were gently centrifuged and, upon resuspending in a smaller volume, plated on a selective plate using glass beads. *Agrobacterium* was transformed using the heat shock method as well, although upon adding plasmid to bacteria the tube was submerged in liquid nitrogen for 1 min, and then transferred to 37°C for 5 min. Regeneration was carried out for 3 h at 28°C and shaking at 200 rpm.

2.8.2 Plant transformation

Ca. 5 weeks old plants were transformed with *Agrobacterium* using the floral dip method (Bent & Clough, 1998). Overnight bacterial cultures were centrifuged and resuspended in buffer (½ MS, 50 g/L sucrose) and upon adding 200-250 µl/L (v/v) Silwet L-77 from PlantMedia, buds were submerged in this bacterial suspension for ca. 1 min. Transformed plants were kept in darkness overnight and then transferred to LD cultivation room. Seeds of T1 generation were selected on MS plates supplemented with adequate antibiotics.

3. Results

3.1 Phenotypic analysis of *jason* suppressors

3.1.1 *jason* suppressors have a wild-type-like phenotype

EMS mutagenesis of the *jas-3* mutant caused random point mutations throughout the genome, resulting in a variety of phenotypes in subsequent generations. Special attention was given to plants, which exhibited wild-type phenotype despite containing mutated *JASON* gene. Therefore, the M2 population was screened doubly. Firstly, the seed set of mature plants was assessed in order to find mutants with no more than 10% of abnormal, i.e. bigger or collapsed seeds per silique; and secondly, the pollen size of the selected plants was measured to confirm the predominance of haploid pollen grains (Fig. 7). Together both features suggest that the meiotic defects of *jason* were restored to a great extent by the second, unknown mutation. Seeds of such double mutant plants were collected, numbered, and stored as the original *jason* suppressor mutants.

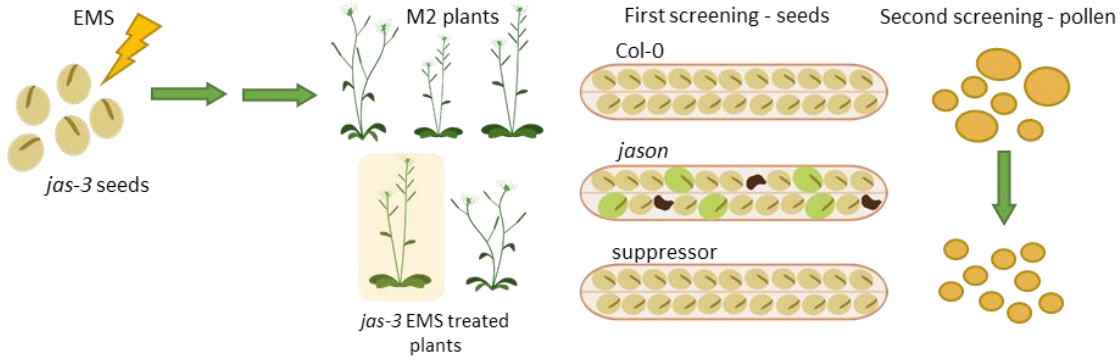

Figure 7 Scheme depicting generation and phenotypic effects of *jason* suppressors.

Several *jason* suppressors were found, varying in the level of phenotype restoration. For the purpose of this project, three of them received special attention and a name after the Argonauts from the Greek mythology: *peleus*, *idas*, and *ankaios*.

Pollen size analysis clearly showed that all three double mutants produced predominantly small, haploid, viable pollen (Fig. 8A). However, since mature pollen is not a direct product of meiosis, as it is generated after two mitotic divisions of microspores' nuclei, a tetrad analysis was performed to validate the presumed reason for this finding. Indeed, each double mutant produced more tetrads than *jason* alone (*peleus*: 80.8%, *idas*: 92%, *ankaios*: 61.1%), although none of them fully suppressed the formation of dyads (*peleus*: 2.4%, *idas*: 1.3%, *ankaios*: 6.1%) (Fig. 8B). Seed set analysis further reaffirmed strong,

although incomplete suppressing abilities of *peleus*, *idas*, and *ankaios*, as all three mutants produced less than 10% of abnormal seeds (Table 1).

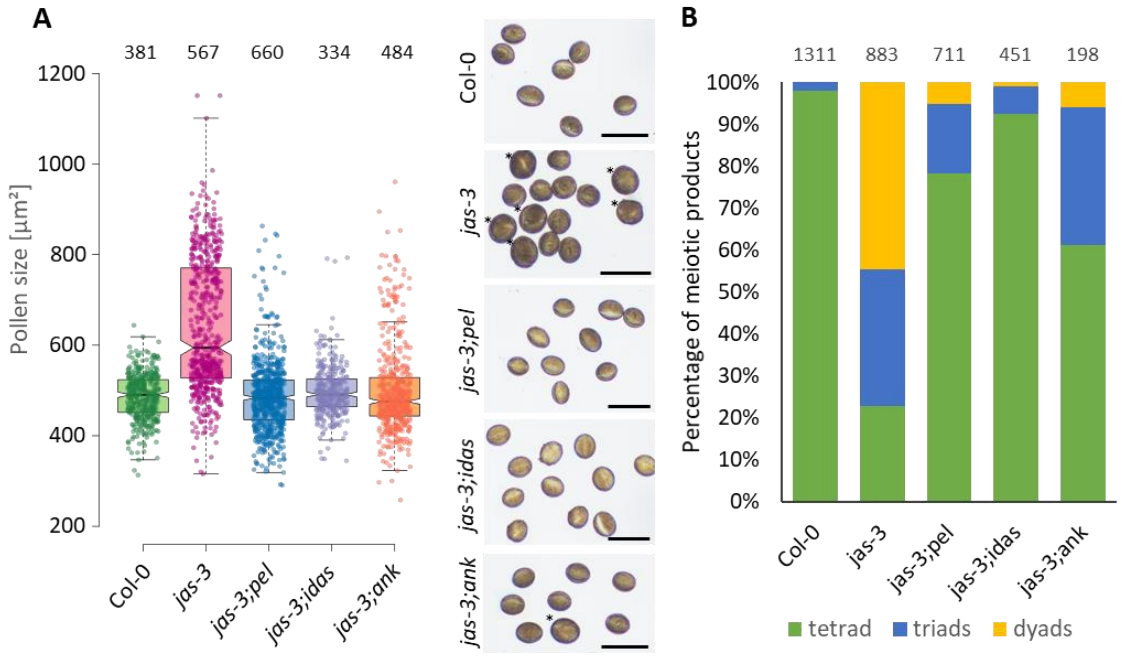

Figure 8 Phenotypic analysis of *jason* suppressors. (A) Distribution of pollen size in *the jason* suppressor double mutants. Asterisks mark the diploid pollen grains. Scale is 50 µm. (B) Percentage of meiotic products in *jason* suppressor lines compared to wild-type and *jason*.

Table 1 Seed set analysis of Col-0, *jason*, and *jason* suppressors. ("Abnormal" means big, viable or collapsed seeds).

Analyzed line	% of abnormal seeds	Average seeds set per silique	Total seeds counted	Standard deviation
Col-0	0	46	273	0
jas-3	37	39	322	0.07
jas-3;pel	4	40	263	0.01
jas-3;idas	2	50	403	0.02
jas-3;ank	7	41	205	0.03

3.1.2 *jason* suppressors contain more organelles in the metaphase II organelle band

The incomplete suppression of *jason* meiotic phenotype led to the question if the organelle band was restored in the double mutants, as a reconstitution of correct organelles' position would be expected to yield 100% of tetrads. All three double mutants seemed to display a special enrichment of organelles within the organelle band, with *jas;ank* showing the highest abundance of organelle signals in-between chromosomes (Fig. 9). However, the band structure was never as distinct as in the wild-type and the

organelles could be found scattered throughout the entire cytoplasm, often close to the chromosomes. The same was observed regarding the "organelle ring" in metaphase I, which was not prominent in any mutant (Fig. 9).

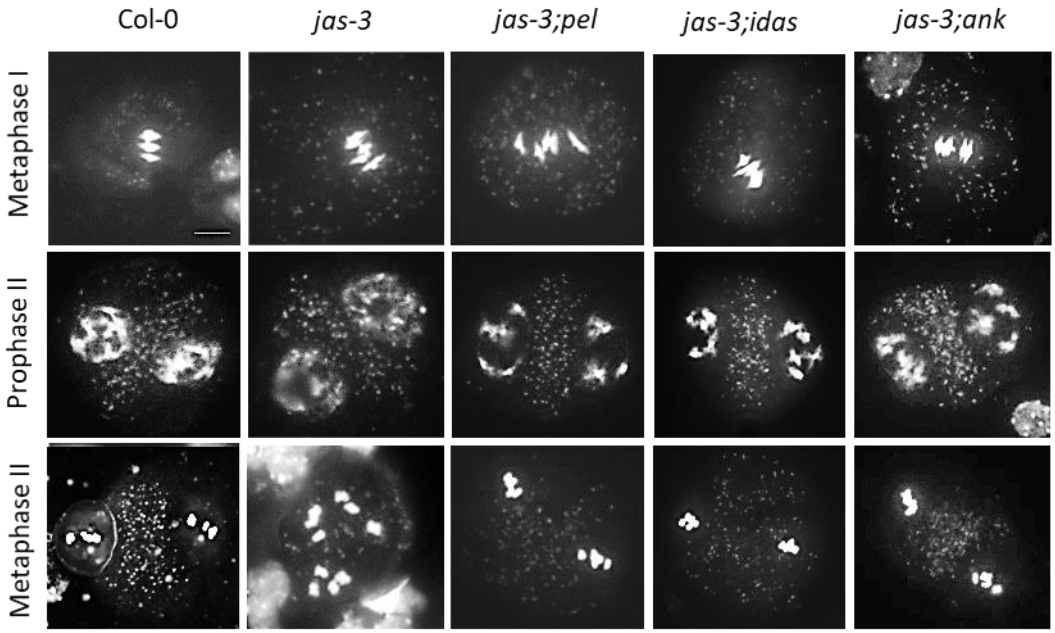

Figure 9 Cytological analysis of *jason* suppressors. Metaphase I and metaphase II were chosen as the stages most important for the mutants' meiotic phenotype. Prophase II was selected to portray the stage, in which no apparent differences can be spotted between the mutants and wild-type. Scale bar is 10 µm for all images.

The finding that neither of the suppressors fully restored the organelle band at metaphase II raises the question what other mechanisms, independently of the full organelle band restoration, could cause the correct meiotic progression and significantly increase tetrad formation in the presence of the *JASON* mutation. To solve this issue, *peleus* was chosen for the further in-depth analysis.

3.1.3 *peleus* suppresses *atps1* meiotic phenotype

Since, *peleus* suppresses the *jason* mutant phenotype, it was interesting to know whether *peleus* could suppress *atps1*, another meiotic mutant characterized by the abnormal spindle positioning. *ATPS1* (*ARABIDOPSIS THALIANA PARALLEL SPINDLE 1*), as mentioned in the introduction, is a gene involved in the diploid gamete formation through unknown mechanisms (D'Erfurth et al., 2008). Mutating this gene causes loss of the organelle band at metaphase II, which results in uncontrolled spindle movement, a phenotype resembling *jason*, although caused by a different mechanism (Brownfield et al., 2015).

The *atps1;pel* double mutant was generated by crossing *jas;pel* with *atps1* and selecting relevant plants in the second generation. The double mutant showed a decreased number

of diploid pollen and only 15.7% of triads and dyads compared to ~70% of abnormal meiotic products in *atps1* itself (Fig. 10A). The occurrence of 84.3% of tetrads in the double mutant strongly resembled the phenotype of suppressed *jason* (Fig. 10B), indicating that *peleus* suppressed *atps1* as well.

In the *atps1* mutant, the organelle band is lost at metaphase II, and not already at prometaphase II as in *jason*, and the phenotype is stronger than in *jason*, as it produces more dyads and more frequently shows touching chromosome sets at metaphase II (Brownfield et al., 2015). In my study, the strength of *atps1* and *jason* mutants was comparable, with both of them generating only up to 33% of tetrads and often showing metaphase II chromosome sets being very close together (Fig. 10B and C). The biggest difference was observed for the *atps1;pel* double mutant, which in contrast to *jas;pel*, in metaphase II meiocytes sometimes also contained intermingled chromosomes (Fig. 10D), confirming the higher impact of the *atps1* mutation on meiotic spindle organization. Nevertheless, the *atps1,pel* double mutant produced predominantly tetrads.

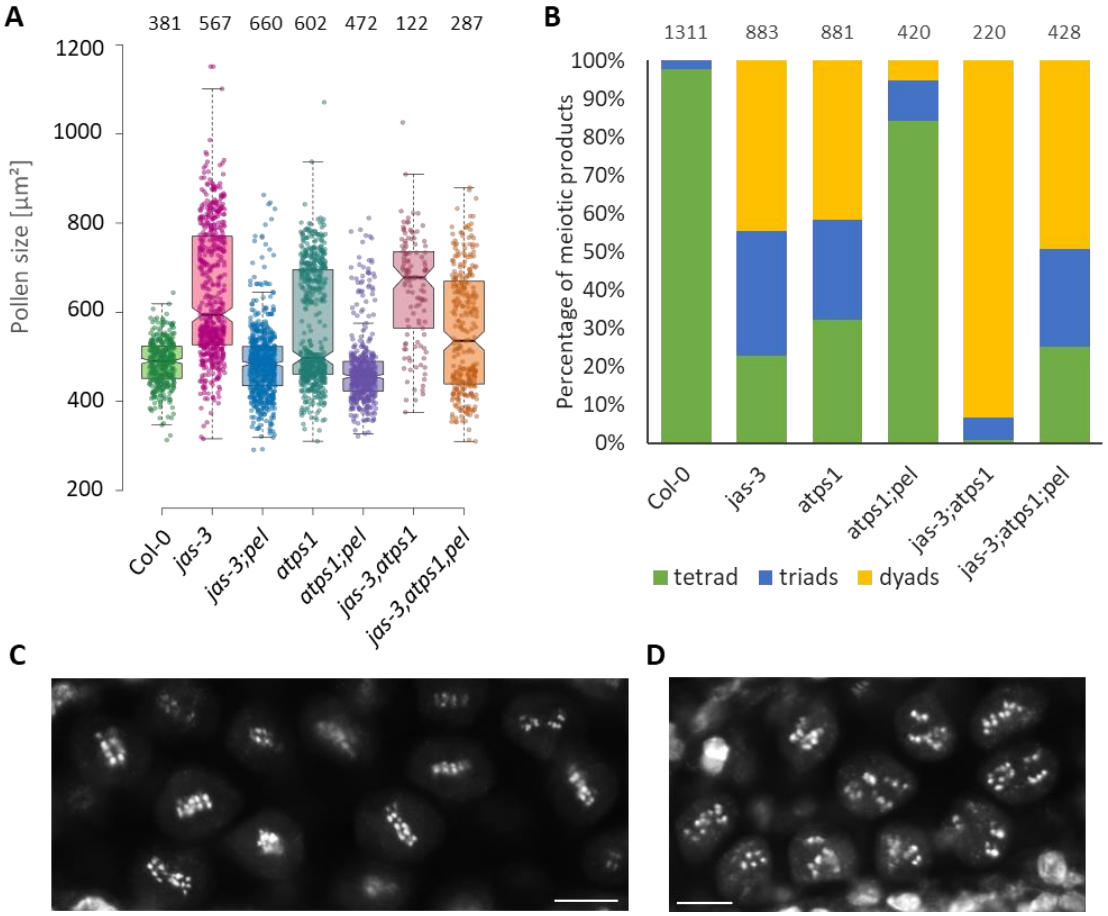

Figure 20 Phenotype of *peleus* crosses with the *atps1* mutant. (A) Pollen size of *atps1;pel*, *jas-3;atps1*, and *jas-3;atps1;pel*. (B) Tetrad formation of *atps1;pel*, *jas-3;atps1*, and *jas-3;atps1;pel*. (C) Anaphase II meiocytes of *atps1*. (D) Anaphase II meiocytes of *atps1;pel*. Scale bars are 10 µm.

Upon finding, that *peleus* suppresses *atps1* as well as *jas*, a triple *jas;atps1;pel* mutant was generated to assess the extent of *peleus'* suppressing capability, considering the fact that *atps1* and *jason* produced unreduced gametes through different genetic pathways. The *jas;atps1* double mutant served as a control. According to Brownfield et al. (2015) the double mutant *jas;atps1* displays an additive phenotype. Indeed, the *jas;atps1* double mutant produced only 1% of tetrads and almost 95% of dyads (Fig. 10B). Due to its severity, this phenotype could not be fully suppressed by introducing *peleus* into the double mutant. Albeit, the number of dyads was decreased by ca. 45%, while the number of tetrads was increased by ca. 25%, resulting in a similar phenotype as *jas* and *atps1* mutants (Fig. 10B). Preliminary analysis of organelle band formation showed intermingled chromosomes in some metaphase II meiocytes, which was not observed in the double mutants, emphasizing that *peleus* cannot fully reverse the strong meiotic defects of *jas;atps1*.

3.2 Elucidating mechanisms of unreduced gamete suppression by *peleus*

3.2.1 *peleus* partially restores the organelle band in the *jason* mutant

Chromosome spreads suggested that *peleus* may restore the organelle band to some extent, although not up to the wild-type level. However, during chromosome spreading cytoplasm is removed, possibly affecting cell component positioning. For this reason, the cytological analysis was revisited, but this time by imaging meiocytes in the whole anthers, which preserves the natural position of cellular components.

This method gave much clearer results than the chromosome spread and the organelle band in metaphase II of the double mutant seemed to be less disorganized than that of the *jas* single mutant. The organelles were often correctly located between the two chromosome sets, not scattered around the cell periphery, and they rarely touched the chromosomes, although the structure of organelle band was never fully wild-type-like. This type of organelle band was called "partial", in contrast to wild-type's "complete" organelle band (without "leakage" of signal in the cytoplasm around chromosomes or near the cell periphery), and *jason*'s "absent" type (no organized structure visible, organelles scattered throughout the cytosol) (Fig. 11A).

Counting the number of metaphase II organelle band types in different mutant meiocytes revealed that no mutant cell contained complete organelle band, which in contrast appeared in all wild-type meiocytes. Instead, organelle bands in both mutants were either partial or absent. However, the number of partially restored organelle bands in *jas;pel* was more than 40% higher than in *jas*, i.e. reaching almost 60% (Fig. 11B). Furthermore,

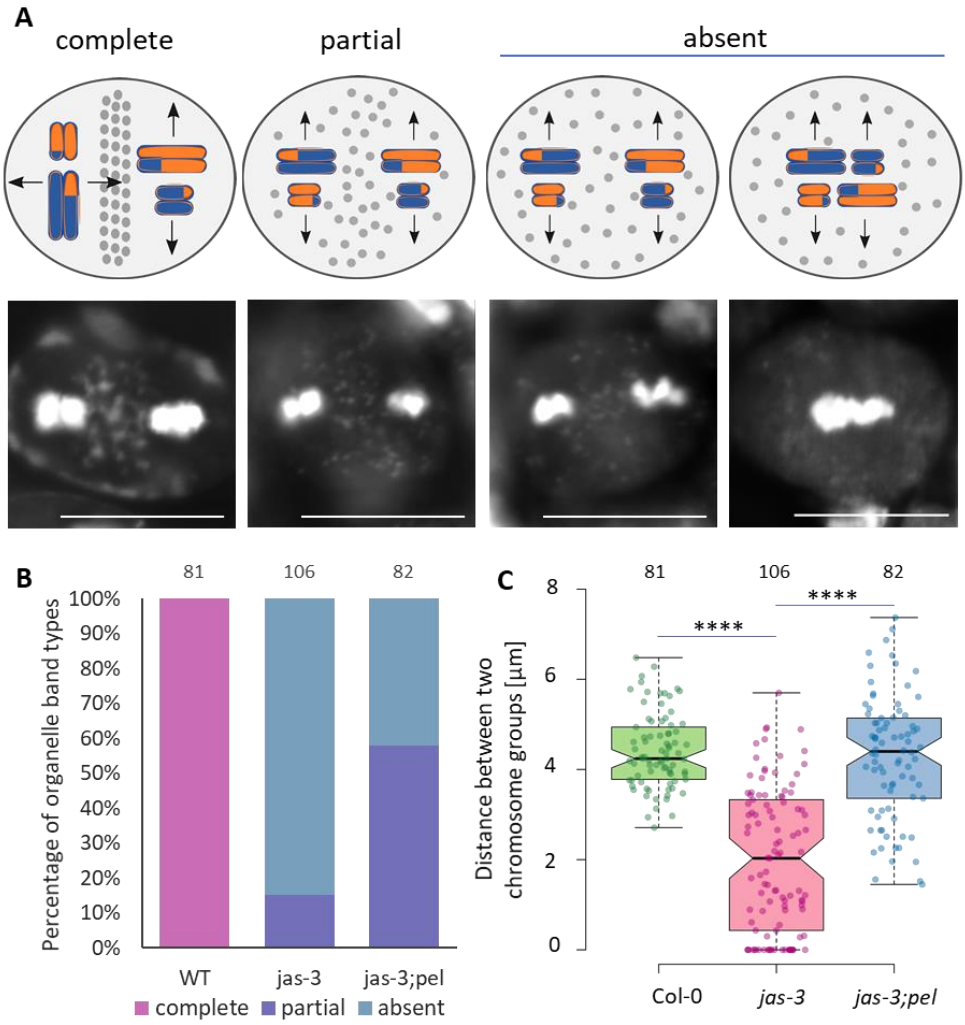

Figure 11 *peleus* suppresses the *jason* mutant phenotype. (A) Schemes depicting three types of organelle band and the corresponding images of metaphase II meiocytes. Scale bar is 10 µm. (B) Percentage of each metaphase II organelle band type in different genetic background. (C) Box plot showing distances between two chromosome sets measured in metaphase II meiocytes. *P* value indicated by asterisks (**** < 0.0001).

many *jas* metaphase II meiocytes displayed minimal distance between chromosome sets. This was never observed in the *jas;pel* double mutant. All metaphase II meiocytes of *jas;pel* contained fully separated chromosome sets, although occasionally the distance between them was shorter than in wild-type (Fig. 11C). Nevertheless, there was no statistically significant difference in the distance of chromosome sets between wild-type and *jas;pel* ($p = 0.091$).

The distance of chromosome sets explains the substantial increase in tetrads in the *jas;pel* mutant. Even though up to 40% of metaphase II meiocytes did not contain a partial organelle band, the chromosome sets in these cells were fully separated from each other, which in many cases enabled their correct segregation into four daughter cells. Therefore,

80% tetrads in the double mutant result from partial organelle band recovery and, in the case of sporadic absence of partial physical barrier, from normal sister chromatid separation due to sufficient distance between chromosome sets.

However, the mechanism(s) underlying a partial organelle band re-formation remained unknown. Therefore, five hypotheses were put forward and subsequently tested to elucidate the cause of the 80% of tetrads in the *jas;pel* double mutant.

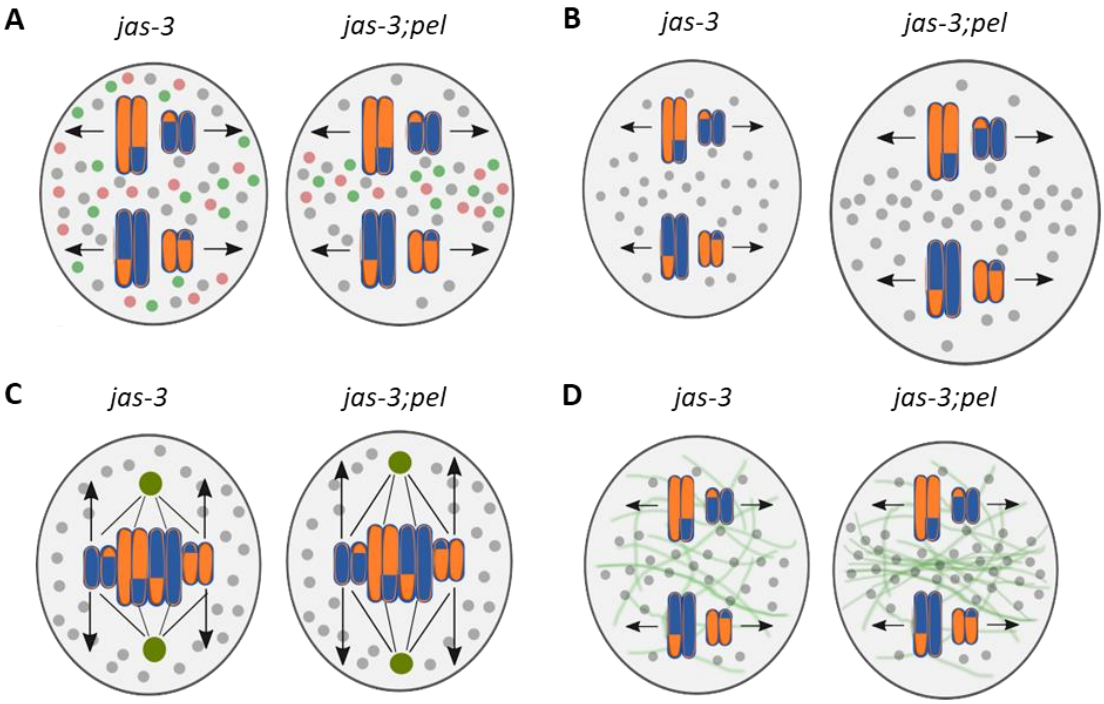

Figure 12 Schemes depicting four out of five hypotheses regarding the reason(s) of tetrad restoration in the *jas;pel* double mutant. (A) Particular vesicle or organelle enrichment in the organelle band. (B) Bigger cell size. (C) Longer meiotic spindles. Green ovals represent spindle poles. (D) Additional structure made of cytoskeleton components.

The first hypothesis regarded the involvement of DNA-free organelles in the organelle band formation (Fig. 12A). DAPI is a blue fluorescent stain that binds to AT-rich regions on the DNA (Williamson & Fennell, 1975), thus the staining limits its use to cell components which contain DNA, i.e. the nucleus, chromosomes, mitochondria and chloroplasts. Different methods need to be utilized in order to uncover the positioning of other organelles in the meiocyte, such as ER, Golgi vesicles, PM vesicles or vacuole. I hypothesized that in the *jas* mutant, all organelles of the cell become randomly scattered at prometaphase II, whereas the *peleus* mutation partially or fully restores the organelles without DNA in the band.

The second hypothesis stated that if *jas;pel* metaphase II meiocytes are bigger than *jas*, the chromosome sets could stay apart from each other in the absence of an organelle band, as it was found to be the cause of *jas* suppression by *telamon* (PhD thesis of Jun Yi, SLU) (Fig. 12B).

The third hypothesis assumed longer metaphase I spindles (Fig. 12C). I hypothesized that if the cell size remained the same in the double mutant as in the single mutant, but the spindle poles in metaphase I were located further away from each other, closer to the cell periphery, homologs could be pulled on a longer distance. If this distance was kept throughout the second meiotic division, it would decrease the chance of chromosomes intermingling in metaphase II and subsequently lead to observed increase in tetrads.

The fourth hypothesis claimed that the meiosis duration in *jas;pel* is longer than in *jas,* as it was observed in the *tam* mutant. The *TAM* gene (*TARDY ASYNCHRONOUS MEIOSIS,* also known as *CYCA1;2*), is a positive regulator of cell cycle progression, similar to *OSD1*. In the absence of TAM protein, meiocytes become arrested in meiosis I, which leads to the production of dyads. Moreover, it was found that in the mutant, meiosis II tends to continue even after callose degradation, resulting in "dyad pollen" with two male gametophytes within the same exine (Magnard et al., 2001). It was thus interesting to know, whether the duration of meiosis influences *peleus*' ability to partially restore the organelle band. I hypothesized that the initial organelle band disruption in *jas* prometaphase II could possibly not be repaired before the sister chromatid separation in anaphase II, but this might be done in *jas;pel* if more time is available.

The fifth hypothesis focused on the involvement of the cytoskeleton in the organelle band formation, due to its function in providing the scaffold for organelle movement within the cell. I suggested that in *jas;pel* the cytoskeleton components – either microtubules or microfilaments – might polymerize into a new, so far unknown structure during metaphase II, acting as a physical barrier between chromosome sets, and complementing the partially restored organelle band (Fig. 12D). It was also possible that the already existing cytoskeleton formations, e.g. phragmoplast, were somehow impaired in the *jas* single mutant and repaired by the mutation in *PELEUS*.

3.2.2 Golgi- and ER-derived vesicles are similarly scattered in metaphase II meiocytes of both mutants

To test the first hypothesis, I utilized a live-cell staining dye within partially dissected anthers of Col-0, *jas* and *jas;pel* to visualize ER- and Golgi-vesicles in meiocytes. Confocal imaging showed a specific enrichment of the metaphase II organelle band with both types of vesicles in wild-type background, which in the case of Golgi localization had been

previously observed (Brownfield et al., 2015). However, in both mutants there was no such enrichment, and vesicles filled the entire cytoplasm except in the close vicinity of the chromosomes (Fig. 13).

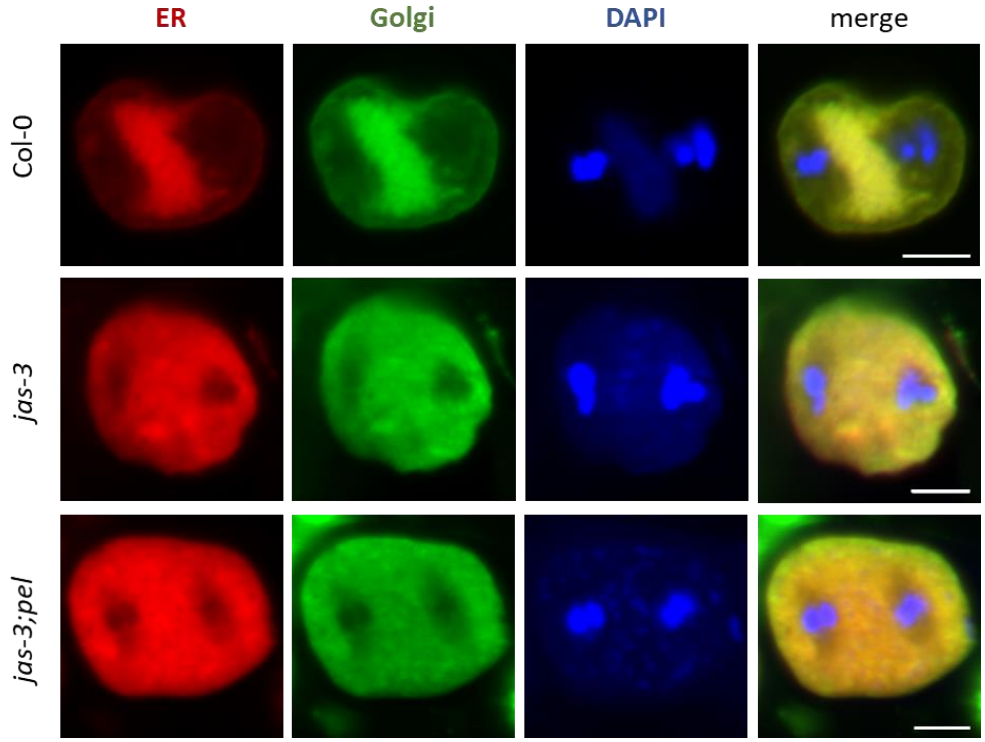

Figure 13 Localization of Golgi- and ER-vesicles in metaphase II meiocytes. Scale bar is 5 µm.

It was observed that *peleus* affected the localization of organelles, which contain DNA (mitochondria and chloroplasts), because DAPI staining showed their increased enrichment within the organelle band in the *jas;pel* mutant. It is thus possible, that *peleus* had a more profound effect only on mitochondria and plastid, whereas little to no effect on others, such as Golgi- and ER-vesicles.

3.2.3 Meiocytes are not larger in *jas;pel* than in *jas*

To test whether mutation in *PELEUS* resulted in the increased meiocyte size, meiocytes were stained with DAPI within intact anthers, imaged under the confocal microscope and the size of metaphase I and II cells was measured using the ZEN software.

The analysis showed that *jas;pel* metaphase I meiocytes were slightly bigger than those of Col-0 and *jas* (138.27 µm^2, 124.3 µm^2, and 134.25 µm^2, respectively), although the difference between *jas* and *jas;pel* was not statistically significant ($p = 0.544$). Metaphase II meiocytes, which are crucial for tetrad formation, exhibited a significant size difference only between wild-type and *jason* (123.91 µm^2 and 134.52 µm^2, $p = 0.00007$), not between

jas and *jas;pel* (p = 0.066), with *jas;pel* cells being even smaller than *jason* cells (127.69 µm^2 *versus* 134.52 µm^2) (Fig. 14). This clearly disproved the second hypothesis.

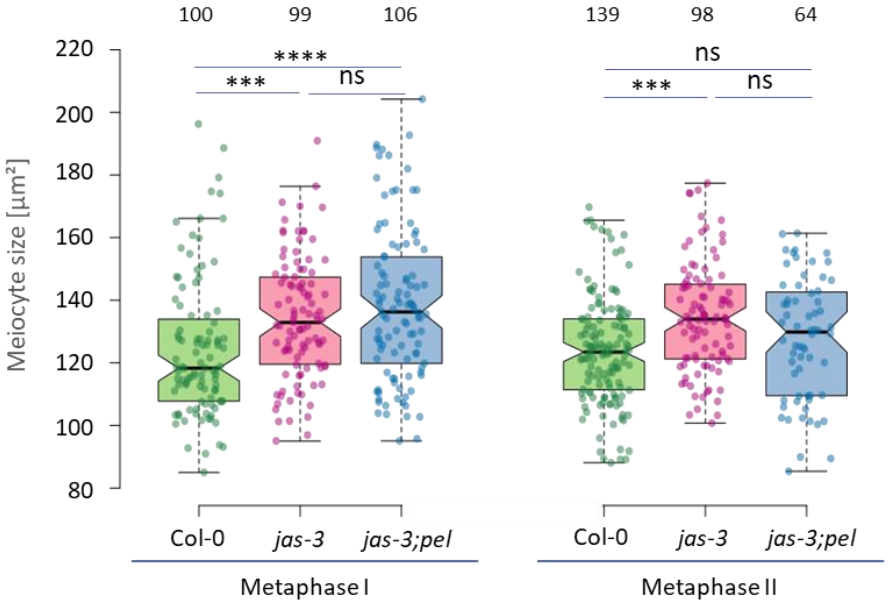

Figure 14 Metaphase I and metaphase II meiocytes' size measurement. *P* value indicated by asterisks (*** < 0.001, **** < 0.0001).

3.2.4 Metaphase I spindles are not longer in *jas;pel* than in *jas*

To test the third hypothesis, marker line of α-tubulin fused with GFP in the *jas;pel* background, was crossed with Col-0 to obtain it in all three necessary backgrounds. Spindles were then observed in the intact anthers and imaged as Z-stacks to capture both ends of each spindle. Their length was measured in ZEN software.

For this analysis, metaphase I meiocytes were more important than those of metaphase II, because if the hypothesis was correct, longer metaphase I spindles would explain why two chromosome groups in the *jas;pel* double mutant were always separated and never came close together. However, measurement did not show longer metaphase I spindles in *jas;pel* than in *jas*, but interestingly, proved that *jason* spindles with their average length of 14.19 µm were significantly longer than those of wild-type (11.66 µm, p = 0) and of the double mutant (12.83 µm, p = 0.0002) (Fig. 15A). The differences between both mutants disappeared in metaphase II, as *jason* spindles had on average the same length as those of the double mutant (8.84 µm and 8.98 µm, respectively), whereas wild-type spindles were significantly shorter (7.94 µm, p = 0 in both comparisons) (Fig. 15B). This disproved the third hypothesis and left the reason for separated chromosome sets in the double mutant open for further discussion.

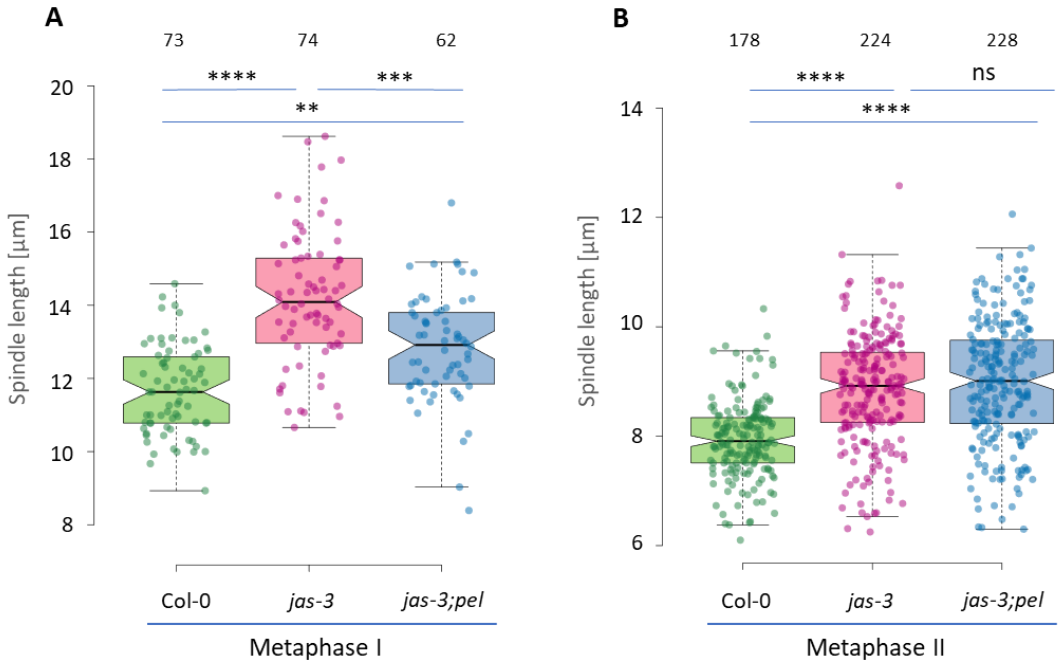

Figure 15 Spindle length measurements. (A) Metaphase I spindle length. (B) Metaphase II spindle length. Each data was collected from 2-4 biological replicates. Only fully visible spindles with clearly defined poles were measured. *P* value indicated by asterisks (** < 0.01, *** < 0.001, **** < 0.0001).

3.2.5 Duration of meiosis is similar in both mutants

To test the fourth hypothesis, the α-tubulin-GFP marker lines were used in collaboration with Dr. Maria Cuacos (IPK Gatersleben) to perform light-sheet microscopy imaging of the entire meiotic process. This method enables live-cell imaging of developing tissues by preserving the fluorescent signal for multiple days without losing its strength. Meiotic buds at the stage of prophase I had their petals and sepals removed, and were subsequently placed under the light-sheet fluorescent microscope for observation.

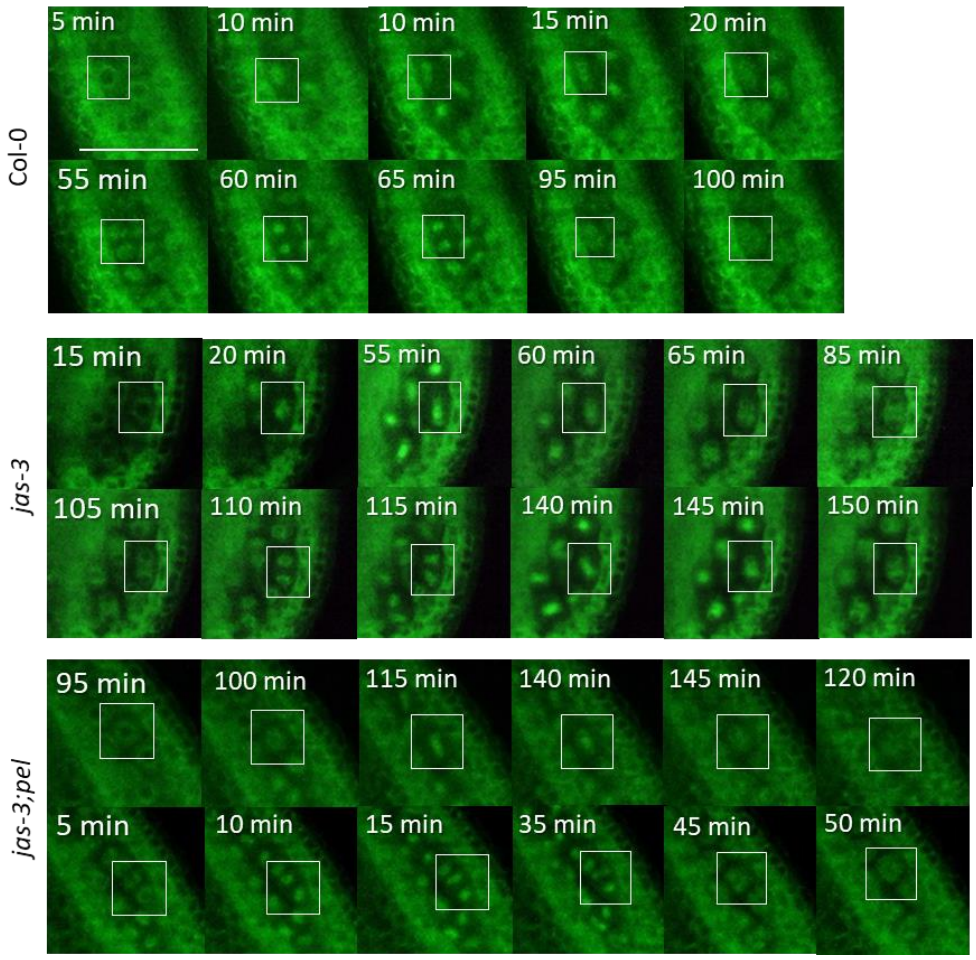

Figure 16 Selected frames from the timelapse of tubulin-GFP dynamics in analyzed lines. White rectangles show a single meiocyte undergoing meiosis, from diakinesis (first frame) to tetrad stage (last frame). Scale bar is 50 µm in each image. The time discontinuity in *jas;pel* was due to loss of focus on the meiocytes and the need to readjust the objective, which required brief stopping of the measurement.

The time needed for completing meiotic divisions was measured from the onset of metaphase I, when tubulin changes its conformation from the "perinuclear ring" structure present during pachytene, diplotene and diakinesis to the metaphase I spindle. Photos were taken every five minutes and assembled into a sequence portraying meiotic progression in living anthers (Fig. 16). Two anthers were assessed for each line (Col-0, *jas*, and *jas;pel*), and the time measured between metaphase I and telophase II was averaged within each line, and compared between the lines. The duration of meiosis between metaphase I and prophase II was approximately 45-50 min in each line, followed by 40-45 min of prophase II stage. The second division lasted on average 37.5 minutes in wild-type and *jas;pel*, and was slightly longer in *jas* (ca. 45 min). However, one of *jas* buds finished the interkinesis quicker and prolonged the second division, which resulted in total duration of divisions equal to that of wild-type and *jas;pel*. Taken together, meiotic

divisions in each line lasted from 120 to 135 minutes, and the differences resulted from natural variation. This observation was similar to the recent study on the effect of heat stress on male meiosis in *A. thaliana*, in which the average duration of meiotic divisions was measured to be 145 minutes (De Jaeger-Braet et al., 2021). Since De Jaeger-Braet et al. proved that elevated temperatures decrease the length of nearly every meiotic stage, it is likely that the plants used in my study were also subjected to slightly increased temperature, which led to the moderately faster meiosis. Nevertheless, since the duration of meiosis was comparable in both mutants, it could not cause the partial organelle band reparation in *jas;pel.*

Despite disproving this hypothesis, the time-lapse tracing of tubulin dynamics revealed a surprising event, which would not have been observed in fixed samples. In *jas*, once the prophase II was finished, two fully separated spindles were created in every meiocyte (frame captured at 115 min and 140 min). These spindles unexpectedly fused shortly after, eventually leading to the generation of dyads (frames captured between 140 and 150 min.). Since meiotic spindles do not appear in prophase II, but only after chromosomes condense, it is almost certain that the stage captured at 115 min was prometaphase II. Thus, the fusion of spindles could coincide with the loss of organelle band. This would confirm the hypothesis that organelles separate the spindles of the second meiotic division (Brownfield et al., 2015; Tchórzewska, 2017). However, to clear any doubts, it is necessary to combine tubulin imaging with DNA visualization in live cells, so that the exact timepoint of both fusion event and the scattering of organelles can be recorded.

3.2.6 The tubulin dynamics are similar in both mutants, whereas actin structure is abnormal

The microtubule dynamics was evaluated using an α-tubulin-GFP marker line and light-sheet microscopy. Due to low resolution of the light-sheet microscope movies, close-up photos of each stage were taken to further compare possible nuances of the structures.

As expected, the microtubule organization was the same in all tested lines (Fig. 17). Particular interest was given to the tubulin structure at telophase I, called Interzonal Microtubule Array (IRA), as it was hypothesized that it is responsible for separating two groups of homologous chromosomes after anaphase I and thus creating enough space for the metaphase II spindles to acquire perpendicular orientation (De Storme & Geelen, 2011). However, no alterations in this structure, e.g. deficient microtubules or their truncated length, were observed in *jas*. Moreover, the wild-type-like phragmoplast, which formed in both mutants during prophase II, successfully separated the two decondensed nuclei.

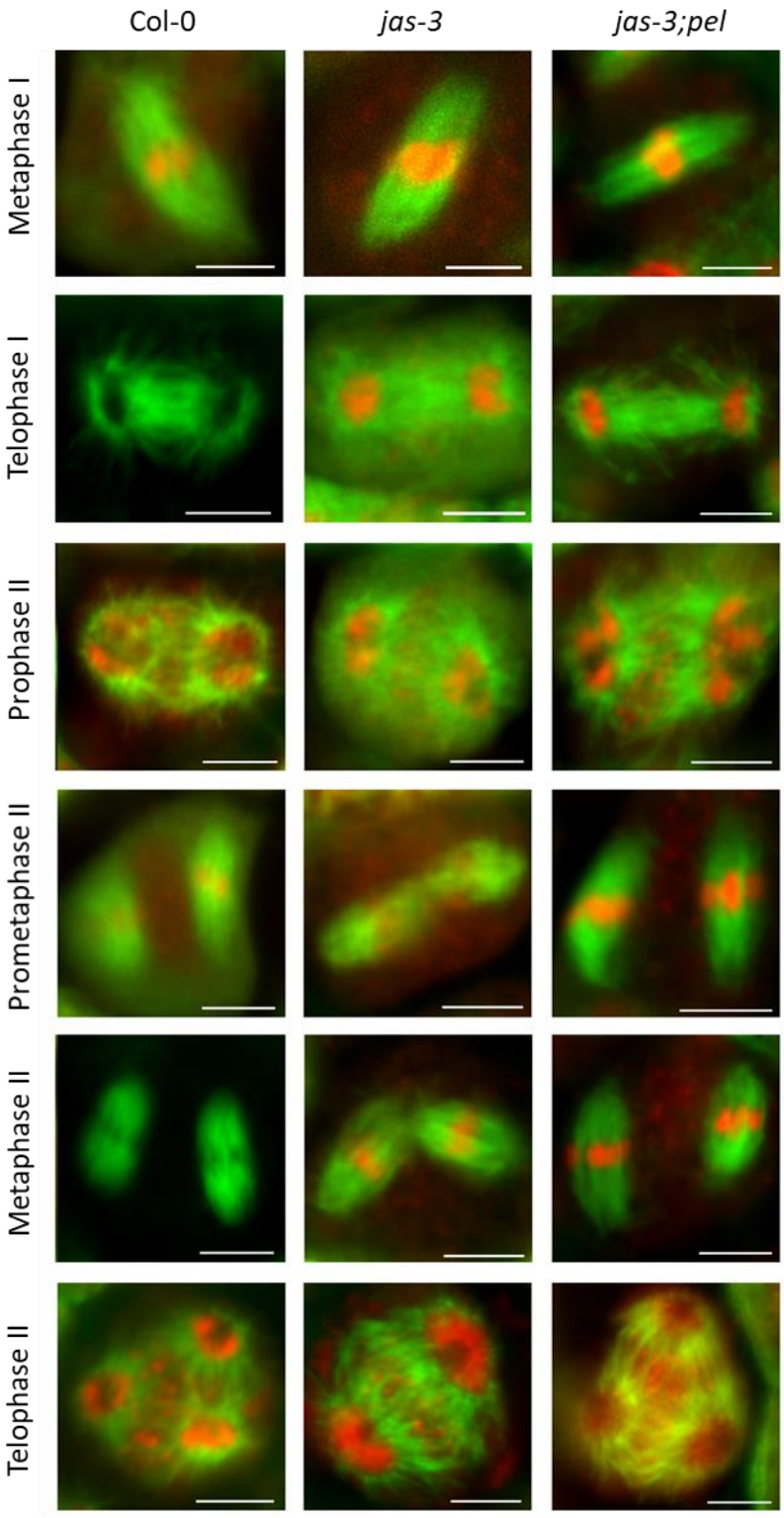

Figure 17 Microtubule dynamics during meiosis. Green is microtubular cytoskeleton, red (false color) are chromosomes. Very faint or no red signals in some images come from weak DAPI staining (most likely due to its usage after expiration date). Scale bars are 5 µm.

The only noticeable difference were metaphase II spindles, which in *jas* were often found to be tripolar or fused, whereas in *jas;pel* they were predominantly separated. This feature of *jason* was already described by Brownfield et al. (2015), while normal spindle

organization in *jas;pel* was expected due to the previously discussed behavior of chromosome sets in metaphase II. Thus, not the spindle structure, but other reasons lead to the suppression of *jason*.

Actin microfilaments were imaged on dissected anthers using phalloidin dye, a bicyclic peptide with high affinity for F-actin, conjugated with a fluorophore. Since phalloidin stabilizes F-actin microfilaments and promotes polymerization of the G-actin (Pozhvanov, 2018), 4% paraformaldehyde was used to fix the actin cytoskeleton prior to sample preparation.

The staining revealed the filamentous network of wild-type actin and a typical enrichment of actin within the microtubular structures of the metaphase I spindle and the RMAs in telophase II. Interestingly, in areas with a high density of organelles and vesicles, such as in the metaphase I organelle ring or the metaphase II organelle band, actin seemed to be less abundant, because the staining was much weaker in these regions (Fig. 18).

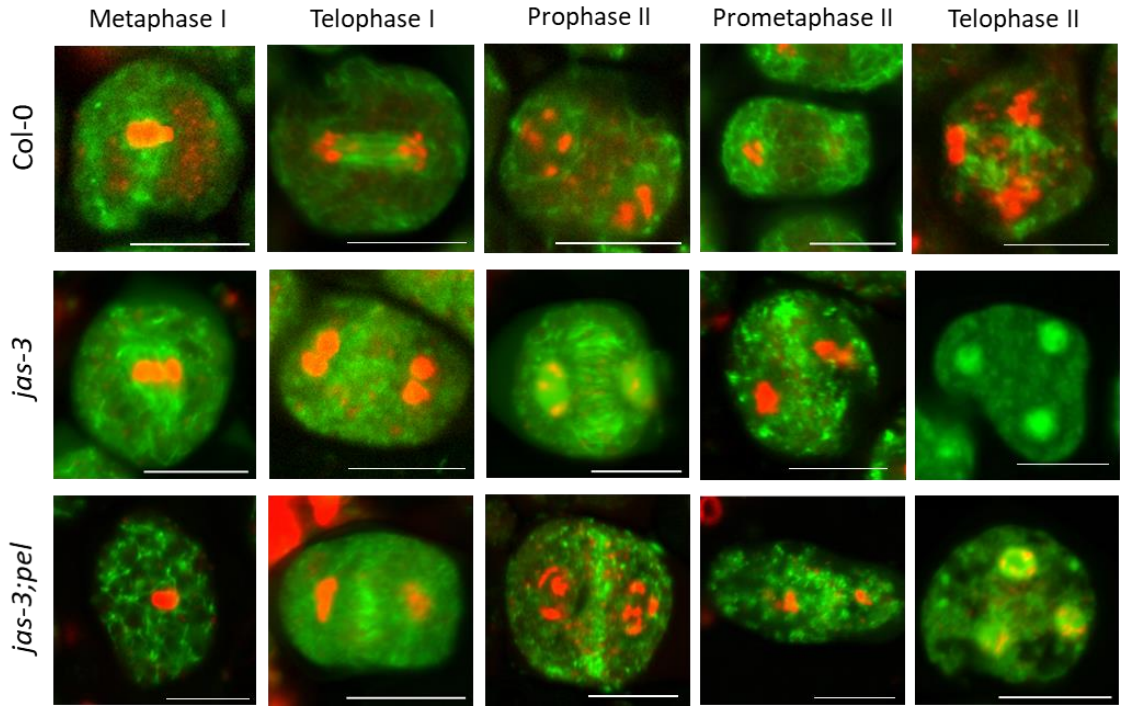

Figure 18 F-actin organization during meiosis. Actin was stained with phalloidin-based dye (green), and nuclei with DAPI (false red). No red signal in *jas-3* telophase II comes from poor DAPI staining. Scale bars are 10 µm.

In contrast to clearly visible microfilaments in wild-type, *jas* and *jas;pel* meiocytes often contained what looked like shorter filaments, dispersed actin and even speckles instead of strands. Actin was sometimes found within the microtubular structures, although its appearance was not consistent. In both mutants some meiocytes showed actin

enrichment, while others did not. Most noticeable was lack of actin enrichment within RMAs in *jas* and in the not fully developed RMAs in *jas,pel*, despite their fully functional microtubular network in this stage (Fig. 17 for comparison). Moreover, in some cells of both mutants a particular, abnormal polymerization of actin occurred, best displayed by *jas;pel* prophase II photo (Fig. 18).

The most noticeable difference was observed at prophase II. In the *jason* mutant, many meiocytes showed actin signal within its decondensed nuclei. Such patterns were observed in multiple meiocytes coming from different anthers, but not in wild-type nor *jas;pel* samples. This would imply that the *jason* mutation affected the actin network structure by causing its partial depolymerization. Actin enrichment within the nuclei was previously observed to be a response to latrunculin B treatment in rat peritoneal mast cells (Pendleton et al., 2003), further indicating its abnormal origin.

These results suggest that loss of JASON disrupts the structure of the actin cytoskeleton. Since actin microfilaments are known to be the scaffold for the transport of organelles and vesicles within the cell, it is likely that altered actin network leads to the organelle dispersion observed in the *jas* mutant. Although the integrity of actin cytoskeleton in *jas;pel* is not repaired, very rare events of actin presence in the prophase II nuclei suggest that the actin deformation progresses slower or is less severe in the *jas;pel* mutant than in the *jas* mutant, which would explain only partial loss of organelles from the organelle band of the double mutant.

3.3 Identification of *PELEUS*

3.3.1 Sequencing *peleus* reveals three candidate genes

In order to analyze the mechanisms of unreduced gamete suppression caused by *peleus*, a forward genetics approach was followed to establish the identity of the gene. For this purpose, a mapping population was generated. *jason* has alleles in both Col (*jas-3*) and L*er* (*jas-1*) ecotypes, which were used to produce a cross that would utilize the Col/L*er* polymorphisms to map the mutation. Therefore, a cross was made between *jas-3*;*pel* and *jas-1* and propagated until F2, so that the suppressor mutation was segregating in *jason* homozygous background (Fig. 19A). In the meantime, the F1 generation of this cross was analyzed for pollen size, revealing that *peleus* mutation was recessive (Fig. 19B). This was later confirmed by the 3:1 ratio of *jason* to *jas;pel* phenotype in the F2 generation. The recessive nature of the mutant allele means that loss of its function causes the suppression of the *jason* phenotype.

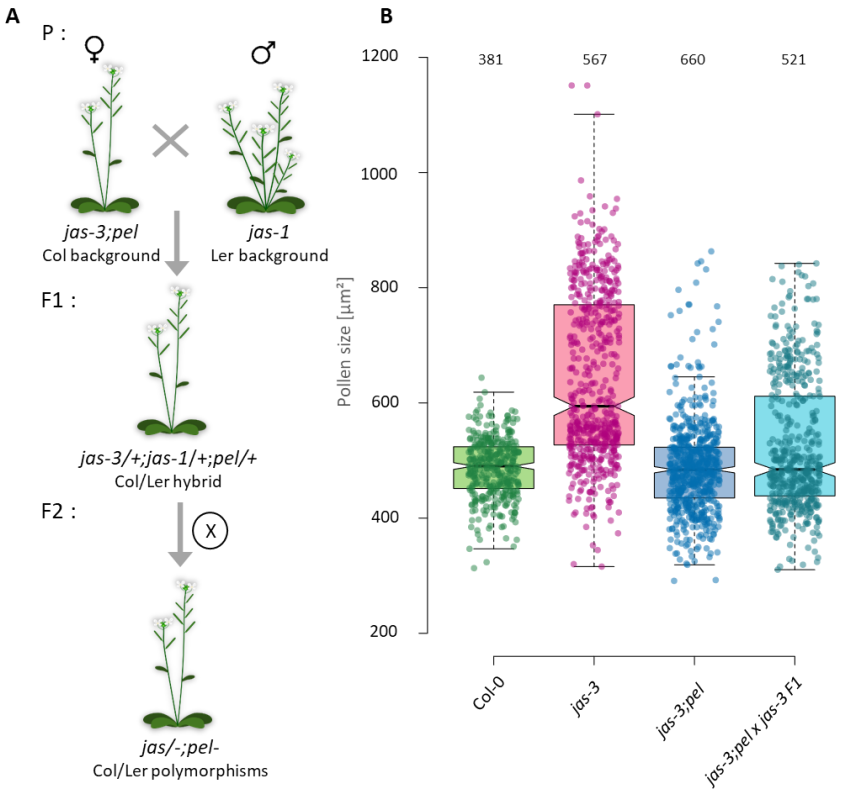

Figure 19 Mapping population of *jason;peleus*. (A) Scheme depicting the process of generating *peleus* mapping population. "X" in a circle symbolizes self-fertilization. (B) Dominancy analysis of the *peleus* point mutation. Plants used for the analysis were the F1 generation (see: A). At least 10 plants of each line were analyzed and the obtained data were merged.

Mapping population of *peleus* (ca. 200 plants) was screened for pollen size, seed set and tetrad formation. Twenty of the strongest suppressors were utilized for positional cloning, which aimed to establish chromosomes containing the polymorphism and narrow down the region of the point mutation. With the use of markers detecting short Col/L*er* polymorphisms (Lukowitz et al., 2000), the *peleus* mutation was mapped on the top arm of chromosome 5, between marker CTR1 at 0.98 Mbp and ciw8 at 7.5 Mbp.

39 plants were used to construct DNA library, which was sent to New-Generation Sequencing (Novogene, UK) with *jason* as a control. According to the obtained results, *peleus* DNA library contained the Col-0 specific non-recombinant region on the top arm of chromosome 5, spanning the area between 2.6 and 3.8 Mbp, which was consistent with the rough mapping result. By limiting the analysis to point mutations found within this region, and setting the discordant chastity to 0.65 to make up for the potential mistakes in the F2 homozygotes assembly, three *PELEUS* candidate genes were revealed: *KIWI* (At5g09250), *AP4B* (At5g11490) and ephrin type-B receptor (AT5G11700, latter referred to by the gene ID for the convenience) (Table 2).

Table 2 Summary of the *PELEUS* gene candidates [modified based on the results of Next-Generation EMS mutation mapping from bar.utoronto.ca/ngm/index.html].

Chrom.	Position	Ref. base	SNP base	Discordant chastity	Accession	Strand	Ref. codon	SNP codon	AA change	BLOSUM 100
5	2876358	C	T	0.74	At5G09250.1	-	AGA	AAA	R → K	3
5	3674314	C	T	0.73	At5G11490.1	+	CTT	TTT	L → F	0
5	3765154	C	T	0.68	At5G11700.1	-	TGG	TAG	W → *	-10

The point mutation in *KIWI* was expected to have little significance on the phenotype (BLOSUM 100 = 3), as it changed the basic arginine into basic lysine. The point mutation in *AP4B* transformed hydrophobic leucine into an aromatic phenylalanine, yet the effect on the peptide was assessed to be insignificant by the algorithm, as the BLOSUM score was equal to 0. Especially promising was the point mutation in *AT5G11700*, as it substituted a tryptophan code with a premature STOP codon, thus truncating the protein and possibly disrupting its functionality. Nevertheless, all three genes were considered candidates and were subsequently tested.

3.3.2 Co-segregation analysis and phenotypic analysis prove that *KIWI* and *AP4B* are not *PELEUS*

The analysis of the candidate genes began with confirming the point mutation in the original *jas;pel* mutant with CAPS analysis (Fig. 20A). *Jason* DNA served as a control to rule out the possibility that the mutation originated in the *jason* background. Additional Sanger sequencing analysis for each point mutation was carried out to ensure correctness of the genotyping result (Fig. 20B-D). Indeed, all three candidate genes were mutated at the expected position in the *jas;pel* double mutant, but not in the *jas* single mutant.

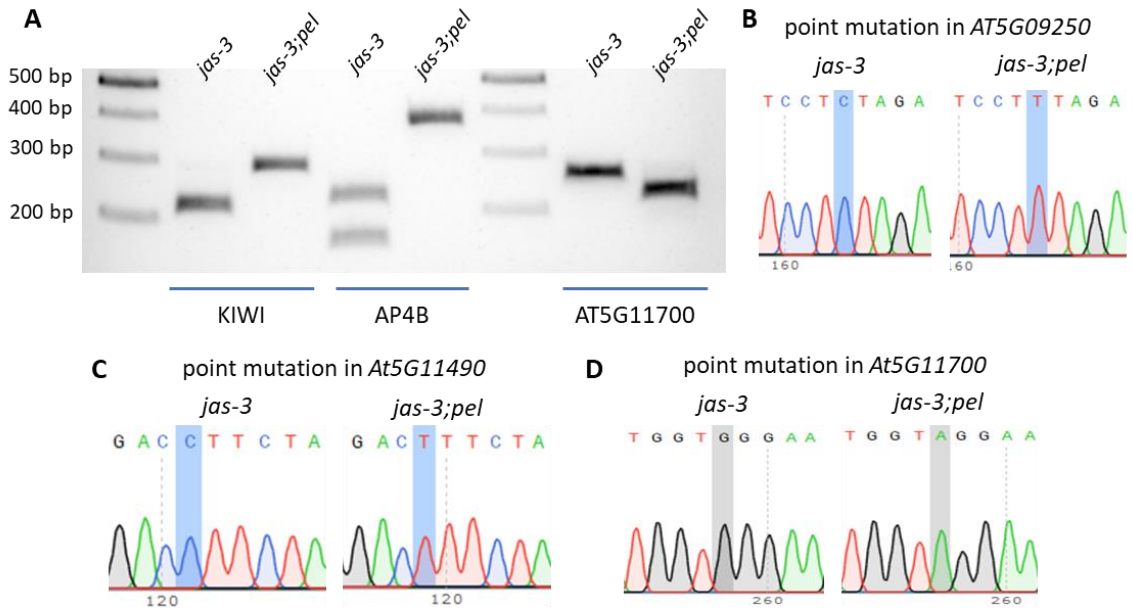

Figure 20 Confirmation of point mutations in three *PELEUS* candidate genes. (A) CAPS and dCAPS analysis for point mutations in *jas-3* and *jas-3;pel*. (B) PCR product sequencing, confirming the point mutation in *KIWI*. The presented sequence is on the forward strand, whereas the KIWI gene lies on the reverse strand. (C) Point mutation in *AP4B*. (D) Point mutation in the ephrin type-B receptor gene.

In order to proceed with the *PELEUS* identification, seeds of 50 F1 plants from the mapping population of the *jas;pel* x *jas* cross were sowed and the obtained F2 plants were analyzed for pollen size. After phenotyping, all plants were genotyped for each candidate's point mutation. Based on the expected segregation ratio of 25% homozygous mutants, 50% heterozygotes and 25% wild-type plants, and the recessive nature of *peleus* mutation, the expected ratio should be 25% WT-like plants (*jas;pel* double mutant phenotype) and 75% plants of *jason* phenotype. Indeed, among 79 analyzed plants, 23 showed suppressed phenotype, which amounted to ca. 29.1% suppressors. All plants homozygous for the mutation in *AP4B* or *AT5G11700* were phenotypically *jason* suppressors. However, this was not the case for the point mutation in *KIWI*. Figure 21 shows only the first seventeen screened plants, as this subset represents the obtained results (Fig. 21A). In this group, plants numbered 4, 5, 10, 12 and 14 were unequivocally *jason* suppressors, but plant nr 10 showed heterozygosity for the *KIWI* point mutation (third asterisk on Fig. 21B). Replicated genotyping confirmed that plant nr 10 was indeed heterozygous for *KIWI* (Fig. 21C). Therefore, co-segregation analysis ruled out the possibility that *KIWI* was *PELEUS*, while indicating that *PELEUS* was located in the vicinity of the other two tested genes.

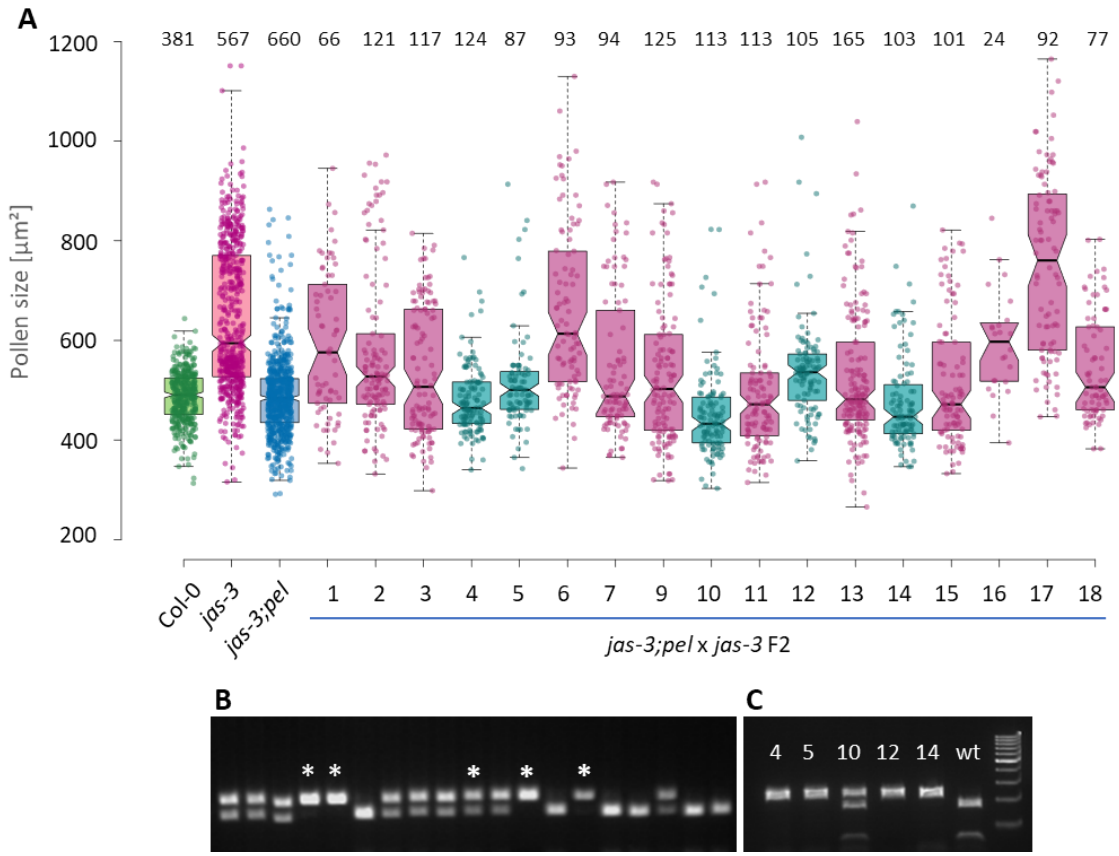

Figure 21 Co-segregation analysis of three *PELEUS* candidates. (A) Pollen size analysis of a representative population of *jas-3;pel* x *jas-3* F2 plants. Teal color of the box plot marks plants with suppressed phenotype, characterized by short body of the plots and relatively few dots ranging above the upper whisker, which is equivalent to the abundance of haploid pollen (main body) versus diploid pollen (area above the main body). Plant nr 8 was genotyped, but did not survive until flowering. (B) Genotyping results for the point mutation of KIWI in the *jas-3;pel* x *jas-3* F2 population. Asterisks mark the plants which had suppressor phenotype in the pollen analysis. (C) Confirmation of the genotyping results of the crucial plants.

AP4B is a subunit of AP-4 complex, responsible for the vacuolar sorting of storage proteins and for plant defense against pathogens associated with the hypersensitive cell death (Hatsugai et al., 2018). Moreover, the *ap4b* mutant presents obvious developmental defects, making it possible to use this characteristic for direct comparison with the *pel* single mutant's phenotype. The plants with the *peleus* mutation under the WT background were identified from a *jas;pel* x Col-0 F2 population. As indicated by the co-segregation analysis, *PELEUS* gene was located either in the close vicinity of *AP4B* and *AT5G11700* genes, or was one of those genes, thus CAPS analysis for any of these two mutations could act as a *pel* genotyping method. Therefore, 40 F2 plants from the aforementioned cross were genotyped, and two putative *pel* mutants had their

morphology compared with *ap4b* mutant. None of them showed any developmental issues, which lead to conclusion that *AP4B* could not be *PELEUS*.

3.3.3 Analysis of the *jas-3* x *at5g11700* T-DNA mutant F2 population leads to identification of *PELEUS*

The last candidate gene, *AT5G11700*, had not been previously analyzed, therefore no phenotypic comparison between *pel* and *at5g11700* mutant could have been conducted. In order to confirm or reject this candidate, a cross between *jas-3* and *AT5G11700* T-DNA insertion mutant (SALK_209914C) was established (Fig. 22). If this putative gene was *PELEUS*, double homozygous mutant obtained in the second generation should imitate *jas;pel* phenotype.

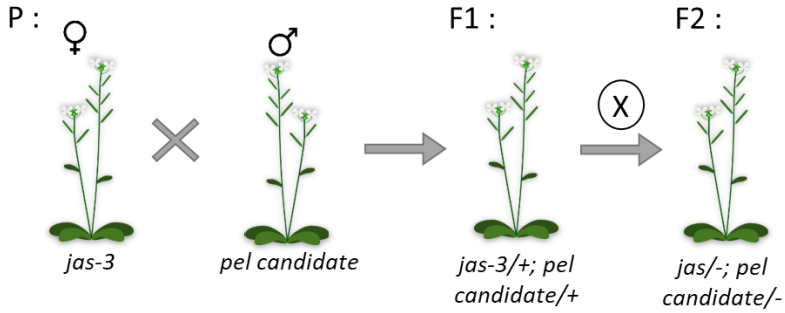

Figure 22 Scheme of a cross between a T-DNA insertion mutant of the *PELEUS* candidate gene and *jas-3*, aimed to replicate the *jas-3;pel* phenotype in the second generation.

A total of ca. 220 F2 seeds was sowed and genotyped for both *jas* mutation and *AT5G11700* T-DNA insertion. 15 double mutants were found and subjected to pollen size analysis (Fig. 23A). Even though there was predominantly haploid pollen characteristic for *jas;pel*, for safer conclusion the tetrad formation had to be analyzed. The results showed that all plants produced at least 75% of tetrads and only up to 10% of dyads (Fig. 23B). Taken both analyses together, I concluded that *PELEUS* was most likely *AT5G11700*.

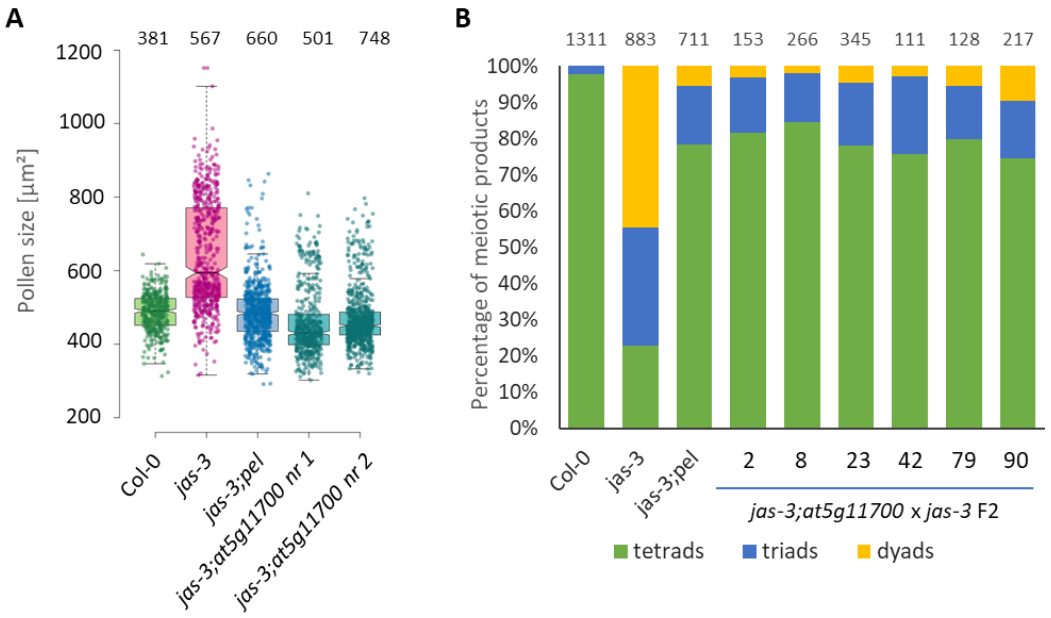

Figure 23 Phenotypic analysis of *jas-3;at5g11700* double mutant plants. (A) Pollen size analysis of two representative *jas-3;at5g11700* double mutants. (B) Tetrad formation analysis of six representative *jas-3;at5g11700* double mutants.

3.3.4 *AT5G11700* complements the *jas;pel* phenotype

In order to ensure the correct identification of *PELEUS*, the WT version of *AT5G11700* needed to be introduced into *jas;pel* to check if the mutant phenotype was complemented. If *PELEUS* was *AT5G11700*, transformed plants would exhibit the *jason* phenotype.

A genomic version of *AT5G11700* under its native promoter (1.5 kb sequence upstream of the START codon) and with a full 5' UTR sequence, adding up to a total of 10590 base pairs, was cloned into the pGWB510 destination vector. The correct construct was then transformed using the *Agrobacterium tumefaciens* strain GV3101 strain into 20 *jas;pel* plants. Positive transformants were selected on a hygromycin plate and later genotyped for hygromycin resistance sequence. 16 plants were considered T1 transformants after additional pollen size and tetrad analysis. 8 of them were propagated and the T2 generation was phenotyped again. Results obtained from representative transformants are listed in the Table 3.

Table 3 Complementation analysis data for representative *jas-3;pel* plants transformed with the pGWB510-pPEL-g*PEL* construct.

T1 plant nr	Pollen size analysis in T1 generation	% of dyads among meiotic products in T1 generation	Hygromycin signal in T2 generation	Pollen size analysis in T2 generation	% of dyads among meiotic products in T2 generation
6	Complemented	75.1% (n = 241)	11 / 12 plants	Complemented: 10 / 10	29.3% (n = 297)
8	Complemented	38.7% (n = 75)	12 / 12 plants	Complemented: 12 / 12	29.3% (n = 198)
9	Complemented	n/a	7 / 10 plants	Complemented: 5 / 6	40.4% (n = 166)
10	n/a	n/a	8 / 10 plants	Complemented: 7 / 8	26.2% (n = 122)
12	Complemented	39.9% (n = 173)	7 / 10 plants	Complemented: 5 / 7	20.1% (n = 209)
14	n/a	n/a	8 / 9 plants	Complemented: 7 / 8	19.2% (n = 172)

The vast majority of the analyzed plants displayed the typical *jason* pollen phenotype with a highly increased number of unreduced, diploid pollen, referred to as "complemented". Moreover, tetrad formation analysis of these plants showed a significant increase in dyads (at least 19.2%) in comparison to 5.3% present on average in *jas;pel*. These results confirmed the conclusion that *PELEUS* was indeed *AT5G11700*.

3.4 Characterization of *PELEUS*

3.4.1 *PELEUS* gene and protein characteristics

AT5G11700 is a protein coding gene located on the top arm of chromosome 5, at ca. 3.77 Mbp. Its genomic version lies on the reverse strand and comprises 9059 nucleotides (including UTRs), and its CDS: 4362 bp. Translated into protein, PELEUS consists of 1453 amino acids and has a mass of ca. 156.5 kDa. It is often referred to as glycine-rich protein, but some databases annotated it specifically as an ephrin type-B receptor due to the presence of a cysteine rich domain of six cysteines within a region of 40 amino acids, creating 3 di-sulfide bonds. Such a domain is found in the third class of plant receptor-like protein kinases (RLKs) – a class with epidermal growth factor-like repeats. Other RLKs classes have no similarity with PELEUS. Moreover, no typical receptor kinase domains are predicted based on the PELEUS protein sequence. Online sources, such as SMART (embl-heidelberg.de) suggest that PELEUS contains ephrin rec-like domain, but BLASTing against non-redundant protein sequences did not corroborate this suggestion. BLAST analysis of the entire PELEUS sequence shows that although it has homologs across multiple flowering plant species, the vast majority of them is described as "unnamed", "hypothetical", "predicted" and "uncharacterized". The ephrin type-B receptor is annotated predominantly within the Arabidopsis genus.

PELEUS has homologs in a variety of flowering plant families, although homologs with more than 75% protein sequence similarity can be found also in mosses (Fig. 24). The most closely related homologs belong to the *Brassicaceae* family, but they are also present in

e.g. cotton (*Gossypium hirsutum* L.), cassava (*Manihot esculenta* Crantz.), purple willow (*Salix purpurea* L.), cacao (*Theobroma cacao* L.), trifoliate orange (*Poncirus trifoliata* L.), and eastern cottonwood (*Populus deltoides* W.Bartram ex Marshall). Homologs with at least 77% of sequence similarity occur also in monocots, such as rice (*Oryza sativa* L.), wheat (*Triticum aestivum* L.) and maize (*Zea mays* L.). Meiosis in monocots differs from that of dicots by successive cytokinesis instead of simultaneous. This means that after first meiotic division, the spore mother cell divides into a dyad and the second meiotic division progresses in each cell individually, thus eliminating the necessity of an organelle band to separate meiotic spindles. The fact, that PELEUS homologs can be found in monocots as well, suggests another unrelated function of PELEUS in these plants.

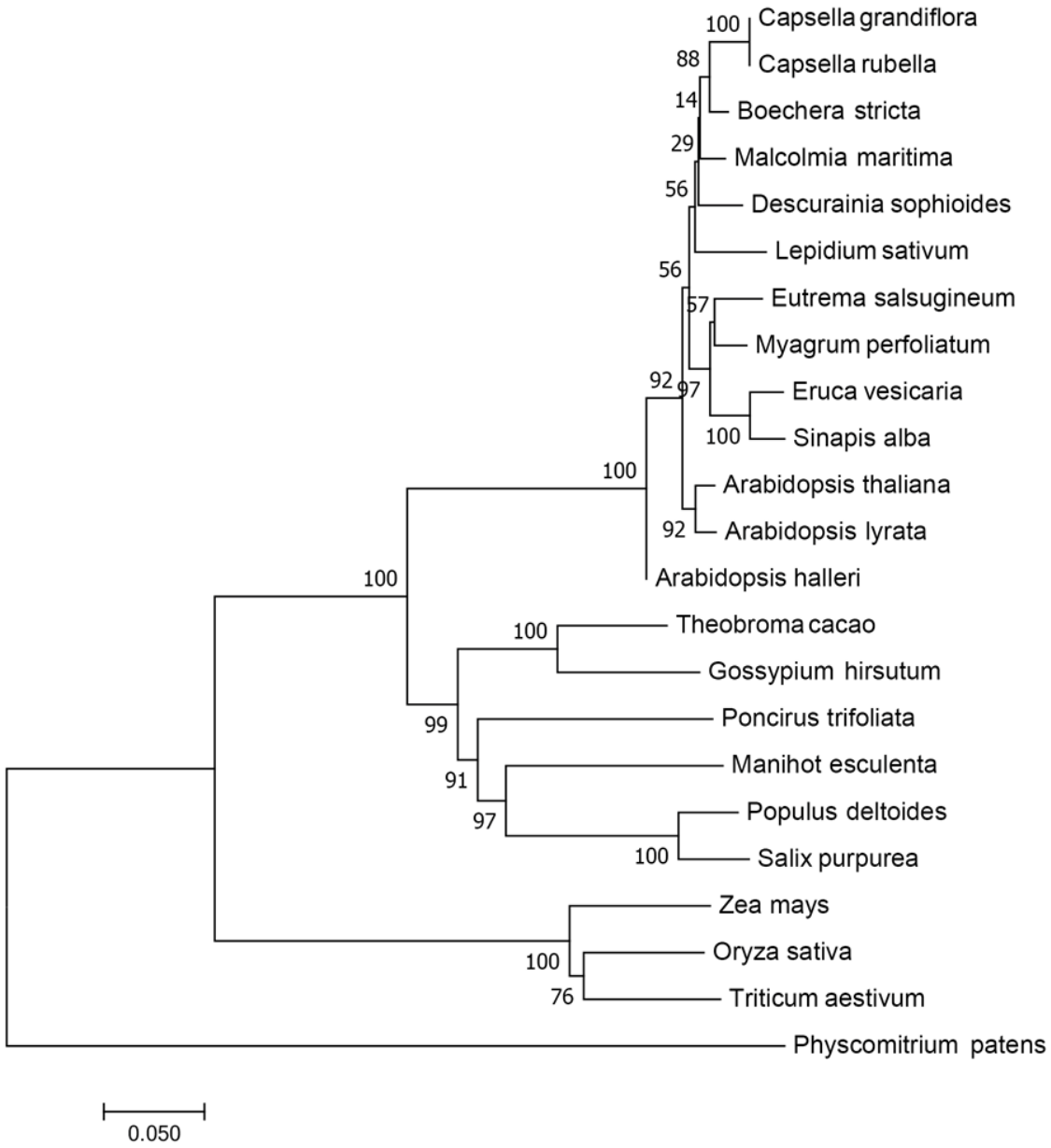

Figure 24 Phylogenetic tree of PELEUS protein homologs. The tree was prepared from protein sequences provided by Phytozome database and analyzed using the MEGA7 software.

The same protein databases imply that PELEUS is a protein with multiple transmembrane domains (Fig. 25). Depending on the program used for the prediction, the number differs from 3 to 10. Moreover, UniProt gathered data from various proteomic studies, which revealed that PELEUS might be localized in plasma membrane, vacuole, and plasmodesmata. The most probable localization seems to be the vacuole, as two independent research papers found it to be localized in the tonoplast and annotated it as a putative multi-transmembrane tonoplast protein of unknown function (Endler et al., 2006; Shimaoka et al., 2004). Almost all prediction programs agree that PELEUS belongs to the secretory pathway, because its N-terminus contains a signaling peptide (although there is no consensus whether it is made of the first 19 amino acids or the SSS-YR motif at position 22-26). This could mean that PELEUS is transported through the secretory pathway to the plasma membrane or the vacuole.

Figure 25 Schematic representation of the PELEUS protein structure. The scheme includes the T-DNA insertion site and most commonly predicted features, such as four transmembrane domains and the cleavable signal peptide at the N-terminus. The amino acid with point mutation in the *peleus* mutant is indicated by the lightning mark.

3.4.2 *PELEUS* is involved in root development

To search for its potential function in wild-type plants, a peleus single mutant (*pel*) was generated by backcrossing *jas;pel* with Col-0 and selecting F2 plants with wild-type *JASON* gene. The T-DNA insertion line SALK_209914C was simultaneously used to support the results from the point mutated single mutant.

Pollen size analysis showed neither diploid nor collapsed pollen, suggesting that reproductive system was unaffected by the mutations (Fig. 26A). Subsequent analysis of meiotic products further confirmed wild-type-like phenotype of *pel*, with nearly 100% of tetrads and 0% of dyads (observed triads were most likely tetrads mistaken for triads due to overlapping cell positions, Fig. 26B). Cytological analysis revealed no chromosome defects, but a fully functional, complete organelle band (Fig. 26C). Therefore, it became obvious that *peleus* is not a meiotic mutant itself. Moreover, morphologically both types of *pel* mutant resembled Col-0, *jas* and, *jas;pel* plants as no developmental defects were observed. To further test this observation, root length of wild-type (control), *jas, jas;pel,* and *pel* were measured under standard LD growth conditions, 6 days after sowing on vertical plates.

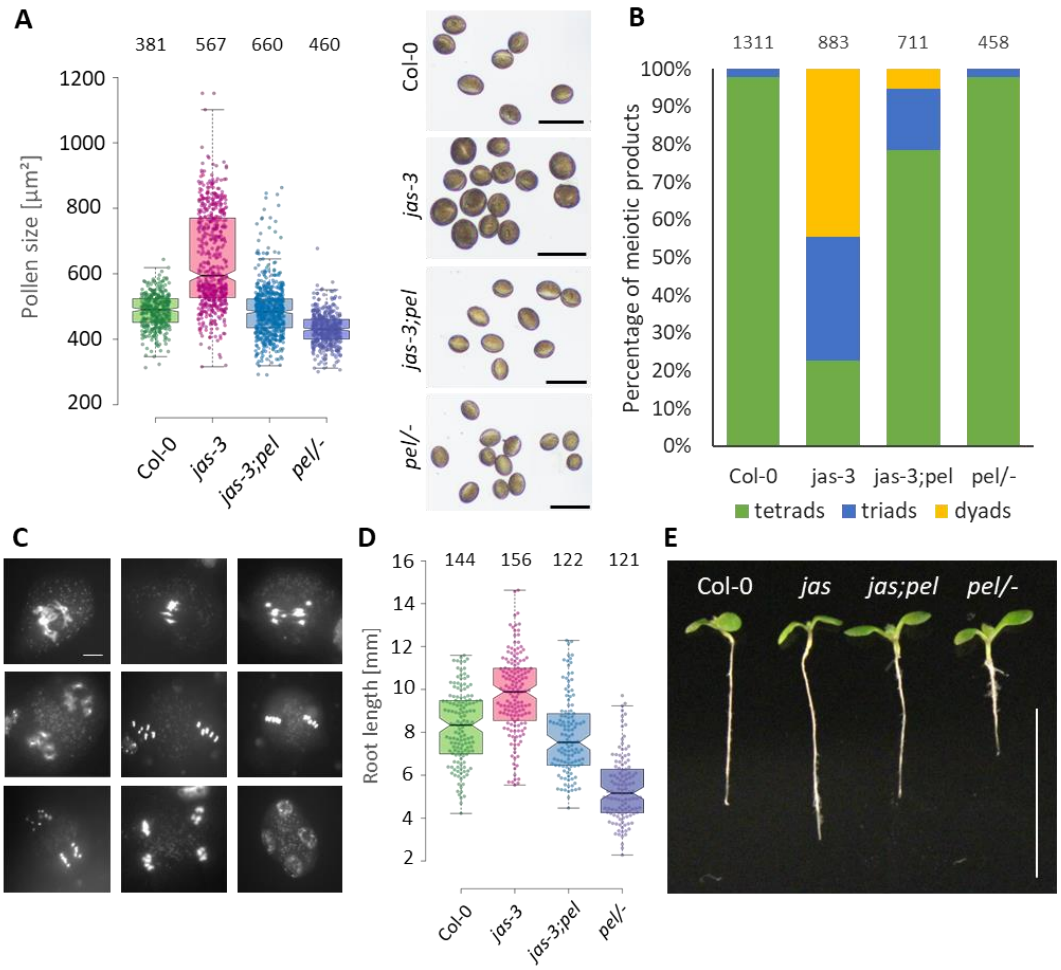

Figure 26 Phenotypic analysis of the *peleus* single mutant. (A) Distribution of pollen size in the *peleus* single mutant and three control lines. Scale bar on pollen photos is 50 µm. (B) Percentage of meiotic products in *pel* and controls. (C) Meiotic stages of *pel*; from left to right: diakinesis, metaphase I, anaphase I, prophase II, prometaphase II, metaphase II, anaphase II, telophase II and four nuclei stage, respectively. Scale bar is 10 µm for all images. (D) Root length of 6-days old seedling. (E) Images of representative 6-days old seedlings. Scale bar is 10 mm.

Interestingly, *pel* roots with an average length of 5.37 mm were shorter than those of wild-type (8.24 mm), *jason* (9.77 mm) and *jas;pel* (7.85 mm) (Fig. 26D and E). This was not caused by the delay in germination, as the growth rate of *pel* was similar to that of wild-type and the double mutant (*pel:* 97.9% germinated seedlings, n=137; *jas;pel*: 99.3%, n=137; wild-type: 94.5%, n=165, counted after 50 hours of germination). Two conclusions could thus be reached from this analysis: 1) PELEUS is required for the correct root development; 2) loss of JASON results in upregulation of root development.

3.4.3 PELEUS co-localizes with vacuolar markers in tissues and somatic cells

To uncover the localization of PELEUS in cells and tissues, a vector carrying the *PELEUS* gene, fused with GFP as a fluorescent tag, was constructed. Additionally, a second

construct carrying the β-Glucuronidase gene under the native *PELEUS* promoter was created to check the pattern of PELEUS expression in the entire plant using the GUS reporter system.

According to the *PELEUS* gene expression profile (Klepikova et al., 2016), the protein is constitutively expressed in almost all plant organs (Fig. 27). The GUS staining assay confirmed this, as the blue staining indicating *PELEUS* expression could be noticed in whole 7 days old seedlings (Fig. 28A and B), 14 days old seedlings (Fig. 28C), mature leaves (Fig. 28D, E and F), inflorescence (Fig. 28G and H) and the husks of mature siliques (Fig. 28I and J). Importantly, both the Klepikova atlas and the GUS staining assay demonstrated the presence of PELEUS in meiotic buds.

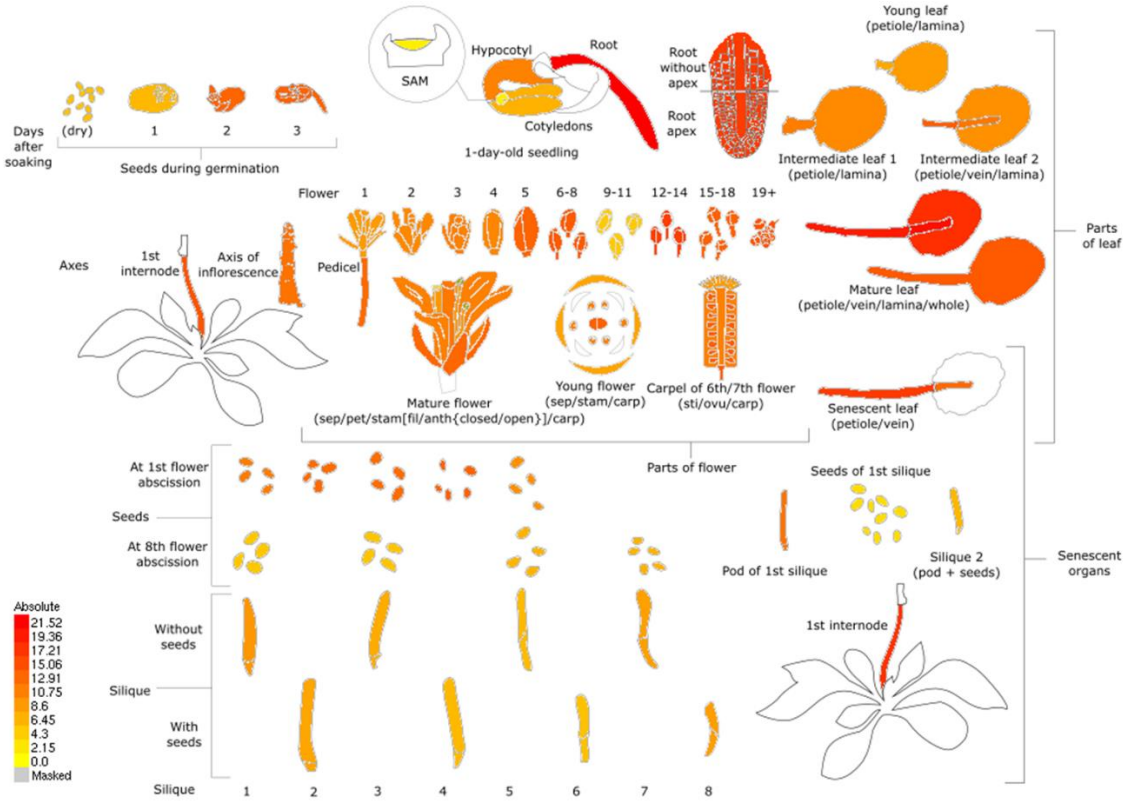

Figure 27 The Klepikova atlas, portraying expression of PELEUS in all developmental stages of *A. thaliana* [modified from arabidopsis.org, based on Klepikova et al., 2016].

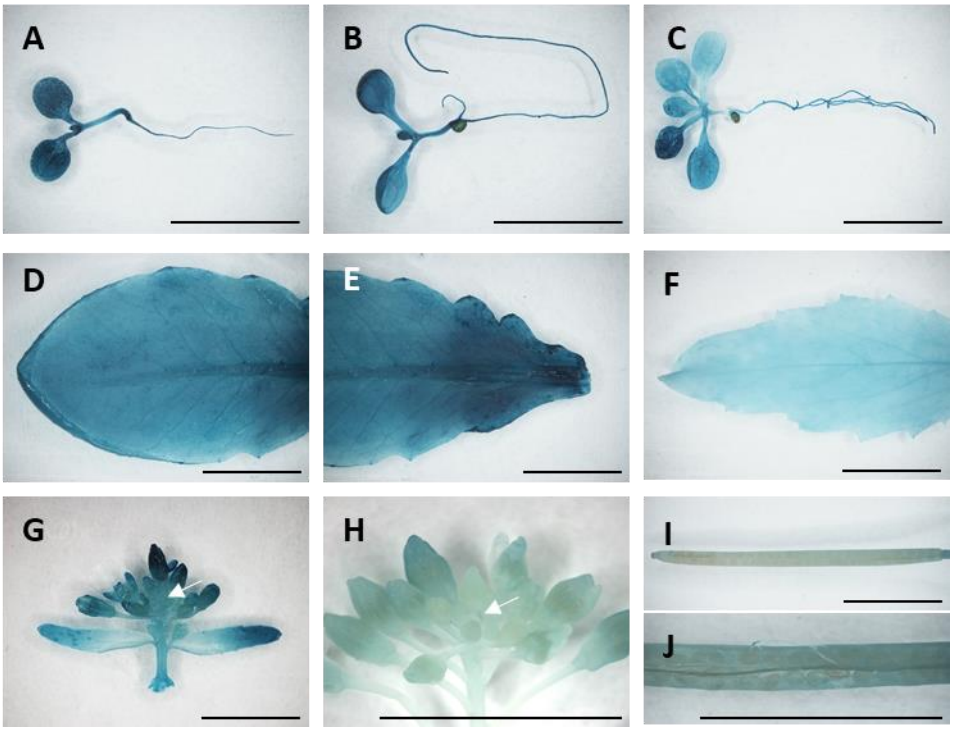

Figure 28 Histochemical GUS staining in tissues of Pro:*PELEUS*-GUS plants. (A) 7-days old seedling. (B) 7-days old seedling, with more visible staining in root. (C) 14-days old seedling. (D) Top of the leaf of a 4-weeks old plant. (E) Bottom of the leaf of a 4-weeks old plants. (F) Cauline leaf of a 5-weeks old plant. (G) Inflorescence of 5-weeks old plant with strong expression. (H) Inflorescence of a 5-weeks old plant with weaker expression of the promoter. Meiotic buds in (G) and (H) are indicated by arrows. (I) Mature silique. (J) Mature silique with seeds visible through the husks. Scale bars are 1 mm.

Since GUS staining assay showed high expression of PELEUS in roots, this organ was chosen to visualize expression of the GFP fusion construct. Moreover, roots are easy to handle, provide clear images and enable fast analysis. Roots of ca. 5 days old Col-0 and *jason* seedlings transformed with pH7FWG0-gPEL-GFP were placed in a drop of water on a microscope slide and imaged under confocal microscope.

Inspecting entire roots confirmed that PELEUS was indeed abundantly expressed in this organ, and that the genetic background of the plant did not affect its localization (Fig. 29A). Moreover, it seemed that PELEUS has two main positions. In old, elongated cells PELEUS was located closely to the plasma membrane, although the irregular signal shape suggests that it was not part of the PM itself. This led to the idea that PELEUS might be located to the tonoplast of the vacuole, as such old cells tend to contain large vacuoles within their cytosols (Fig. 29B). In younger cells, closer to the root tip, PELEUS was located on the surface of a large, circular organelle, likely the vacuole (Fig. 29C) and in a small organelle of which the identity remained elusive. Depending on the viewed fragment of

the root, the GFP signal was observed to be either part of the vacuole or contained within cytoplasm as an individual structure.

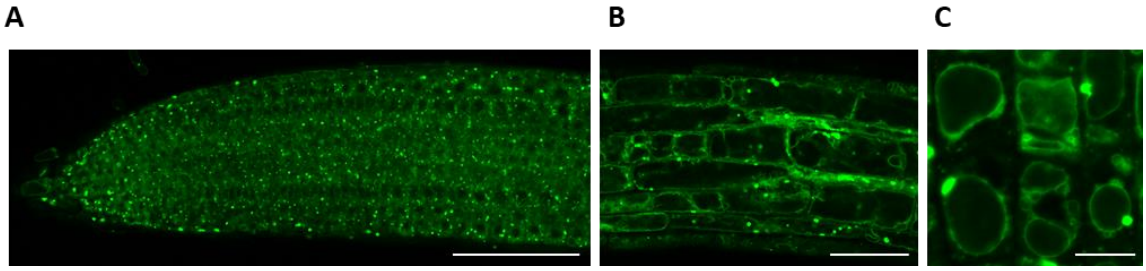

Figure 29 PELEUS's cellular localization, imaged in roots of 5-days old *jason* seedlings. Only *jason* seedlings are shown, as the localization in Col-0 roots is identical (as shown in Fig. 30). (A) A view on the whole root tip, portraying the abundance of signal. Scale bar is 100 µm. (B) Root section with old, vacuolated cells. Scale bar is 50 µm. (C) A zoomed in photo of young root cells. Scale bar is 10 µm.

To confirm PELEUS's cellular localization, a cross between PELEUS-GFP and various marker lines from the wave lines collection (Geldner et al., 2009) was established. All markers were fused with mCherry to easily distinguish their red signal from PELEUS's green signal, and to enable the possible use of DAPI for chromosome staining. The signals were imaged in 4-6 days old roots, in the layers of cells beneath the surface. Chosen marker lines are listed in the Supplemental Table 1.

It quickly became apparent, that the large, circular structures visualized by PELEUS-GFP overlapped with the signal generated by RabG3F, which is a GTPase essential for trafficking between late endosome and vacuole (Cui et al., 2014), as well as with the vacuolar marker VAMP711 (Fig. 30). Interestingly, there was no overlap between PELEUS-GFP and RabF2a, which is another GTPase involved in the trafficking of soluble proteins between the pre-vacuolar compartment (PVC, also known as multivesicular body, MVB) and the central vacuole (Jung et al., 2011). Thus, colocalization analysis confirmed vacuolar localization of PELEUS and, in agreement with the aforementioned proteomic analyses by Endler et al., and Shimaoka et al., strongly suggested that PELEUS was localized on the vacuolar membrane, tonoplast. However, colocalization analysis did not uncover the identity of the bright signal spots. It was excluded that they belong to the Golgi apparatus or to MVBs, since PELEUS-GFP did not colocalize with any of them. Furthermore, they could not have been related to plasma membrane nor ER, which are structurally different. Although this signal was abundant in roots, its origin remained elusive.

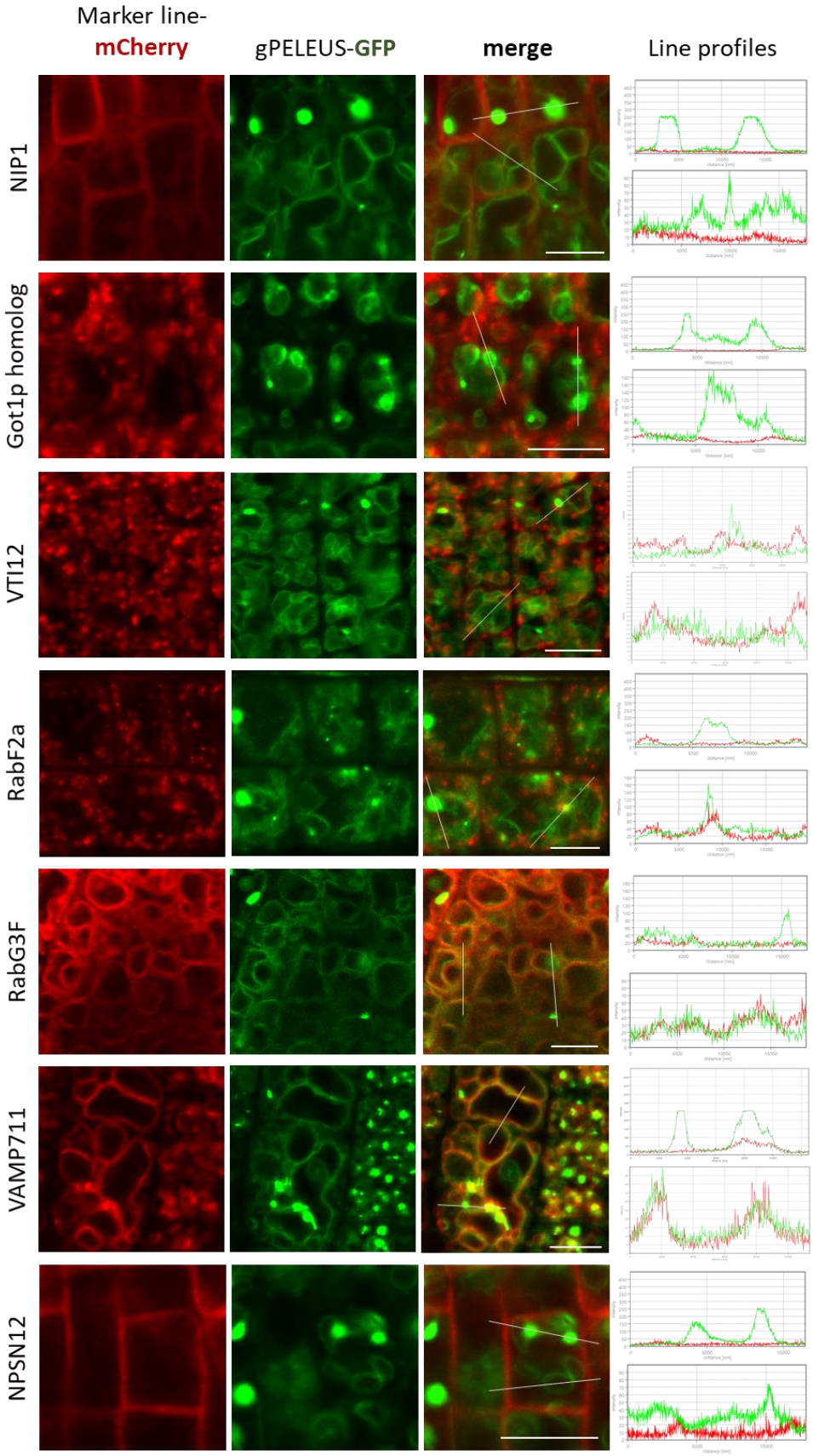

Figure 30 Co-localization analysis of genomic PELEUS fused with GFP (gPEL-GFP, green signal) and marker lines from the wave lines collection (red signal), imaged in 4-6 days old wild-type roots. Scale bar is 10 µm. The upper line profile from each pair includes the bright spot.

3.4.4 PELEUS partially maintains the vacuolar localization in meiocytes

Upon discovering that PELEUS localized to the vacuole in somatic tissues, the question was whether PELEUS shared the same localization during meiosis. To assess that, selected seedlings used for co-localization analysis in roots were propagated until flowering, and the intact anthers were stained with DAPI for confocal imaging.

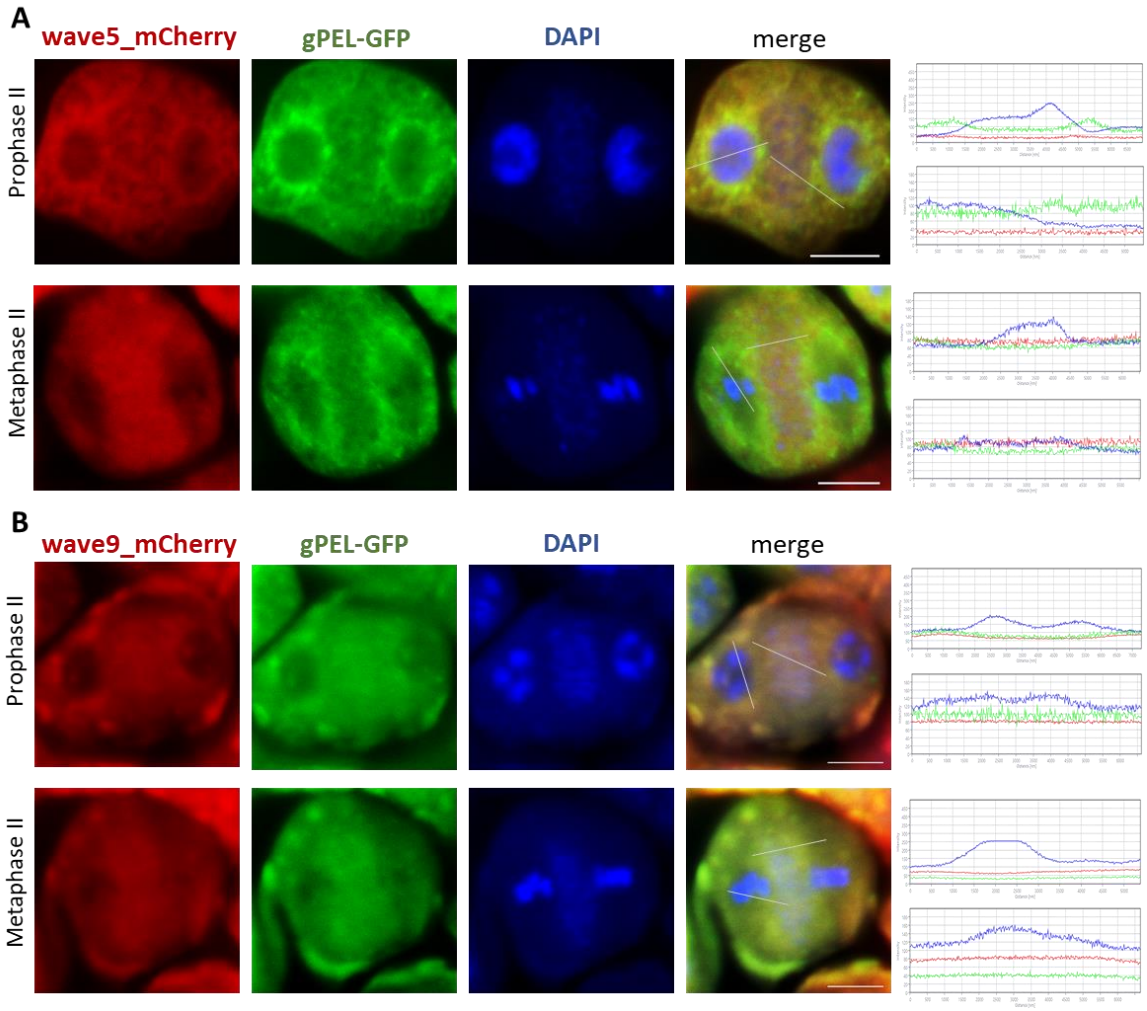

Figure 31 Co-localization of vacuole markers with PELEUS-GFP in wild-type meiocytes. (A) RabG3F (wave5_mCherry, red signal) and gPEL-GFP (green signal). (B) VAMP711 (wave9_mCherry, red signal) and PELEUS-GFP (green signal). Scale bars are 5 µm. The upper line profile from each pair always includes the chromosomes, whereas the lower one – the organelle band.

At prophase II, RabG3F localized to the phragmoplast and the nuclear envelope, while PELEUS did not share phragmoplast localization, but occurred at the nuclear envelope. PELEUS remained partially overlapped with RabG3F at metaphase II, as both signals were detected on the rim of the organelle band and the chromosomes (Fig. 31A). However, RabG3F was observed within the organelle band, whereas PELEUS was not. The co-localization of VAMP711 and PELEUS around prophase II nuclei and metaphase II organelle

band further supported the vacuolar localization of PELEUS (Fig. 31B). Taken together, PELEUS partially co-localizes with vacuole not only in roots, but also in meiocytes.

Since the co-localization analysis was performed under the wild-type background, it was important to assess the PELEUS localization in *jason* meiocytes. Therefore, *jason* plants transformed with the gPEL-GFP construct were prepared for the whole anther analysis and metaphase II meiocytes inside intact anthers were inspected with a confocal microscope.

As observed in the co-localization analysis, in wild-type metaphase II PELEUS surrounded both chromosomes and the organelle band, creating a distinct, previously not observed structure (Fig. 32). Knowing that the JASON protein maintains the organelle band in metaphase II and belongs to it, as it co-localized with both Golgi- and PM-derived vesicles (Brownfield et al., 2015), it was surprising to note that PELEUS was not a part of that same structure, despite impacting it. Moreover, PELEUS's metaphase II distribution in *jason* background was significantly affected by the loss of JASON protein. Upon disruption of the organelle band, PELEUS scattered in the cytoplasm in the disorganized manner, similarly to how organelles and vesicles disperse in the *jason* mutant (Fig. 32). This finding shows that the localization of PELEUS during meiosis depends on the functional JASON protein.

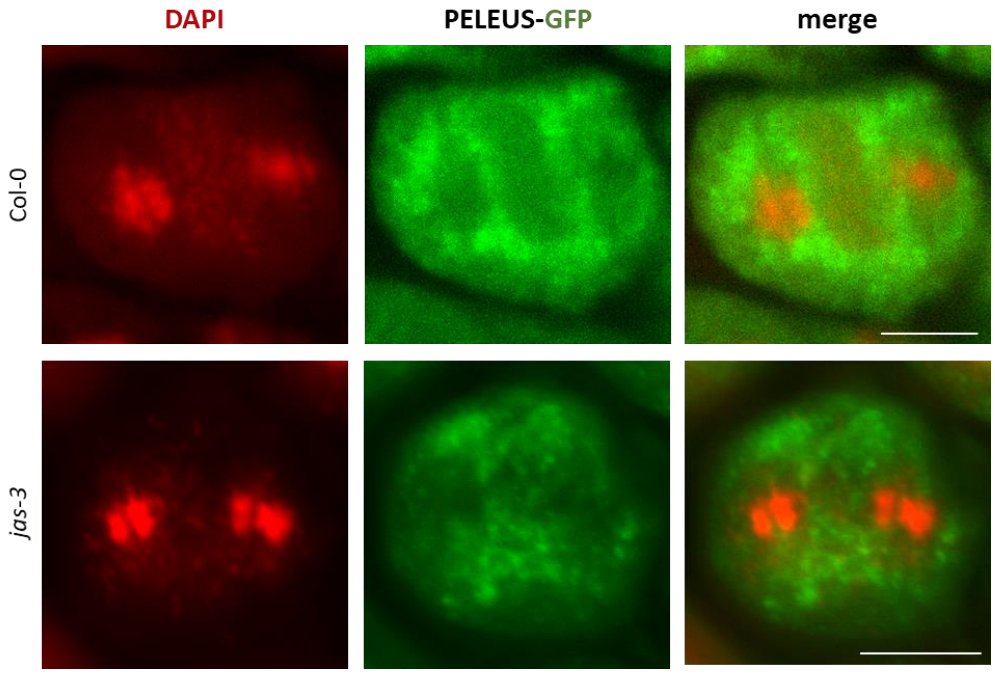

Figure 32 Localization of PELEUS in metaphase II meiocytes under wild-type and *jason* backgrounds. Chromosomes were stained with DAPI (false red) and PELEUS is visible in green. Scale bar is 5 µm.

3.4.5 PELEUS acts upstream of UBQ-LIKE1 as its negative regulator

It was reported that AT5G11700 interacts with the ubiquitin-like protein 1 (UBQ-like1, AT5G42220) in a proteome-wide binary protein-protein interaction map for *A. thaliana* (Dreze et al., 2011). UBQ-like1 consists of 879 amino acids, is found in the cytosol and presumably also in the nucleus, and is annotated as part of the BAT3 complex. In mammals, this complex is responsible for transferring tail-anchored proteins from the SGTA (Small glutamine-rich tetratricopeptide repeat-containing protein alpha) onto GET3 (Guided entry of tail-anchored proteins factor 3) ATPase, in order to target them to the endoplasmic reticulum (ER). The BAT3 complex also functions as a chaperone for polypeptides targeted to the proteasome for degradation in the ER-associated protein degradation pathway (ERAD) (Leznicki et al., 2010). Unsurprisingly, UBQ-like1 was annotated to be involved in this process as well. Moreover, it putatively binds mRNA, misfolded protein and polyubiquitinylated protein (Gaudet et al., 2011) and interacts with PUB22 – an E3 ubiquitin-protein ligase (Stegmann et al., 2012). Interaction between UBQ-like1 and AT5G11700 would mean that PELEUS is either involved in the protein degradation process, or is degraded in this process itself.

Protein degradation is an important process aimed at keeping homeostasis in the cell by removing misfolded proteins. This process is ongoing also during meiosis, since many important regulatory proteins, such as cyclins or CDK inhibitors, need to be recycled in order to progress through the divisions. Thus, it was interesting to know, whether the involvement of PELEUS in the protein degradation process is the cause of its suppressing function. To address this question, *jas;pel* was crossed with the *ubq-like1* single mutant to generate *jas;ubq-like1* and *jas;pel*;*ubq-like1* mutants. Pollen size analysis of the *ubq-like1* single mutant displayed its wild-type-like pollen phenotype and revealed the typical *jason* phenotype of the new *jas;ubq-like1* double mutant, making it clear that UBQ-like1 itself was not involved in the meiosis regulation (Fig. 33A). However, the increased amount of diploid pollen in the *jas;pel*;*ubq-like1* triple mutant, especially very large pollen grains with the area bigger than 800 μm^2, suggested that upon *ubq-like1* mutation, *peleus* was no longer able to suppress *jason* as efficiently as in the *jas;pel* double mutant (Fig. 33B). Meiotic products of four different triple mutants were subsequently tested to confirm this finding. Indeed, all triple mutant plants displayed nearly as many dyads and triads as the *jas* single mutant and clearly more than the *jas;pel* double mutant [percentage of dyads in each triple mutant: 24.5% (n=106), 42.6% (n=115), 28.6% (n=329) and 22.5% (n=191)].

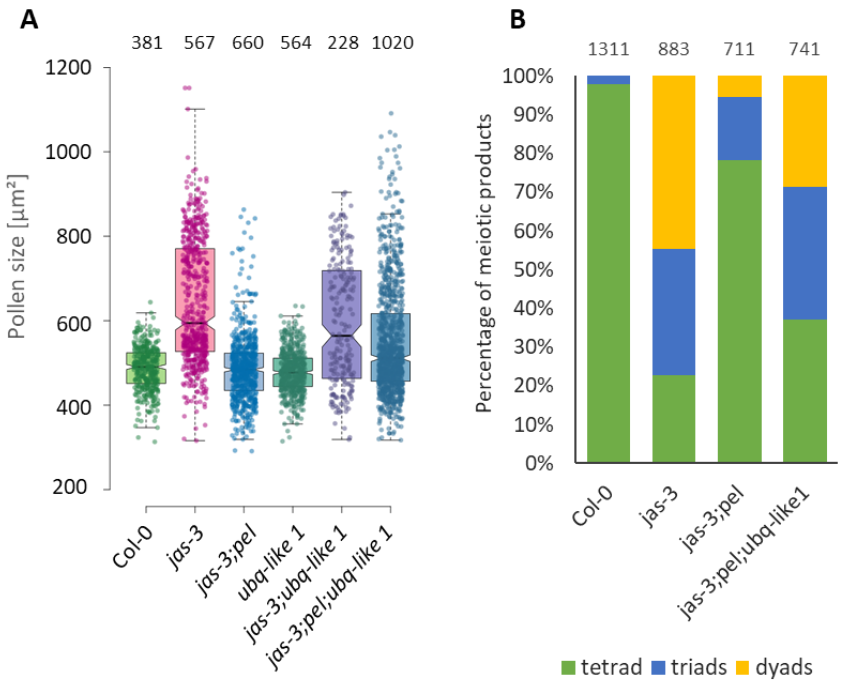

Figure 33 Phenotypic analysis of *jas;pel;ubq-like1* triple mutant. (A) Pollen size analysis. (B) Tetrad formation analysis. In both cases the results are the averaged data from 4-5 plants.

This finding implies that suppression of *jason* by *peleus* relies on UBQ1-mediated protein degradation and that defects in this process may enhance abnormal meiotic progression in meiosis II.

4. Discussion

My aim is to elucidate the mechanisms of unreduced gamete formation by uncovering the genetic mechanisms governing this process. This was performed by analyzing the *Arabidopsis thaliana* male meiotic mutant *jason* and its suppressor: *peleus*. The *jason* mutant produces a mix of normal and abnormal meiotic products, the latter correlating with the loss of the organelle band at metaphase II, a subsequent disorganized movement of meiotic spindles and eventual mis-segregation of sister chromatids (Erilova et al., 2009, Brownfield et al., 2015). Suppressors of the *jason* mutant are genes, which upon mutation, revert the *jason* phenotype to wild-type. Such suppressors were found by screening an EMS-mutagenized population of *jason* plants. During this PhD study, a forward genetics approach was utilized to identify *peleus* as one of these suppressors that was further characterized. *PELEUS* encodes an unknown protein localized in the vacuolar membrane, the tonoplast, and is expressed almost constitutively in all organs throughout plant development. The mutation of *PELEUS* does not interfere with meiotic progression, but mutating this gene in the *jason* mutant caused partial organelle band recovery, leading to the significant increase in correct meiotic products. Interestingly, the same *peleus* mutation suppressed also *atps1* – another male meiotic mutant which disrupts the organelle band at metaphase II similar to *jason* (D'Erfurth et al., 2008; Brownfield et al., 2015). An in-depth analysis of the causes underlying this phenotype ruled out several hypothetical explanations, leaving one convincing model: loss of PELEUS leads to the enrichment of a particular type of vesicles within the organelle band, eventually partially restoring its function.

4.1 *PELEUS* negatively regulates *JASON* and *ATPS1*

The most important characteristics of *PELEUS* is its function during male meiosis. The *peleus* single mutant did not exhibit any meiotic phenotype, unless the mutation was caused under the *jason* or *atps1* background. The latter two mutants cause disruption in the organelle band after prophase II, which is believed to be the primary reason for the spindles to move freely within the cytoplasm. Depending on the random positioning of the spindles during metaphase II, chromosome segregation can yield either dyads, triads, or tetrads (D'Erfurth et al., 2008; Erilova et al., 2009; Brownfield et al., 2015). Mutation of *PELEUS* did not fully restore the organelle band, but often led to a decreased loss of organelles from the band, which, if sufficiently established, physically prevented chromosome sets and spindles from coming into contact with each other. So far, this finding was made predominantly for the organelles which contain DNA (mitochondria and

chloroplasts), while Golgi- and ER-derived vesicles were proved not to be affected by mutation of *PELEUS*, because they remained dispersed in the cell just as in *jason* (Fig. 13).

Another important observation regarding the meiotic phenotypes of both *jas* and *jas;pel* mutants was the lack of polyads among the abnormal gametes. Polyads are meiotic products consisting of more than four nuclei and usually the result of lagging chromosomes, which do not merge with the remaining chromosomes of their sets before cytokinesis. Absence of polyads indicates that separation of sister chromatids was correct, and emphasizes that the observed dyads and triads in mutant meiocytes were caused by incorrect (fused or tripolar) spindle orientation in the *jas* mutant. However, those two abnormal types of spindles were never observed in the *jas;pel* mutant, the parallel spindle being the only one noted in the double mutant, which suggests that some other factor must have influenced the generation of triads and dyads. The most likely explanation is the occasionally detected closer distance between the metaphase II chromosome sets (Fig. 11C), indicating the closer distance between the meiotic spindles. If this was caused by the absence of the organelle band, the segregated sister chromatids may be pulled too close to another set of sister chromatids at telophase II, preventing the division plane to be established between them and thus forming one nucleus instead of two.

The fact that *peleus* suppressed both *jason* and *atps1* through efficient distancing of the homolog sets and/or spindles at metaphase II, despite both meiotic mutants presumably acting through different genetic pathways (Brownfield et al., 2015) suggests that the PELEUS protein acts downstream of JASON and ATPS1 as their negative regulator.

4.2 *peleus* suppresses *jason* by mediating actin cytoskeleton rearrangement

In the *jason* mutant meiocytes, actin cytoskeleton was discovered to be altered. The filamentous actin was first observed at metaphase I, but gradually depolymerized during meiotic progression and formed a mix of thicker bundles and short specks (Fig. 18). Moreover, actin was located in the decondensed nuclei in both prophase II and telophase II nuclei, which is indicative of the microfilaments' abnormal characteristics (Pendleton et al., 2003). Actin depolymerization was also found in the *jas;pel* meiocytes, although the progression of this process was visibly slower. There was no enrichment of actin within prophase II nuclei and the density of filamentous actin in many metaphase II meiocytes was higher than in the *jas* meiocytes. Additional abnormal polymerization of actin within the organelle band was spotted in both mutants, although it was usually more pronounced in the double mutant. Moreover, telophase II meiocytes of the double mutant often retained the actin structures observed in wild-type, despite the general depolymerization of the cytoskeleton at this stage.

In plants, actin cytoskeleton (rather than the microtubules) is considered to be more important for the intracellular transport of the organelles such as ER, Golgi, mitochondria or peroxisomes (Verchot-Lubicz & Goldstein, 2010). This movement is mediated by myosins – motor proteins, which utilize energy from the hydrolysis of ATP to walk on the microfilaments. There are three models representing the transport of the organelles induced by the cytoskeleton: 1) active transport by myosins binding individual organelles and carrying them along the microfilaments, which generates cytoplasmic streaming; 2) in-direct transport, in which the ER is transported by myosins, and other organelles are associated with the ER surface; 3) passive movement, in which some organelles are carried by the hydrodynamic flow generated by the cytoplasmic streaming (reviewed in Geitmann & Nebenführ, 2015; Nebenführ & Dixit, 2018). Although it is unknown which model is valid in the case of chondriokinesis (the rearrangement of organelles during cell division; Bakowski, 1938), the actin cytoskeleton is believed to play an important role in the positioning of organelles during cell division (Sheahan et al., 2004; Tchórzewska & Bednara, 2011). Nevertheless, the involvement of microtubules should not be omitted, as in some species microtubules were found to encapsulate the organelles, forcing them into a specific configuration (Tchórzewska et al., 2008).

The only abnormal characteristic of the microtubular cytoskeleton of the *jas* mutant is the presence of fused, parallel and tripolar spindles. Since the actin microfilaments are mostly depolymerized, it prevents the myosins from travelling along them and generating the cytoplasmic streaming. As such, the dispersion of the organelles in prometaphase II cannot be caused by the active process of redistributing organelles in the cytoplasm by myosins, but rather through a passive process of diffusion. This may be possible due to the observable low density of actin strands in the cytoplasm (Fig. 18). The *peleus* mutation was observed to slow down the depolymerization process and often trigger the abnormal polymerization within the organelle band, which could act as an additional scaffold for the organelles in the cell equator. Both of those occurrences are likely to be responsible for the partial organelle band reformation at metaphase II. More so, since chloroplasts (visualized with DAPI staining) may be less mobile and less prone to diffuse outside of the cell center due to their large size than the small Golgi- and ER-derived vesicles.

The denser actin cytoskeleton in the *jas;pel* mutant also explains the maintained chromosome distance at metaphase II. In the study on mouse oocytes, it was proven that dense and immobile actin network prevents the microtubular spindle from migrating to the cell pole (Holubcová et al., 2013). It is thus very likely, that actin cytoskeleton functions as a stabilizer of meiotic spindles. I hypothesize that this can happen either by causing the neighboring cytoplasm to become dense and immobilize the spindle, or by generating an

abnormally polymerized structure at the cell equator, that acts as a physical barrier in the absence of complete organelle band, which prevents the spindles from fusing with each other. Moreover, the aforementioned study demonstrated how Rab11a-positive vesicles, actin cytoskeleton, and myosins cooperate in regulating asymmetric spindle positioning (Holubcová et al., 2013). Rab11a-positive vesicles were found to be sequestering and clustering actin nucleators, which regulate the density of actin network in a myosin-Vb-dependent manner and eventually allow the microtubular spindle to migrate to the required position in the cell. JASON and PELEUS are highly unlikely to be myosins or formins (plant actin nucleators, Blanchoin & Staiger, 2010) due to lack of any of the conserved domains. Nevertheless, the relationship presented in that study highlights the involvement of vesicles in cytoskeleton regulation and shows a very interesting direction for further research.

Taken together, I propose that loss of PELEUS under the *jason* background slows down or alleviates the effects of the actin depolymerization caused by the mutation of *JASON*. As such, dense enough actin filaments are able to keep some of the chloroplasts and/or mitochondria in the organelle band either by forming an impenetrable, dense cytosol areas surrounding the spindles, or by aggregating in the cell equator and thus providing additional physical barrier. In the case of the 40% of metaphase II meiocytes, which were observed to lack the organelle band (Fig. 11B), the actin network should still be sufficiently dense around the chromosomes and spindles to prevent them from merging, resulting in the maintained chromosome sets distance (Fig. 11C). The occasional occurrence of the abnormal F-actin polymerization within the organelle band at prophase II and prometaphase II may act as an additional physical barrier for the chromosomes and spindles or as a scaffold for the organelles, supporting their correct positioning within the band.

4.3 PELEUS is a vacuole membrane-localized protein

In somatic tissues, e.g. in roots, PELEUS was found at two positions: the membrane of a large, semi-circular organelle and a large spot of high signal intensity. The membrane organelle was identified as belonging to vacuole, because PELEUS-GFP co-localized with RabG3F, a marker of vesicles traveling from prevacuolar compartments to vacuoles, and with VAMP711, a SNARE protein localized in the vacuolar membrane, the tonoplast. This localization was confirmed by two proteomic papers analyzing proteins of the tonoplast, which found AT5G11700 to be an unidentified, glycine-rich, multi-transmembrane domain protein (Endler et al., 2006; Shimaoka et al., 2004). Preliminary analysis of the co-localization in meiocytes seems to corroborate this finding, especially for the RabG3F co-

localization. Crosses with other selected marker lines did not give an answer as to the second localization, but plasma membrane, ER, Golgi, TGN and RabF2a-positive vesicles, transporting proteins from pre-vacuolar compartments to the central vacuole, can be excluded (Fig. 30).

Multiple studies confirm vacuoles to be highly dynamic organelles, capable of creating various structures, such as large vacuoles, tubular vacuoles (Hicks et al., 2004), transvacuolar strands, sheets (Uemura et al., 2002) and bulbs (Saito et al., 2002, also reviewed in Oda et al., 2009). Bulbs are small, spherical, often double-membraned structures characterized by the strong fluorescence, and thus fit the characteristics of the unrecognized structure observed during the co-localization analysis. Although the fluorescence was not observed within the bulbs (Saito et al., 2002), the strong signal within the spherical structures in the tissues expressing PELEUS-GFP may be attributed to the GFP artefacts. As such, alternative methods must be used in order to confirm that PELEUS localizes to various forms of the vacuole.

An interesting localization was observed by studying the signal of PELEUS-GFP in meiocytes. As expected, the localization of PELEUS was dynamic in both wild-type and *jas*, following the movement of variety of organelles during meiotic progression. When the nuclei were decondensed at prophase II, PELEUS localized closely to the chromosomes, nearly touching the nuclear envelope (Fig. 31A). Remarkably, during metaphase II in wild-type, PELEUS was surrounding the intact organelle band, without being part of it, as if it was part of a cage-like structure holding the organelles in place. This structure was not visible in the *jas* background, as the GFP signal was scattered throughout the cytoplasm and around the meiotic spindle. The disorganized pattern observed in *jason* metaphase II suggests that PELEUS localizes to vesicles, because upon loss of JASON protein, PELEUS disperses similarly to mitochondria, chloroplasts, Golgi- and ER-derived vesicles (Fig. 9, 13 and 32). High-quality images of PELEUS and vacuole markers are crucial to determine, whether this localization pattern is related to a spatial organization of the vacuole. More so, since the fate of this organelle during meiosis remains unclear.

It is unknown whether vacuoles are inherited from the PMC or created *de novo* from fusion of post-Golgi vesicles with prevacuoles, from fusion of young vacuoles or from enlargement of the ER tubules (Lin et al., 2001). In meiosis of summer snowflake (*Leucojum aestivum* L.), vacuoles were observed to exist in pollen mother cells, but decrease in size and number during meiotic divisions (Ekici & Dane, 2012), most likely to provide space for spindles and chromosomes. Vacuoles were also found in post-meiotic haploid microspores of *A. thaliana* undergoing pollen development (Yamamoto et al.,

2003). Study on *jason*, which did not detect any tonoplast signal in male meiocytes, seems to corroborate the hypothesis regarding vacuole *de novo* formation in *A. thaliana* (Fig. 4) (Brownfield et al., 2015). As such, it is likely that *A. thaliana* pollen inherits vacuoles from PMC in the form of vesicles, and that PELEUS protein localizes to the surface of these vesicles.

The location of PELEUS raises the question how the vacuole is involved in the suppression of *jason*. Since PELEUS was predicted by several programs to be a multi-transmembrane protein, it is expected to be an integral part of the tonoplast. In this case, whatever its role in the suppression of *jason* is, it needs to be carried out from the surface of the vacuole. Little is known about plant Ephrin receptors; therefore, it is possible that their primary localization is the tonoplast and they participate in protein degradation by interacting with UBQ-LIKE1. It is also possible that PELEUS is interacting with the cytoskeleton, because multiple studies point to a connection between vacuoles and actin. The actin depolymerizing agents cytochalasin D, latrunculin B, or bistheonellide A, affected vacuole dynamics in *A. thaliana* leaf epidermal cells (Uemura et al., 2002), as well as vacuolar morphology and motion in lily pollen tubes (Lovy-Wheeler et al., 2007). Direct evidence of the interaction between vacuole and actin cytoskeleton was provided by partial co-localization of these two structures (Higaki et al., 2006; Kutsuna et al., 2003) and proteomic analysis, which revealed that myosins – motor proteins travelling on microfilaments – are part of the vacuolar proteome (Carter et al., 2004). Most importantly, depolymerization of actin caused disruption of tubular vacuole membranes in tobacco BY-2 cells in favor of spherical vacuoles formation (Kutsuna et al., 2003). Altered actin cytoskeleton and an abundance of PELEUS-GFP-colocalized speckles of high fluorescence intensity were both noted in the *jason* mutant, solidifying the notion that actin may act as a regulator of the vacuole structure (discussed in Wang et al., 2017). These findings provide an exciting direction for further research to uncover the involvement of vacuole in the correct meiotic progression.

4.4 The *peleus* mutant requires a functional protein degradation pathway to suppress *jason*

PELEUS was found to physically interact with UBQ-like1 (At5g42220) through Yeast two hybrid (Y2H) assay (Dreze et al., 2011). In line with the protein interaction, the *jas;pel;ubq-like1* triple mutant showed an enhanced *jason* phenotype, indicating the existence of the functional relationship between PELEUS and UBQ-LIKE1.

UBQ-like1 is presumably a part of the BAT3 complex, which in mammals participates in the ER-associated protein degradation (ERAD), a pathway involved in protein quality

control by dislocating misfolded, ubiquitin-tagged proteins from ER to the cytoplasm for proteasomal degradation. In plants, the ERAD pathway was found to be required e.g. for optimal plant growth under selenate stress (Van Hoewyk, 2018) or for plant survival under high-salt stress (Liu et al., 2011). Overloaded or dysfunctional ERAD pathway is assumed to be one of the factors causing programmed cell-death in early tapetal cells under stressful conditions, which results in male sterility (De Storme & Geelen, 2014). UBQ-LIKE1 itself is also supposed to function in mRNA binding, misfolded protein binding, and polyubiquitin modification-dependent protein binding. Ubiquitination is important during prophase I, when the three complexes SCF, APC/C, and HEI10 regulate correct meiotic progression by successively targeting for degradation various proteins responsible for maintenance of chromosome structure, homologous recombination, axis assembly, and for the formation of the synaptonemal complex (reviewed in Bolaños-Villegas et al., 2018 and Orr et al., 2021). These three complexes are multi-protein E3 ligases, which share the RING domain, that interacts with the E2 ubiquitin-conjugating enzyme to mark proteins for degradation in the proteasome by transferring ubiquitin from E2 onto a target's lysine. APC/C is also necessary for the regulation of transition from the first to the second division by the degradation of A- and B-type cyclins (Bulankova et al., 2013), which was described in more detail in chapter 2.2.3 on the examples of the *TAM* and *OSD1* genes.

Since protein degradation is crucial for the transition from meiosis I to meiosis II, the *ubq-like1* mutant was expected to display a meiotic phenotype. However, similarly to *peleus*, no phenotype was found unless *UBQ-LIKE1* gene was mutated in the *jas;pel* double mutant. This triple mutant showed a phenotype reverted to that of *jas;pel*, suggesting that suppression of *jason* by *peleus* requires a functional protein degradation system.

Despite the cross-talk of PELEUS and UBQ-LIKE1, and the involvement of UBQ-LIKE1 in protein degradation, it seems unlikely that PELEUS is a target of UBQ-LIKE1. If that was the case, then *jas* and *jas;pel* mutants should exhibit the same phenotype, because PELEUS should be marked for degradation by UBQ-LIKE1 in *jason* background. As this is not the case, UBQ-LIKE1 should be acting downstream of PELEUS. The current working model of this interaction is portrayed in the figure 34.

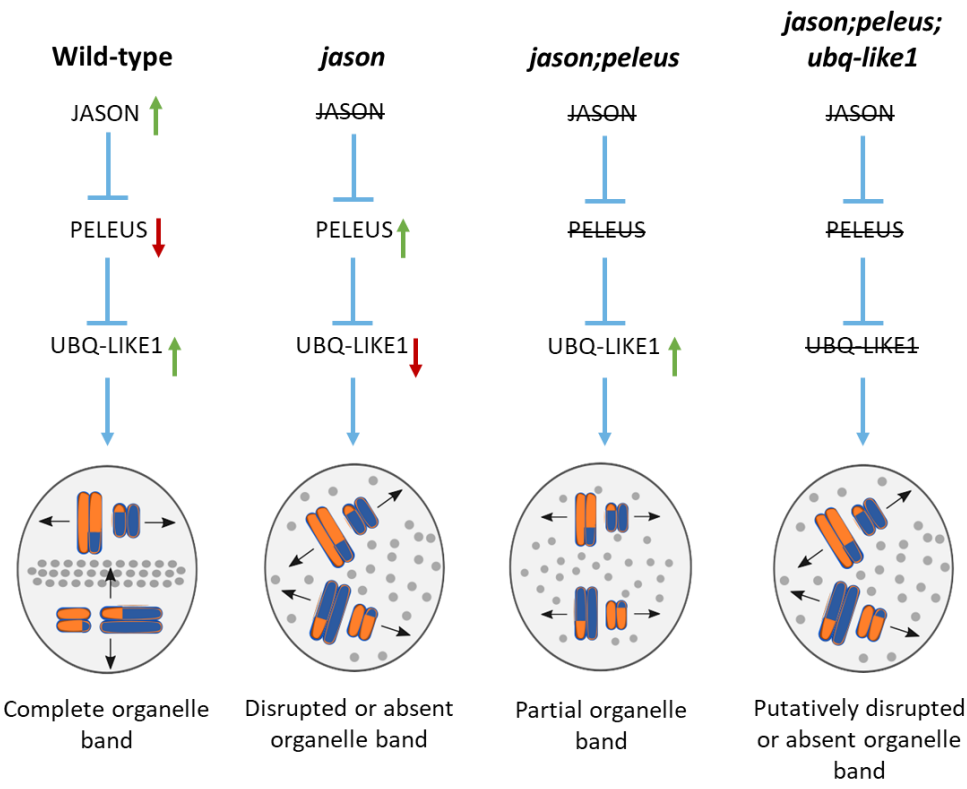

Figure 34 Proposed scheme of the molecular pathway involving all important proteins described in this study. Green arrow indicates activity, whereas red arrow – lack of activity. Crossed out protein name indicates loss of functionality.

According to the findings, functional JASON is the primary reason for the maintenance of the organelle band at metaphase II in wild-type *Arabidopsis*. Upon loss of JASON, the organelle band becomes disrupted and the organelles spread in the cytoplasm. As previously described, the scattering of the organelles is likely to be initiated by the gradually depolymerizing actin cytoskeleton, which loses its thickness and thus is unable to generate the density gradient holding the organelles in the cell equator.

In the *jas;pel* mutant, lack of functional PELEUS causes the meiotic phenotype to partially revert, corroborating the finding that *PELEUS* is a negative regulator of meiosis. The *peleus* mutation is likely slowing down the depolymerization of the actin cytoskeleton, which allows the microfilaments to partially retain their functionality at prometaphase II and metaphase II. As such, many mitochondria and/or chloroplasts remain in the organelle band, providing the physical barrier for the chromosome sets. Moreover, even in the occasional absence of the organelle band, actin network is dense enough to separate chromosome sets and/or the spindles, which increases the chance of the correct sister chromatid segregation at anaphase II.

In the *jas;pel;ubq-like1* triple mutant, loss of functional UBQ-LIKE1 results in the phenotype reverting to the *jas*-like. Although the organelle band was not observed in the triple mutant, the quantitative analysis of the meiotic products strongly indicates the disruption of this structure. This suggests that the protein degradation pathway is involved in the regulation of meiosis II progression, although the cytoplasmic components, which is marked for degradation by the UBQ-LIKE1, remains to be discovered.

Taken together, I suggest that JASON, the protein located in the Golgi- and PM-derived vesicles and responsible for the maintenance of organelle band at prometaphase II, is also involved in the regulation of the actin cytoskeleton structure. PELEUS – a putative ephrin type-B receptor located on the tonoplast – is a negative meiotic regulator, which mediates the depolymerization of the actin network downstream of JASON. UBQ-LIKE1, the last known component of the pathway, is a putatively cytoplasmic protein involved in the ERAD pathway and a positive meiotic regulator. I believe this study documents the existence of the connection between endomembrane system, actin cytoskeleton, and the degradation pathway, and sheds more light on the importance of their interaction in the regulation of meiosis.

5. Summary

Meiosis is essential for sexual reproduction, and abnormalities in this process often lead to ploidy instability. In wild-type organism, meiocytes undergo one round of DNA replication and two subsequent nuclear divisions in order to produce gametes with half of the somatic diploid DNA amount. In many dicotyledonous plants, such as *Arabidopsis thaliana*, cytokinesis is simultaneous, as in: it occurs after completion of meiosis, dividing mother cell into four daughter cells at once. In plants with this type of cytokinesis, two perpendicular meiotic spindles at metaphase II are separated by organelles and vesicles forming the "organelle band" located in the cell equator. This structure is believed to provide a physical barrier between two chromosome sets, preventing them from coming into contact and mediating their correct segregation.

In Arabidopsis, JASON (JAS) protein is required for maintaining the organelle band during male meiosis. In the *jas* mutant, the absence of JASON in the organelle band causes this structure to disrupt, thus allowing the meiotic spindles to move freely and rearrange into fused, tripolar or parallel orientations. Abnormal meiotic spindle positioning leads to incorrect chromosome segregation and eventually yields an increased amount of unreduced (2n) male gametes, which mature into viable diploid pollen grains.

To further investigate the mechanisms of unreduced gamete formation, a suppressor screen was performed, aimed to find mutants that form reduced (1n) gametes in the presence of *jas* mutation. One of the mutants, *peleus*, was able to suppress 2n gamete formation in the *jas* background through partial recovery of the organelle band and maintaining the distance between chromosome sets at metaphase II. *PELEUS* was subsequently identified to be the gene encoding a putative ephrin type-B receptor. The PELEUS protein was found to be located on the tonoplast in both somatic and germline cells and to interact with UBQ-LIKE1 protein involved in the ER-associated degradation pathway.

The wild-type-like phenotype of the *peleus* single mutant suggests that PELEUS is a negative regulator of JASON, whereas *jason*-like phenotype of the *jas;pel;ubq-like1* mutant implies that UBQ-LIKE1 acts downstream of PELEUS, and that protein degradation pathway is required for the suppressing mechanism. The relationship between vacuolar localization of PELEUS and PELEUS's function in *jason* was not yet uncovered, although it is hypothesized that there is a connection between tonoplast's motor proteins and actin cytoskeleton; more so, since microfilaments were found to be severely altered in both *jason* and *jas;pel*. Lastly, partial recovery of the mitochondria and/or chloroplasts within

the organelle band and the maintenance of chromosome distance at metaphase II of *jas;pel* indicate the involvement of the actin network in the regulation of meiotic progression. I suggest that the density of the actin cytoskeleton is one of the main components responsible for the maintenance of the organelle band shape, and that loss of JASON causes the actin network to destabilize and depolymerize. Additional mutation in the *PELEUS* gene reverts the *jason* phenotype by slowing down the depolymerization process and allows the microfilaments to retain their partial functionality in the crucial metaphase II stage.

Taken together, the observations made throughout the course of this Ph.D. study led me to propose that unreduced gamete formation in *jason* and suppression of this process by *peleus* depend on the correlation between vacuolar network, actin cytoskeleton, and protein degradation, although the specific pathway remains to be determined. I believe these findings provide new insights into the mechanisms of unreduced gamete formation in Arabidopsis, especially the involvement of the endomembrane system and degradation pathway in regulating meiotic progression.

6. References

Adams, K. L., & Wendel, J. F. (2005). Polyploidy and genome evolution in plants. *Current Opinion in Plant Biology*, *8*(2), 135–141. https://doi.org/10.1016/j.pbi.2005.01.001

Albertin, W., & Marullo, P. (2012). Polyploidy in fungi: Evolution after whole-genome duplication. *Proceedings of the Royal Society B: Biological Sciences*, *279*(1738), 2497–2509. https://doi.org/10.1098/rspb.2012.0434

Ambrose, J. C., & Cyr, R. (2007). The kinesin ATK5 functions in early spindle assembly in Arabidopsis. *Plant Cell*, *19*(1), 226–236. https://doi.org/10.1105/tpc.106.047613

Ascough, G. D., Van Staden, J., & Erwin, J. E. (2008). Effectiveness of colchicine and oryzalin at inducing polyploidy in Watsonia lepida N.E. Brown. *HortScience*, *43*(7), 2248–2251. https://doi.org/10.21273/hortsci.43.7.2248

Assaad, F. F., Huet, Y., Mayer, U., & Jürgens, G. (2001). The cytokinesis gene KEULE encodes a Sec1 protein that binds the syntaxin KNOLLE. *Journal of Cell Biology*, *153*(3), 531–543. https://doi.org/10.1083/jcb.152.3.531

Augustine, R. C. (2018). Nuclear positioning requires a tug-of-war between kinesin motors. *Plant Cell*, *30*(7), 1383–1384. https://doi.org/10.1105/tpc.18.00499

Bakowski, Z. (1938): Versuch einer Klassifizierung der Chondriokinese bei Korrnophyten. Acta Soc. Bot. Pol. 15: 323-369.

Bannigan, A., Lizotte-Waniewski, M., Riley, M., & Baskin, T. I. (2008). Emerging molecular mechanisms that power and regulate the anastral mitotic spindle of flowering plants. *Cell Motility and the Cytoskeleton*, *65*(1), 1–11. https://doi.org/10.1002/cm.20247

Barba-Gonzalez, R., Miller, C.T., Ramanna, M.S., van Tuyl, J.M. (2006) Nitrous oxide (N2O) induces 2n gametes in sterile F1 hybrids between Oriental 9 Asiatic lily (Lilium) hybrids and leads to intergenomic recombination. Euphytica 148:303–309

Bent, A. F., & Clough, S. J. (1998). Floral dip: a simplified method for Agrobacterium-mediated transformation of Arabidopsis thaliana. *Plant Journal*, *16*(6), 735–743.

Bicknell, R. A., & Koltunow, A. M. (2004). Understanding apomixis: Recent advances and remaining conundrums. *Plant Cell*, *16*(SUPPL.), 228–245. https://doi.org/10.1105/tpc.017921

Birchler, J. A., Auger, D. L., & Riddle, N. C. (2003). In Search of the Molecular Basis of Heterosis. *Plant Cell*, *15*(10), 2236–2239. https://doi.org/10.1105/tpc.151030

Birchler, J. A., & Veitia, R. A. (2007). The gene balance hypothesis: From classical genetics to modern genomics. *Plant Cell*, *19*(2), 395–402. https://doi.org/10.1105/tpc.106.049338

Blanc, G., Barakat, A., Guyot, R., Cooke, R., & Delseny, M. (2000). Extensive duplication and reshuffling in the Arabidopsis genome. *Plant Cell*, *12*(7), 1093–1101. https://doi.org/10.1105/tpc.12.7.1093

Blanc, G., Hokamp, K., & Wolfe, K. H. (2003). A recent polyploidy superimposed on older large-scale duplications in the Arabidopsis genome. *Genome Research*, *13*(2), 137–144. https://doi.org/10.1101/gr.751803

Blanchoin, L., & Staiger, C. J. (2010). Plant formins: Diverse isoforms and unique molecular mechanism.

Biochimica et Biophysica Acta - Molecular Cell Research, *1803*(2), 201–206. https://doi.org/10.1016/j.bbamcr.2008.09.015

Bogart, J. P. (1980). *Plenum Press, New York 1980*. 341–378.

Bolaños-Villegas, P., Xu, W., Martínez-García, M., Pradillo, M., & Wang, Y. (2018). Insights Into the Role of Ubiquitination in Meiosis: Fertility, Adaptation and Plant Breeding. *The Arabidopsis Book*, *16*, e0187. https://doi.org/10.1199/tab.0187

Bretagnolle, F., & Thompson, J. D. (1995). Gametes with the somatic chromosome number: mechanisms of their formation and role in the evolution of autopolyploid plants. *New Phytologist*, *129*(1), 1–22. https://doi.org/10.1111/j.1469-8137.1995.tb03005.x

Brown, R. C., & Lemmon, B. E. (1989). *Minispindles and cytoplasmic domains in microsporogenesis of orchids*. 26–32.

Brown, R. C., & Lemmon, B. E. (2001). *The cytoskeleton and spatial control of cytokinesis in the plant life cycle*. 35–49.

Brown, R. O. Y. C., & Lemmon, B. E. (1992). *Control of division plane in normal and griseofulvin-treated microsporocytes of Magnolia*. *1038*, 1031–1038.

Brown, S. S., & Spudich, J. A. (1979). Cytochalasin inhibits the rate of elongation of actin filament fragments. *Journal of Cell Biology*, *83*(3), 657–662. https://doi.org/10.1083/jcb.83.3.657

Brownfield, L., & Köhler, C. (2011). Unreduced gamete formation in plants: Mechanisms and prospects. *Journal of Experimental Botany*, *62*(5), 1659–1668. https://doi.org/10.1093/jxb/erq371

Brownfield, L., Yi, J., Jiang, H., Minina, E. A., Twell, D., & Köhler, C. (2015). Organelles maintain spindle position in plant meiosis. *Nature Communications*, *6*. https://doi.org/10.1038/ncomms7492

Bulankova, P., Akimcheva, S., Fellner, N., & Riha, K. (2013). Identification of Arabidopsis Meiotic Cyclins Reveals Functional Diversification among Plant Cyclin Genes. *PLoS Genetics*, *9*(5). https://doi.org/10.1371/journal.pgen.1003508

Burk, L. G. (1967). An Interspecific Bridge-Cross. *Journal of Heredity*, *58*(5), 215–218. https://doi.org/10.1093/oxfordjournals.jhered.a107591

Cabout, S., Leask, M. P., Varghese, S., Yi, J., Peters, B., Conze, L. L., Köhler, C., & Brownfield, L. (2017). The meiotic regulator JASON utilizes alternative translation initiation sites to produce differentially localized forms. *Journal of Experimental Botany*, *68*(15), 4205–4217. https://doi.org/10.1093/jxb/erx222

Carputo, D., Basile, B., Cardi, T., & Frusciante, L. (2000). Erwinia resistance in backcross progenies of Solanum tuberosum × S. tarijense and S. tuberosum (+) S. Commersonii hybrids. *Potato Research*, *43*(2), 135–142. https://doi.org/10.1007/BF02357954

Carter, C., Pan, S., Zouhar, J., Avila, E. L., Girke, T., & Raikhel, N. V. (2004). The vegetative vacuole proteome of Arabidopsis thaliana reveals predicted and unexpected proteins. Plant Cell, 16(12), 3285–3303. https://doi.org/10.1105/tpc.104.027078

Chen, C., Marcus, A., Li, W., Hu, Y., Vielle Calzada, J. P., Grossniklaus, U., Cyr, R. J., & Ma, H. (2002). The Arabidopsis ATK1 gene is required for spindle morphogenesis in male meiosis. *Development*, *129*(10), 2401–2409. https://doi.org/10.1242/dev.129.10.2401

Comai, L. (2005). The advantages and disadvantages of being polyploid. *Nature Reviews Genetics*, *6*(11),

836–846. https://doi.org/10.1038/nrg1711

Consiglio, F., Carputo, D., Monti, L., & Conicella, C. (2004). Exploitation of genes affecting meiotic non-reduction and nuclear restitution: Arabidopsis as a model? *Sexual Plant Reproduction*, *17*(2), 97–105. https://doi.org/10.1007/s00497-004-0215-y

Cui, Y., Zhao, Q., Gao, C., Ding, Y., Zeng, Y., Ueda, T., Nakano, A., & Jiang, L. (2014). Activation of the Rab7 GTPase by the MON1-CCZ1 complex is essential for PVC-to-vacuole trafficking and plant growth in Arabidopsis. *Plant Cell*, *26*(5), 2080–2097. https://doi.org/10.1105/tpc.114.123141

D'Erfurth, I., Jolivet, S., Froger, N., Catrice, O., Novatchkova, M., & Mercier, R. (2009). Turning meiosis into mitosis. *PLoS Biology*, *7*(6). https://doi.org/10.1371/journal.pbio.1000124

D'Erfurth, I., Jolivet, S., Froger, N., Catrice, O., Novatchkova, M., Simon, M., Jenczewski, E., & Mercier, R. (2008). Mutations in AtPS1 (Arabidopsis thaliana Parallel Spindle 1) lead to the production of diploid pollen grains. *PLoS Genetics*, *4*(11), 1–9. https://doi.org/10.1371/journal.pgen.1000274

Dawe, R. K. (1998). Meiotic chromosome organization and segregation in plants. *Annual Review of Plant Biology*, *49*, 371–395. https://doi.org/10.1146/annurev.arplant.49.1.371

Dawe, R. K., Lowry, E. G., Gent, J. I., Stitzer, M. C., Swentowsky, K. W., Higgins, D. M., Ross-Ibarra, J., Wallace, J. G., Kanizay, L. B., Alabady, M., Qiu, W., Tseng, K. F., Wang, N., Gao, Z., Birchler, J. A., Harkess, A. E., Hodges, A. L., & Hiatt, E. N. (2018). A Kinesin-14 Motor Activates Neocentromeres to Promote Meiotic Drive in Maize. *Cell*, *173*(4), 839-850.e18. https://doi.org/10.1016/j.cell.2018.03.009

De Jaeger-Braet, J., Krause, L., Buchholz, A., & Schnittger, A. (2021). Heat stress reveals a specialized variant of the pachytene checkpoint in meiosis of Arabidopsis thaliana . The Plant Cell. https://doi.org/10.1093/plcell/koab257

De Storme, N., & Geelen, D. (2011). The arabidopsis mutant jason produces unreduced first division restitution male gametes through a parallel/ fused spindle mechanism in meiosis II. *Plant Physiology*, *155*(3), 1403–1415. https://doi.org/10.1104/pp.110.170415

De Storme, N., & Geelen, D. (2013). Sexual polyploidization in plants - cytological mechanisms and molecular regulation. *New Phytologist*, *198*(3), 670–684. https://doi.org/10.1111/nph.12184

De Storme, N., & Geelen, D. (2014). The impact of environmental stress on male reproductive development in plants: Biological processes and molecular mechanisms. *Plant, Cell and Environment*, *37*(1), 1–18. https://doi.org/10.1111/pce.12142

Dhonukshe, P., Baluška, F., Schlicht, M., Hlavacka, A., Šamaj, J., Friml, J., & Gadella, T. W. J. (2006). Endocytosis of cell surface material mediates cell plate formation during plant cytokinesis. *Developmental Cell*, *10*(1), 137–150. https://doi.org/10.1016/j.devcel.2005.11.015

Dinis, A. M., & Mesquita, J. F. (1993). The F-actin distribution during microsporogenesis in Magnolia soulangeana Soul. (Magnoliaceae). *Sexual Plant Reproduction*, *6*(1), 57–63. https://doi.org/10.1007/BF00227584

Dissmeyer N, Nowack MK, Pusch S, Stals H, Inzé D, Grini PE, Schnittger A (2007) T-loop phosphorylation of Arabidopsis CDKA;1 is required for its function and can be partially substituted by an aspartate residue. Plant Cell 19: 972 – 985

Dowling, T. E., & Secor, C. L. (1997). The role of hybridization and introgression in the diversification of animals. *Annual Review of Ecology and Systematics*, *28*(33), 593–619.

https://doi.org/10.1146/annurev.ecolsys.28.1.593

Dreze, M., Carvunis, A.-R., Charloteaux, B., Galli, M., Pevzner, S. J., Tasan, M., Ahn, Y.-Y., Balumuri, P., Barabasi, A.-L., Bautista, V., Braun, P., Byrdsong, D., Chen, H., Chesnut, J. D., Cusick, M. E., Dangl, J. L., de los Reyes, C., Dricot, A., Duarte, M., … Yazaki, J. (2011). Evidence for Network Evolution in an Arabidopsis Interactome Map. *Science*, *333*(6042), 601–607. https://doi.org/10.1126/science.1203877

Edwards, K., Johnstone, C., & Thompson, C. (1991). A simple and rapid method for the preparation of plant genomic DNA for PCR analysis. *Nucleic Acids Research*, *19*(6), 1349. https://doi.org/10.13031/aim.20141900217

Ekici, N., & Dane, F. (2012). Ultrastructural studies on the sporogenous tissue and anther wall of Leucojum aestivum (amaryllidaceae) in different developmental stages. Anais Da Academia Brasileira de Ciencias, 84(4), 951–960. https://doi.org/10.1590/S0001-37652012005000061

Endler, A., Meyer, S., Schelbert, S., Schneider, T., Weschke, W., Peters, S. W., Keller, F., Baginsky, S., Martinoia, E., & Schmidt, U. G. (2006). Identification of a vacuolar sucrose transporter in barley and arabidopsis mesophyll cells by a tonoplast proteomic approach. *Plant Physiology*, *141*(1), 196–207. https://doi.org/10.1104/pp.106.079533

Erilova, A., Brownfield, L., Exner, V., Rosa, M., Twell, D., Scheid, O. M., Hennig, L., & Köhler, C. (2009). Imprinting of the Polycomb group gene MEDEA serves as a ploidy sensor in Arabidopsis. *PLoS Genetics*, *5*(9). https://doi.org/10.1371/journal.pgen.1000663

Falconer, M. M., Donaldson, G., & Seagull, R. W. (1988). *MTOCs in Higher Plant Cells : an Immunofluorescent Study of Microtubule Assembly Sites Following Depolymerization by APM*. 46–55.

Fan, L., Li, R., Pan, J., Ding, Z., & Lin, J. (2015). Endocytosis and its regulation in plants. *Trends in Plant Science*, *20*(6), 388–397. https://doi.org/10.1016/j.tplants.2015.03.014

Fang, J., Yuan, S., Li, C., Jiang, D., Zhao, L., Peng, L., Zhao, J., Zhang, W., & Li, X. (2018). Reduction of ATPase activity in the rice kinesin protein Stemless Dwarf 1 inhibits cell division and organ development. *Plant Journal*, *96*(3), 620–634. https://doi.org/10.1111/tpj.14056

Fullmer, E.L. (1899) The development of the microsporangia and microspores of Hemerocallis fulva. Bot Gaz 28:8–18

Führer, E. (2004). Polyploid spermatozoa in Pityogenes chalcographus and Ips typographus (Coleoptera: Scolytidae). *European Journal of Entomology*, *101*(1), 21–27. https://doi.org/10.14411/eje.2004.005

Furt, F., Liu, Y. C., Bibeau, J. P., Tüzel, E., & Vidali, L. (2013). Apical myosin XI anticipates F-actin during polarized growth of Physcomitrella patens cells. *Plant Journal*, *73*(3), 417–428. https://doi.org/10.1111/tpj.12039

Gaudet, P., Livstone, M. S., Lewis, S. E., & Thomas, P. D. (2011). Phylogenetic-based propagation of functional annotations within the Gene Ontology consortium. *Briefings in Bioinformatics*, *12*(5), 449–462. https://doi.org/10.1093/bib/bbr042

Geitmann, A., & Nebenfähr, A. (2015). Navigating the plant cell: Intracellular transport logistics in the green kingdom. *Molecular Biology of the Cell*, *26*(19), 3373–3378. https://doi.org/10.1091/mbc.E14-10-1482

Geldner, N., Dénervaud-Tendon, V., Hyman, D.L., Mayer, U., Stierhof, Y.D., Chory, J. (2009) Rapid, combinatorial analysis of membrane compartments in intact plants with a multicolor marker set. Plant J.;59(1):169-78. PMID: 19309456

Grant, V. (1953). Cytogenetics of the hybrid Gilia millefoliata x achilleaefolia. Chromosoma, 5(1), 372–390. https://doi.org/10.1007/bf01271494

Gould, S. J., & Vrba, E. S. (1982). Exaptation—a Missing Term in the Science of Form. *Paleobiology*, *1*(N/A), 4–15. https://doi.org/10.1017/S0094837300004310

Haig, D. & Westoby, M. (1991). Genomic im- printing in endosperm: its effect on seed development in crosses between species, and between different ploidies ofthe same species, and its implications for the evo- lution of apomixis. Philos. Trans. R. Soc. London Ser. B 333:1–13

Haider, N. (2013). The origin of the B-genome of bread wheat (Triticum aestivum L.). *Russian Journal of Genetics*, *49*(3), 263–274. https://doi.org/10.1134/S1022795413030071

Hamada, T. (2014). Microtubule organization and microtubule-associated proteins in plant cells. In International Review of Cell and Molecular Biology (1st ed., Vol. 312). Elsevier Inc. https://doi.org/10.1016/B978-0-12-800178-3.00001-4

Hartwig, J. H., & Stossel, T. P. (1979). Cytochalasin B and the structure of actin gels. *Journal of Molecular Biology*, *134*(3), 539–553. https://doi.org/10.1016/0022-2836(79)90366-8

Hatsugai, N., Nakatsuji, A., Unten, O., Ogasawara, K., Kondo, M., Nishimura, M., Shimada, T., Katagiri, F., & Hara-Nishimura, I. (2018). Involvement of adapter protein complex 4 in hypersensitive cell death induced by avirulent bacteria. *Plant Physiology*, *176*(2), 1824–1834. https://doi.org/10.1104/pp.17.01610

Hicks, G. R., Rojo, E., Hong, S., Carter, D. G., & Raikhel, N. V. (2004). Geminating pollen has tubular vacuoles, displays highly dynamic vacuole biogenesis, and requires VACUOLESS1 for proper function. *Plant Physiology*, *134*(3), 1227–1239. https://doi.org/10.1104/pp.103.037382

Higaki, T., Kutsuna, N., Okubo, E., Sano, T., & Hasezawa, S. (2006). Actin microfilaments regulate vacuolar structures and dynamics: Dual observation of actin microfilaments and vacuolar membrane in living tobacco BY-2 cells. *Plant and Cell Physiology*, *47*(7), 839–852. https://doi.org/10.1093/pcp/pcj056

Higgins, D. M., Nannas, N. J., & Dawe, R. K. (2016). The maize Divergent spindle-1 (Dv1) gene encodes a kinesin-14A motor protein required for meiotic spindle pole organization. *Frontiers in Plant Science*, *7*(AUG2016), 1–11. https://doi.org/10.3389/fpls.2016.01277

Hiwatashi, Y., Sato, Y., & Doonan, J. H. (2014). Kinesins have a dual function in organizing microtubules during both tip growth and cytokinesis in physcomitrella patens. *Plant Cell*, *26*(3), 1256–1266. https://doi.org/10.1105/tpc.113.121723

Holubcová, Z., Howard, G., & Schuh, M. (2013). Vesicles modulate an actin network for asymmetric spindle positioning. *Nature Cell Biology*, *15*(8), 937–947. https://doi.org/10.1038/ncb2802

Jaillon, O., Aury, J. M., Noel, B., Policriti, A., Clepet, C., Casagrande, A., Choisne, N., Aubourg, S., Vitulo, N., Jubin, C., Vezzi, A., Legeai, F., Hugueney, P., Dasilva, C., Horner, D., Mica, E., Jublot, D., Poulain, J., Bruyère, C., … Wincker, P. (2007). The grapevine genome sequence suggests ancestral hexaploidization in major angiosperm phyla. *Nature*, *449*(7161), 463–467. https://doi.org/10.1038/nature06148

Jiao, Y., Wickett, N. J., Ayyampalayam, S., Chanderbali, A. S., Landherr, L., Ralph, P. E., Tomsho, L. P., Hu, Y.,

Liang, H., Soltis, P. S., Soltis, D. E., Clifton, S. W., Schlarbaum, S. E., Schuster, S. C., Ma, H., Leebens-Mack, J., & Depamphilis, C. W. (2011). Ancestral polyploidy in seed plants and angiosperms. *Nature*, *473*(7345), 97–100. https://doi.org/10.1038/nature09916

Jung, C., Lee, G. J., Jang, M., Lee, M., Lee, J., Kang, H., Sohn, E. J., & Hwang, I. (2011). Identification of Sorting Motifs of AtβFruct4 for Trafficking from the ER to the Vacuole Through the Golgi and PVC. *Traffic*, *12*(12), 1774–1792. https://doi.org/10.1111/j.1600-0854.2011.01276.x

Kang, XY., Zhu, ZT. (1997). A study on the 2n pollen vitality and germinant characteristics of white populars. Acta Bot Yunnanica. 1997;19:402–6.

Katepa-Mupondwa, F. M., Christie, B. R., & Michaels, T. E. (2002). An improved breeding strategy for autotetraploid Alfalfa (Medicago sativa L.). *Euphytica*, *123*(1), 139–146. https://doi.org/10.1023/A:1014488307000

Kellis, M., Birren, B. W., & Lander, E. S. (2004). Proof and evolutionary analysis of ancient genome duplication in the yeast. *Nature*, *428*(3), 617–624. http://www.broad.mit.edu/seq/YeastDuplication

Kidwell, K. K., Bingham, E. T., Woodfield, D. R., & Osborn, T. C. (1994). Relationships among genetic distance, forage yield and heterozygosity in isogenic diploid and tetraploid alfalfa populations. *Theoretical and Applied Genetics*, *89*(2–3), 323–328. https://doi.org/10.1007/BF00225162

Kim, D., Paggi, J. M., Park, C., Bennett, C. and Salzberg, S. L. (2019). Graph-based genome alignment and genotyping with HISAT2 and HISAT-genotype. Nat Biotechnol 37, 907-915.

Kim, S. J., & Brandizzi, F. (2014). The plant secretory pathway: An essential factory for building the plant cell wall. *Plant and Cell Physiology*, *55*(4), 687–693. https://doi.org/10.1093/pcp/pct197

Kitamura, S., Akutsu, M., & Okazaki, K. (2009). Mechanism of action of nitrous oxide gas applied as a polyploidizing agent during meiosis in lilies. *Sexual Plant Reproduction*, *22*(1), 9–14. https://doi.org/10.1007/s00497-008-0084-x

Klepikova, A.V., Kasianov, A.S., Gerasimov, E.S, Logacheva, M.D., Penin, A.A. (2016) A high resolution map of the Arabidopsis thaliana developmental transcriptome based on RNA-seq profiling. https://doi.org/10.1111/tpj.13312

Köhler, C., Mittelsten Scheid, O., & Erilova, A. (2010). The impact of the triploid block on the origin and evolution of polyploid plants. *Trends in Genetics*, *26*(3), 142–148. https://doi.org/10.1016/j.tig.2009.12.006

Kosetsu, K., Matsunaga, S., Nakagami, H., Colcombet, J., Sasabe, M., Soyano, T., Takahashi, Y., Hirt, H., & Machida, Y. (2010). The MAP kinase MPK4 Is required for cytokinesis in Arabidopsis thaliana. *Plant Cell*, *22*(11), 3778–3790. https://doi.org/10.1105/tpc.110.077164

Kutsuna, N., & Hasezawa, S. (2002). Dynamic organization of vacuolar and microtubule structures during cell cycle progression in synchronized tobacco BY-2 cells. *Plant and Cell Physiology*, *43*(9), 965–973. https://doi.org/10.1093/pcp/pcf138

Kutsuna, N., Kumagai, F., Sato, M. H., & Hasezawa, S. (2003). Three-Dimensional Reconstruction of Tubular Structure of Vacuolar Membrane Throughout Mitosis in Living Tobacco Cells. *Plant and Cell Physiology*, *44*(10), 1045–1054. https://doi.org/10.1093/pcp/pcg124

Lee, Y. R.J., Giang, H. M., & Liu, B. (2001). A novel plant kinesin-related protein specifically associates with the phragmoplast organelles. *Plant Cell*, *13*(11), 2427–2439. https://doi.org/10.1105/tpc.13.11.2427

Lee, Yuh Ru Julie, & Liu, B. (2007). Cytoskeletal motor proteins in plant cell division. *Plant Cell*

Monographs, *9*(August), 169–193. https://doi.org/10.1007/7089_2007_127

Leznicki, P., Clancy, A., Schwappach, B., & High, S. (2010). Bat3 promotes the membrane integration of tail-anchored proteins. *Journal of Cell Science*, *123*(13), 2170–2178. https://doi.org/10.1242/jcs.066738

Li, J., Blanchoin, L., & Staiger, C. J. (2015). Signaling to actin stochastic dynamics. *Annual Review of Plant Biology*, *66*, 415–440. https://doi.org/10.1146/annurev-arplant-050213-040327

Lim, K. B., Ramanna, M. S., De Jong, J. H., Jacobsen, E., & Van Tuyl, J. M. (2001). Indeterminate meiotic restitution (IMR): A novel type of meiotic nuclear restitution mechanism detected in interspecific lily hybrids by GISH. *Theoretical and Applied Genetics*, *103*(2–3), 219–230. https://doi.org/10.1007/s001220100638

Lin, Y., Seals, D. F., Randall, S. K., & Yang, Z. (2001). Dynamic localization of rop GTPases to the tonoplast during vacuole development. Plant Physiology, 125(1), 241–251. https://doi.org/10.1104/pp.125.1.241

Liqin, G., Jianguo, Z., Xiaoxia, L., & Guodong, R. (2019). Polyploidy-related differential gene expression between diploid and synthesized allotriploid and allotetraploid hybrids of Populus. *Molecular Breeding*, *39*(5). https://doi.org/10.1007/s11032-019-0975-6

Liu, L., Cui, F., Li, Q., Yin, B., Zhang, H., Lin, B., Wu, Y., Xia, R., Tang, S., & Xie, Q. (2011). The endoplasmic reticulum-associated degradation is necessary for plant salt tolerance. *Cell Research*, *21*(6), 957–969. https://doi.org/10.1038/cr.2010.181

Liu, Z., Gao, J., Cui, Y., Klumpe, S., Xiang, Y., Erdmann, P. S., & Jiang, L. (2021). Membrane imaging in the plant endomembrane system. Plant Physiology, 185(3), 562–576. https://doi.org/10.1093/PLPHYS/KIAA040

Lopes, M. A., & Larkins, B. A. (1993). Endosperm origin, development, and function. *Plant Cell*, *5*(10), 1383–1399. https://doi.org/10.1105/tpc.5.10.1383

Lovy-Wheeler, A., Cárdenas, L., Kunkel, J. G., & Hepler, P. K. (2007). Differential organelle movement on the actin cytoskeleton in lily pollen tubes. *Cell Motility and the Cytoskeleton*, *64*(3), 217–232. https://doi.org/10.1002/cm.20181

Lukowitz, W., Gillmor, C. S., & Scheible, W.-R. R. (2000). Positional cloning in Arabidopsis. Why it feels good to have a genome initiative working for you. *Plant Physiology*, *123*(3), 795–805. https://doi.org/10.1104/pp.123.3.795

Magnard, J. L., Yang, M., Chen, Y. C. S., Leary, M., & McCormick, S. (2001). The Arabidopsis gene tardy asynchronous meiosis is required for the normal pace and synchrony of cell division during male meiosis. *Plant Physiology*, *127*(3), 1157–1166. https://doi.org/10.1104/pp.010473

Makarevitch, I., Phillips, R. L., & Springer, N. M. (2008). Profiling expression changes caused by a segmental aneuploid in maize. *BMC Genomics*, *9*, 1–13. https://doi.org/10.1186/1471-2164-9-7

Marasek-Ciolakowska, A., Ramanna, M. S., Arens, P., & Van Tuyl, J. M. (2012). Breeding and cytogenetics in the genus Tulipa. *Floriculture and Ornamental Biotechnology*, *6*(SPEC.ISS.1), 90–97.

Marcus, A. I., Ambrose, J. C., Blickley, L., Hancock, W. O., & Cyr, R. J. (2002). Arabidopsis thaliana protein, ATK1, is a minus-end directed kinesin that exhibits non-processive movement. *Cell Motility and the Cytoskeleton*, *52*(3), 144–150. https://doi.org/10.1002/cm.10045

Marcus, A.I., Li, W., Ma, H., Cyr, R.J. (2003) A kinesin mutant with an atypical bipolar spindle undergoes normal mitosis. Mol. Biol. Cell 14:1717–26

Marquette, W. (1907) Manifestations of polarity in plant cells which apparently are without centrosomes. Beih Bot Centralbl Abt I 21:281–303

Marquette, W. (1908) Concerning the organization of the spore mother-cells of Marsilia quadrifolia. Trans Wisconsin Acad Sci Arts Let 16:81–106

Mason, A. S., Nelson, M. N., Yan, G., & Cowling, W. A. (2011). Production of viable male unreduced gametes in Brassica interspecific hybrids is genotype specific and stimulated by cold temperatures. *BMC Plant Biology*, *11*. https://doi.org/10.1186/1471-2229-11-103

McCoy, T. J., & Rowe, D. E. (1986). Single cross alfalfa (Medicago sativa L.) hybrids produced via 2n gametes and somatic chromosome doubling: experimental and theoretical comparisons. *Theoretical and Applied Genetics*, *72*(1), 80–83. https://doi.org/10.1007/BF00261459

McLysaght, A., Hokamp, K., & Wolfe, K. H. (2002). Extensive genomic duplication during early chordate evolution. *Nature Genetics*, *31*(2), 200–204. https://doi.org/10.1038/ng884

Mendoza, H. A., & Haynes, F. L. (1974). Genetic basis of heterosis for yield in the autotetraploid potato. *Theoretical and Applied Genetics*, *45*(1), 21–25. https://doi.org/10.1007/BF00281169

Menges, M., De Jager, S. M., Gruissem, W., & Murray, J. A. H. (2005). Global analysis of the core cell cycle regulators of Arabidopsis identifies novel genes, reveals multiple and highly specific profiles of expression and provides a coherent model for plant cell cycle control. *Plant Journal*, *41*(4), 546–566. https://doi.org/10.1111/j.1365-313X.2004.02319.x

Mercier, R., Armstrong, S. J., Horlow, C., Jackson, N. P., Makaroff, C. A., Vezon, D., Pelletier, G., Jones, G. H., & Franklin, F. C. H. (2003). The meiotic protein SWI1 is required for axial element formation and recombination initiation in Arabidopsis. *Development*, *130*(14), 3309–3318. https://doi.org/10.1242/dev.00550

Mercier, R., Vezon, D., Bullier, E., Motamayor, J. C., Sellier, A., Lefèvre, F., Pelletier, G., & Horlow, C. (2001). SWITCH1 (SWI1): A novel protein required for the establishment of sister chromatid cohesion and for bivalent formation at meiosis. *Genes and Development*, *15*(14), 1859–1871. https://doi.org/10.1101/gad.203201

Mercier, R., Mézard, C., Jenczewski, E., Macaisne, N., & Grelon, M. (2015). The molecular biology of meiosis in plants. *Annual Review of Plant Biology*, *66*, 297–327. https://doi.org/10.1146/annurev-arplant-050213-035923

Miao, H., Guo, R., Chen, J., Wang, Q., Lee, Y. R. J., & Liu, B. (2019). The γ-tubulin complex protein GCP6 is crucial for spindle morphogenesis but not essential for microtubule reorganization in Arabidopsis. *Proceedings of the National Academy of Sciences of the United States of America*, *116*(52), 27115–27123. https://doi.org/10.1073/pnas.1912240116

Michaelis, P. (1955) Cytologia 20:315

Moody, M. E., Mueller, L. D., & Soltis, D. E. (1993). Genetic variation and random drift in autotetraploid populations. *Genetics*, *134*(2), 649–657. https://doi.org/10.1093/genetics/134.2.649

Morgan, E. R., Seelye, J. F., Hofmann, B. L., & Grant, J. E. (2004). Production of triploid Sandersonia aurantiaca plants. *South African Journal of Botany*, *70*(2), 210–214. https://doi.org/10.1016/S0254-6299(15)30237-4

Morita, M. T., & Shimada, T. (2014). The plant endomembrane system-A complex network supporting plant development and physiology. *Plant and Cell Physiology*, *55*(4), 667–671. https://doi.org/10.1093/pcp/pcu049

Nebei, B. R. (1937). Mechanism of polyploidy through colchicine. *Nature*, *140*(1932), 1101.

Nebenführ, A., & Dixit, R. (2018). Kinesins and Myosins: Molecular Motors that Coordinate Cellular Functions in Plants. *Annual Review of Plant Biology*, *69*(February), 329–361. https://doi.org/10.1146/annurev-arplant-042817-040024

Nishihama, R., Soyano, T., Ishikawa, M., Araki, S., Tanaka, H., Asada, T., Irie, K., Ito, M., Terada, M., Banno, H., Yamazaki, Y., & Machida, Y. (2002). Expansion of the cell plate in plant cytokinesis requires a kinesin-like protein/MAPKKK complex. *Cell*, *109*(1), 87–99. https://doi.org/10.1016/S0092-8674(02)00691-8

Oakley, B. R. (2000). An abundance of tubulins. Trends in Cell Biology, 10(12), 537–542. https://doi.org/10.1016/S0962-8924(00)01857-2

Oda, Y., Higaki, T., Hasezawa, S., & Kutsuna, N. (2009). Chapter 3 New Insights into Plant Vacuolar Structure and Dynamics. In *International Review of Cell and Molecular Biology* (1st ed., Vol. 277, Issue C). Elsevier Inc. https://doi.org/10.1016/S1937-6448(09)77003-0

Ogburia, M. N., Yabuya, T., & Adachi, T. (2002). A cytogenetic study of bilateral sexual polyploidization in cassava (Manihot esculenta Crantz). *Plant Breeding*, *121*(3), 278–280. https://doi.org/10.1046/j.1439-0523.2002.00694.x

Olsen, R. T., Ranney, T. G., & Viloria, Z. (2006). Reproductive behavior of induced allotetraploid xChitalpa and in vitro embryo culture of polyploid progeny. *Journal of the American Society for Horticultural Science*, *131*(6), 716–724. https://doi.org/10.21273/jashs.131.6.716

Orr, J. N., Waugh, R., & Colas, I. (2021). Ubiquitination in Plant Meiosis: Recent Advances and High Throughput Methods. *Frontiers in Plant Science*, *12*(April), 1–22. https://doi.org/10.3389/fpls.2021.667314

Ortiz, R., Franco, J., & Iwanaga, M. (1997). Transfer of resistance to potato cyst nematode (Globodera pallida) into cultivated potato Solanum tuberosum through first division restitution 2n pollen. *Euphytica*, *96*(3), 339–344. https://doi.org/10.1023/A:1003049618218

Otegui, M. S., Mastronarde, D. N., Kang, B. H., Bednarek, S. Y., & Staehelin, L. A. (2001). Three-dimensional analysis of syncytial-type cell plates during endosperm cellularization visualized by high resolution electron tomography. *Plant Cell*, *13*(9), 2033–2051. https://doi.org/10.1105/tpc.13.9.2033

Ovechkina, Y., & Oakley, B. R. (2001). Gamma tubulin in plant cells. *Methods in Cell Biology*, *67*(67), 195–212. https://doi.org/10.1016/s0091-679x(01)67014-6

Pendleton, A., Pope, B., Weeds, A., Koffer, A. (2003) Latrunculin B or ATP Depletion Induces Cofilin-dependent Translocation of Actin into Nuclei of Mast Cells. MECHANISMS OF SIGNAL TRANSDUCTION| VOLUME 278, ISSUE 16, P14394-14400. https://doi.org/10.1074/jbc.M206393200

Peremyslov, V.V., Prokhnevsky, A.I., Avisar, D., Dolja, V.V. (2008) Two class XI myosins function in organelle trafficking and root hair development in Arabidopsis thaliana. Plant Physiol. 146:1109–16

Peremyslov, V.V., Prokhnevsky, A.I., Dolja, V.V. (2010). Class XI myosins are required for development, cell expansion, and F-actin organization in Arabidopsis. Plant Cell 22:1883–97

Pozhvanov, G. (2018). Visualization and analysis of actin cytoskeleton organization in plants. *Biological*

Communications, *63*(1), 59–69. https://doi.org/10.21638/spbu03.2018.107

Ramsey, J., & Schemske, D. W. (1998). Pathways, mechanisms, and rates of polyploid formation in flowering plants. *Annual Review of Ecology and Systematics*, *29*, 467–501. https://doi.org/10.1146/annurev.ecolsys.29.1.467

Ravi, M., Marimuthu, M. P. A., & Siddiqi, I. (2008). Gamete formation without meiosis in Arabidopsis. *Nature*, *451*(7182), 1121–1124. https://doi.org/10.1038/nature06557

Renny-Byfield, S., & Wendel, J. F. (2014). Doubling down on genomes: Polyploidy and crop plants. *American Journal of Botany*, *101*(10), 1711–1725. https://doi.org/10.3732/ajb.1400119

Riddle, N. C., Kato, A., & Birchler, J. A. (2006). Genetic variation for the response to ploidy change in Zea mays L. *Theoretical and Applied Genetics*, *114*(1), 101–111. https://doi.org/10.1007/s00122-006-0414-z

Saito, C., Ueda, T., Abe, H., Wada, Y., Kuroiwa, T., Hisada, A., Furuya, M., & Nakano, A. (2002). A complex and mobile structure forms a distinct subregion within the continuous vacuolar membrane in young cotyledons of Arabidopsis. *Plant Journal*, *29*(3), 245–255. https://doi.org/10.1046/j.0960-7412.2001.01189.x

Sato, S., Katoh, N., Iwai, S., & Hagimori, M. (2005). Frequency of spontaneous polyploidization of embryos regenerated from cultured anthers or microspores of Brassica rapa var. pekinensis L. and B. oleracea var. capitata L. *Breeding Science*, *55*(1), 99–102. https://doi.org/10.1270/jsbbs.55.99

Sattler, M. C., Carvalho, C. R., & Clarindo, W. R. (2016). The polyploidy and its key role in plant breeding. *Planta*, *243*(2), 281–296. https://doi.org/10.1007/s00425-015-2450-x

Schlegel, R. (2006) Rye (Secale cereale L): a younger crop plant with a bright future. In: Singh RJ, Jauhar PP (eds) Genetic resources, chromosome engineering, and crop improvement: cereals, vol 2. CRC Press, New York NASC

Scott, R. J., Spielman, M., Bailey, J., & Dickinson, H. G. (1998). Parent-of-origin effects on seed development in Arabidopsis thaliana. *Development*, *125*(17), 3329–3341. https://doi.org/10.1242/dev.125.17.3329

Sémon, M., & Wolfe, K. H. (2007). Consequences of genome duplication. *Current Opinion in Genetics and Development*, *17*(6), 505–512. https://doi.org/10.1016/j.gde.2007.09.007

Shamina, N. V., Gordeeva, E. I., Kovaleva, N. M., Seriukova, E. G., & Dorogova, N. V. (2007). Formation and function of phragmoplast during successive cytokinesis stages in higher plant meiosis. *Cell Biology International*, *31*(6), 626–635. https://doi.org/10.1016/j.cellbi.2006.12.001

Shaw, S. L., Kamyar, R., & Ehrhardt, D. W. (2003). *Esearch rticles*. *300*(June), 1715–1719.

Sheahan, M. B., Rose, R. J., & McCurdy, D. W. (2004). Organelle inheritance in plant cell division: The actin cytoskeleton is required for unbiased inheritance of chloroplasts, mitochondria and endoplasmic reticulum in dividing protoplasts. *Plant Journal*, *37*(3), 379–390. https://doi.org/10.1046/j.1365-313X.2003.01967.x

Sheldon, J.M. & Hawes, C. (1988) The actin cytoskeleton during male meiosis in Lilium. Cell Biol Int Rep 12:471–476

Shimamura, M., Brown, R. C., Lemmon, B. E., Akashi, T., Mizuno, K., Nishihara, N., Tomizawa, K. I., Yoshimoto, K., Deguchi, H., Hosoya, H., Horio, T., & Mineyuki, Y. (2004). γ-Tubulin in Basal Land Plants: Characterization, Localization, and Implication in the Evolution of Acentriolar Microtubule Organizing

Centers. Plant Cell, 16(1), 45–59. https://doi.org/10.1105/tpc.016501

Shimaoka, T., Ohnishi, M., Sazuka, T., Mitsuhashi, N., Hara-Nishimura, I., Shimazaki, K. I., Maeshima, M., Yokota, A., Tomizawa, K. I., & Mimura, T. (2004). Isolation of intact vacuoles and proteomic analysis of tonoplast from suspension-cultured cells of Arabidopsis thaliana. *Plant and Cell Physiology*, *45*(6), 672–683. https://doi.org/10.1093/pcp/pch099

Simon, P. W., & Peloquin, S. J. (1976). Pollen vigor as a function of mode of 2n gamete formation in potatoes. *Journal of Heredity*, *67*(4), 204–208. https://doi.org/10.1093/oxfordjournals.jhered.a108710

Spielman, M., Preuss, D., Li, F. L., Browne, W. E., Scott, R. J., & Dickinson, H. G. (1997). TETRASPORE is required for male meiotic cytokinesis in Arabidopsis thaliana. *Development*, *124*(13), 2645–2657. https://doi.org/10.1242/dev.124.13.2645

Staiger, C. J., & Cande, W. Z. (1991). Microfilament distribution in maize meiotic mutants correlates with microtubule organization. *Plant Cell*, *3*(6), 637–644. https://doi.org/10.2307/3869192

Stegmann, M., Anderson, R.G., Ichimura, K., Pecenkova, T., Reuter, P., Žárský, V., McDowell, J.M., Shirasu, K., Trujillo, M. (2012). he Ubiquitin Ligase PUB22 Targets a Subunit of the Exocyst Complex Required for PAMP-Triggered Responses in *Arabidopsis*. *The Plant Cell*, Volume 24, Issue 11, November 2012, Pages 4703–4716, https://doi.org/10.1105/tpc.112.104463

Tchórzewska, D., Winiarczyk, K., Pietrusiewicz, J., & Bednara, J. (2008). A new type of microtubular cytoskeleton in microsporogenesis of Lavatera thuringiaca L. *Protoplasma*, *232*(3–4), 223–231. https://doi.org/10.1007/s00709-007-0281-8

Tchórzewska, D. (2017). Chondriokinesis during microsporogenesis in plants. *Planta*, *246*(1), 1–18. https://doi.org/10.1007/s00425-017-2706-8

Tchórzewska, D. & Bednara, J. (2011). The dynamics of the actin cytoskeleton during sporogenesis in Psilotum nudum L. *Protoplasma*, *248*(2), 289–298. https://doi.org/10.1007/s00709-010-0167-z

Traas, J. A., Burgain, S., & Vaulx, R. D. D. E. (1989). The Organization of the Cytoskeleton During Meiosis in Eggplant (Solanum Melongena (L.)): Microtubules and F-Actin are Both Necessary for Coordinated Meiotic Division. *Journal of Cell Science*, *92*(4), 541–550.

Tuyet, N.T., Jisen, S., Đo Đinh, Ca. (2011). Study on the meiosis of pollen mother cells and mechanism producing 2n pollens in Dien and Phuctrach pummelo. Science & Technology Journal of Agriculture & Rural Development. 2011;23–27.

Ueda, H., Yokot,a E., Kutsuna, N., Shimada, T., Tamura, K., et al. (2010) Myosin-dependent endoplasmic reticulum motility and F-actin organization in plant cells. PNAS 107:6894–99

Uemura, T., Yoshimura, S. H., Takeyasu, K., & Sato, M. H. (2002). Vacuolar membrane dynamics revealed by GFP-AtVam3 fusion protein. *Genes to Cells*, *7*(7), 743–753. https://doi.org/10.1046/j.1365-2443.2002.00550.x

Van Breukelen, E. W. M. (1982). Competition between 2x and x pollen in styles of Solanum tuberosum determined by a quick in vivo method. *Euphytica*, *31*(3), 585–590. https://doi.org/10.1007/BF00039196

Van Hoewyk, D. (2018). Defects in endoplasmic reticulum-associated degradation (ERAD) increase selenate sensitivity in Arabidopsis. *Plant Signaling and Behavior*, *13*(4), 1–5. https://doi.org/10.1080/15592324.2016.1171451

Van Lammeren, A. A. M., Bednara, J., & Willemse, M. T. M. (1989). Organization of the actin cytoskeleton during pollen development in Gasteria verrucosa (Mill.) H. Duval visualized with rhodamine-phalloidin. *Planta*, *178*(4), 531–539. https://doi.org/10.1007/BF00963823

Verchot-Lubicz, J., & Goldstein, R. E. (2010). Cytoplasmic streaming enables the distribution of molecules and vesicles in large plant cells. *Protoplasma*, *240*(1), 99–107. https://doi.org/10.1007/s00709-009-0088-x

Waizenegger, I., Lukowitz, W., Assaad, F., Schwarz, H., Jürgens, G., & Mayer, U. (2000). The Arabidopsis KNOLLE and KEULE genes interact to promote vesicle fusion during cytokinesis. *Current Biology*, *10*(21), 1371–1374. https://doi.org/10.1016/S0960-9822(00)00775-2

Wang, P., Hawkins, T. J., & Hussey, P. J. (2017). Connecting membranes to the actin cytoskeleton. *Current Opinion in Plant Biology*, *40*, 71–76. https://doi.org/10.1016/j.pbi.2017.07.008

Wang, Y., Magnard, J. L., McCormick, S., & Yang, M. (2004). Progression through meiosis I and meiosis II in arabidopsis anthers is regulated by an A-type cyclin predominately expressed in prophase I. *Plant Physiology*, *136*(4), 4127–4135. https://doi.org/10.1104/pp.104.051201

Wiedemeier, A.M., Judy-March, J.E., Hocart, C.H., Wasteneys, G.O., Williamson, R.E., Baskin, T.I. (2002) Mutant alleles of Arabidopsis RADIALLY SWOLLEN 4 and 7 reduce growth anisotropy without altering the transverse orientation of cortical micro- tubules or cellulose microfibrils. Development 129:4821–4830.

Williamson, D. H., & Fennell, D. J. (n.d.). *The Use of Flzcorescent DNA-Binding Mitochondria1 D N A*.

Wood, T.E. et al. (2009) The frequency of polyploid speciation in vascular plants. Proc. Natl. Acad. Sci. U.S.A. 106, 13875–13879

Wu, S. Z., & Bezanilla, M. (2014). Myosin VIII associates with microtubule ends and together with actin plays a role in guiding plant cell division. *ELife*, *3*, 1–20. https://doi.org/10.7554/eLife.03498

Wyatt, R. et al. (1988) Allopolyploidy in bryophytes – multiple origins of Plagiomnium medium. Proc. Natl. Acad. Sci. U.S.A. 85, 5601–5604

Xu, C., Liu, Z., Zhang, L., Zhao, C., Yuan, S., & Zhang, F. (2013). Organization of actin cytoskeleton during meiosis I in a wheat thermo-sensitive genic male sterile line. *Protoplasma*, *250*(1), 415–422. https://doi.org/10.1007/s00709-012-0386-6

Xu, T., Sun, X., Jiang, S., Ren, D., Liu, G. (2007) Cotton GhKCH2, a plant specific kinesin, is low-affinitive and nucleotide-independent as binding to microtubule. Journal of Biochemistry and Molecular Biology 40,723–730. doi:10.5483/bmbrep.2007.40.5.723

Yamamoto, Y., Nishimura, M., Hara-Nishimura, I., & Noguchi, T. (2003). Behavior of Vacuoles during Microspore and Pollen Development in Arabidopsis thaliana. Plant and Cell Physiology, 44(11), 1192–1201. https://doi.org/10.1093/pcp/pcg147

Yang, C. Y., Spielman, M., Coles, J. P., Li, Y., Ghelani, S., Bourdon, V., Brown, R. C., Lemmon, B. E., Scott, R. J., & Dickinson, H. G. (2003). TETRASPORE encodes a kinesin required for male meiotic cytokinesis in Arabidopsis. *Plant Journal*, *34*(2), 229–240. https://doi.org/10.1046/j.1365-313X.2003.01713.x

Yasuhara, H., Sonobe, S. and Shobaoka, H. (1995) Effects of brefeldin A on the formation of the cell plate in tobacco BY-2 cells. Eur. J. Cell Biol. 66: 274-281.

Yasuhara, H., & Shibaoka, H. (2000). Inhibition of cell-plate formation by brefeldin A inhibited the depolymerization of microtubules in the central region of the phragmoplast. *Plant and Cell*

Physiology, *41*(3), 300–310. https://doi.org/10.1093/pcp/41.3.300

Zhou, S., Wang, Y., Li, W., Zhao, Z., Ren, Y., Wang, Y., Gu, S., Lin, Q., Wang, D., Jiang, L., Su, N., Zhang, X., Liu, L., Cheng, Z., Lei, C., Wang, J., Guo, X., Wu, F., Ikehashi, H., … Wan, J. (2011). Pollen semi-sterility1 encodes a kinesin-1-like protein important for male meiosis, anther dehiscence, and fertility in rice. *Plant Cell*, *23*(1), 111–129. https://doi.org/10.1105/tpc.109.073692

7. Appendix

Supplemental table 1 List of plants from the wave lines collection used in this study.

NASC Code	Wave nr	Gene name	AGI	Marker
781670	5	RabG3F	At3g18820	late endosome/vacuole
781671	6	NIP1	At4g19030	ER/plasma membrane
781672	7	RabF2a	AT5g45130	late endosome/pre-vacuolar
781673	9	VAMP711	AT4g32150	vacuole
781675	13	VTI12	At1g26670	TGN/early endosome
781676	18	Got1p homolog	At3g03180	Golgi
781677	22	SYP32	At3g24350	Golgi
781686	131	NPSN12	At1g48240	Plasma membrane
781687	138	PIP1;4	At4g00430	Plasma membrane

Supplemental table 2 List of primers used in this study.

Gene	5‘ … 3‘ sequence	Aim
AT5G11700	TCGACGAAATCAACTCTATAGCTGCATACCTATGGT	*peleus* EMS mutant genotyping F
	ATTCTCAAAATGTGTAGTCCTGTTACCTTCAGA	*peleus* EMS mutant genotyping R
	CCTCCTCCTCCATCTAAATGC	*peleus* T-DNA mutant genotyping LP
	AAGATTTTTGTGCATGGTTCG	*peleus* T-DNA mutant genotyping RP
AT1G06660	TCTGTCCGGTTTGAATGTGA	*jas-1* EMS mutant genotyping F
	TATGACACCGACTCCTGGTG	*jas-1* EMS mutant genotyping R
	CACTTCAAATGGTGTTGCATG	*jas-3* T-DNA mutant genotyping LP
	TCTTCCCATTTTCACTCATGG	*jas-3* T-DNA mutant genotyping RP
AT1G34355	AAGAACAGAAGCAGCTTTCCC	*atps1* genotyping LP
	CTGAACCAGTCGCTAAAGCTG	*atps1* genotyping RP
AT5G42220	TGTCTGTCGTTTCCTTCCATC	*ubq-like1* genotyping LP
	TGCTCCATCCGATTAATGAAC	*ubq-like1* genotyping RP
AT5G09250	ACTCTGGTCTGAAGAGAACA	*kiwi* CAPS F
	ACCCATAAGCTCACTGCTA	*kiwi* CAPS R
AT5G11490	AAGGACTATGTGACCGCTGA	*ap4b* CAPS F
	TACCTCGGCTGAATGCTCTT	*ap4b* CAPS R

AT5G11700	ATAAGCTTGATATC**GAATTC**ttggaatccgcgaaaatgttatg	In-fusion cloning of genomic PELEUS into TSK108 F
	ACTAGTGGATCC**CCCGGG**gaaggggaagatgagggaatga	In-fusion cloning of genomic PELEUS into TSK108 R
	ACTAGTGGATCC**CCCGGG**CGACTGCCAAAACAGCTCAT	In-fusion cloning of genomic PELEUS (no STOP codon) into TSK108 R

8. Acknowledgement

I'd like to extend my sincerest gratitude to:

my supervisor Jun.-Prof. Hua Jiang, who took me into his lab and gave me this project. Working on *jason* suppressors made me realize what scientific path I want to follow and prepared me for the challenges I will be facing in the field of plant genetics. I will be forever grateful for the vast knowledge and support I received during the course of my Ph.D. study and for shaping me into a scientist I've always wanted to become;

Prof. Ingo Schubert for the immense unconditional support and guidance on how to better my scientific and personal skills. Thank you for helping me stay on the right track and for maintaining my love for science, while providing invaluable advice and professionalism;

Prof. Andreas Houben and Dr Stefan Heckmann – for the willingness to share their knowledge and materials with the new members of the IPK chromosome community and for instilling and maintaining the passion for plant genetics in new generations of young scientists;

Dr Twan Rutten for the guidance on how to produce best quality confocal images regardless of the given material and Dr Maria Cuacos – for using the light-sheet microscope expertise for the most enjoyable collaboration and providing me with one of my favorite data in this thesis: the tubulin dynamics movies;

all the members of the Chromosome Applied Biology laboratory, who shared my ups and downs, who greeted me with a smile, who helped me out and let me learn from them. To Jinping Cheng and Linhao Xu for all the amazing memories we shared during our three-year long journey and for letting me experience some of your fascinating culture. To Leane Gottschalk for being the great technician and a wonderful person, and for all the unforgettable trips we had, which showed us the beautiful piece of Germany we were lucky to be in. To Yingrui Ma for taking on this project with a smile. And to everybody who was part of our ACB team. Hopefully all of our paths will cross again as we venture further into the scientific world!

Bianka Jacobi and Dr Britt Leps for their passion and professionalism in helping the students. Thank you for making the non-scientific aspects of our lives completely non-stressful and helping us focus on the work without any other worries;

and to my Parents and Family, who showed me never-ending support for my choices throughout all those years. Especially to my Mom, who is the reason why I kept on going. Dziękuję, Mamo. Bez Ciebie i Twojej miłości nie byłoby mnie tu, gdzie jestem.

Thank you!

9. Curriculum Vitae

EWA WERONIKA PISKORZ

PERSONAL INFORMATION

Date of Birth: 21st July 1993

Place of Birth: Wrocław, Lower Silesia, Poland

EDUCATION

2018-2021 Ph.D. studies in Biology at Martin Luther University of Halle-Wittenberg, Germany.

PhD thesis prepared in Applied Chromosome Biology laboratory at Leibniz Institute of Plant Genetics and Crop Plant Research (IPK) Gatersleben, Germany, title: "Elucidating mechanisms of unreduced gamete formation in *Arabidopsis thaliana*".

PhD thesis supervisor: Jun.-Prof. Hua Jiang.

2015-2017 M.Sc. studies in Biotechnology (specialization: Molecular Biology) at the University of Wrocław, Poland.

Master thesis prepared in Molecular Cell Biology laboratory, title: „Preliminary characteristic of *Arabidopsis thaliana ftsh4* mutants with inactivated ATPase or proteolytic domain – studies on the stages of germination and seedling development".

Master thesis supervisor: Dr Małgorzata Heidorn-Czarna.

2012-2015 B.Sc. studies in Biotechnology at the University of Wrocław, Poland.

Bachelor thesis in Molecular Cell Biology laboratory, title: „Processes of mitophagy and mitochondria-derived vesicles formation in mitochondrial quality control".

Bachelor thesis supervisor: Dr Małgorzata Heidorn-Czarna.

SELECTED SCIENTIFIC EXPERIENCE

10.2017-03.2018 The University of Sheffield; LLP Erasmus traineeship in dr Jarema Malicki Laboratory.

Title of the traineeship: "Studies on cilia in zebrafish – vertebrate model organism".

Internship supervisor: Dr Jarema Malicki †.

07.2016 University of Wrocław; master internship in Biotransformation laboratory.

Title of the internship: "Labeling of CDR1 protein in *Candida albicans*".

Internship supervisor: Dr Joanna Szczepaniak.

08-12.2015 Norwegian University of Life Sciences; LLP Erasmus internship in Molecular Cell Biology laboratory.

Research project title: „Studies on a food-grade Lactobacillus-based oral vaccine delivery system". Internship supervisor: Prof. Tor Lea.

CONFERENCES AND PAPERS

2021 Oral presentation at the GPZ Chromosome Meeting "Chromosome Biology in context of Evolution and Plant Breeding", Görlitz, Germany;

2021 Participant in the 23rd International Chromosome Conference (ICC) and the 24th International Colloquium in Animal Cytogenetics and Genomics (ICACG);

2021 Participant in the Plant Science Student Conference, IPK Gatersleben;

2021 Participant in MAYosis 2021;

2019 Poster presentation at the Plant Science Student Conference, IPB Halle;

2018 Poster presentation at the 6th Annual CMIAD Retreat in Sheffield;

2017 Acknowledgment in publication: Kuczkowska et al. (2017) Immunogenic Properties Of *Lactobacillus plantarum* Producing Surface-Displayed *Mycobacterium tuberculosis* Antigens, *Applied and Environmental Microbiology*, 83(2): e02782-16.

ACHIEVEMENTS

2021	Jun.-Prof. Hua Jiang's DFG grant following up my PhD project;
2016/2017	Rector's Scholarship for the best students;
2012-2015	Ordered Course Scholarship at the University of Wrocław.

10. Eidesstattliche Erklärung/Declaration under Oath

Ich erkläre an Eides statt, dass ich die Arbeit selbstständig und ohne fremde Hilfe verfasst, keine anderen als die von mir angegebenen Quellen und Hilfsmittel benutzt und die den benutzten Werken wörtlich oder inhaltlich entnommenen Stellen als solche kenntlich gemacht habe.

I declare under penalty of perjury that this thesis is my own work entirely and has been written without any help from other people. I used only the sources mentioned and included all the citations correctly both in word or content.

_____ _____

Datum / *Date*

Unterschrift des Antragstellers /

Signature of the applicant

11. Erklärung über bestehende Vorstrafen und anhängige Ermittlungsverfahren/Declaration concerning Criminal Record and Pending Investigations

Hiermit erkläre ich, dass ich weder vorbestraft bin noch, dass gegen mich Ermittlungsverfahren anhängig sind. / *I hereby declare that I have no criminal record and that no preliminary investigations are pending against me.*

_____ _____

Datum / *Date*

Unterschrift des Antragstellers / *Signature of the applicant*